COMBUSTION & FLAME

Quarterly Journal of The Combustion Institute

Contents

VOLUME 11 NO. 4 DECEMBER 1958

	Page
EXPERIMENTAL STUDY OF A REVERSED JET FLAMEHOLDER. *G. A. Agoston, A. W. Noon and T. D. Witherly*	333
ON THE DECOMPOSITION FLAME OF LIQUID OZONE-OXYGEN MIXTURES IN A TUBE. *R. Sandri*	348
SPECTROSCOPIC STUDIES ON TEMPERATURE GRADIENTS IN FLAMES. *R. H. Tourin*	353
SPEED OF FLAME IN SLOWLY MOVING CLOUDS OF CORK DUST. *R. H. Essenhigh and D. W. Woodhead*	365
CONFINED JETS AND RECIRCULATION PHENOMENA WITH COLD AIR. *R. Curtet*	383
ON THE CALCULATION OF PROPERTIES OF GASES AT ELEVATED TEMPERATURES. *I. Amdur and J. Ross*	412
RECENT DEVELOPMENTS AND NOTES. *W. A. Kirkby*	421
PUBLICATIONS	435
LETTERS TO THE EDITORS: A NOTE ON POLYCYCLIC HYDROCARBONS IN ASSOCIATION WITH THE CARBONACEOUS RESIDUES FROM DIFFUSION FLAMES. *A. Badakshan, F. H. Garner and R. Long;* THE RELATION BETWEEN FUEL INJECTION AND COMBUSTION IN DIESEL ENGINES. *W. T. Lyn;* NOTE ON THE INFLUENCE OF HYDROCARBON STRUCTURE ON ALDEHYDE FORMATION DURING LOW TEMPERATURE OXIDATION. *D. H. Allen and R. Long;* BURNING TIMES OF LIQUID FUEL DROPS IN A CONVECTION-RADIATION FIELD. *E. G. Masdin and R. H. Essenhigh;* THE HYDROGEN DIFFUSION FLAME AS AN INFLAMMABLE GAS DETECTOR. *P. D. Edwards and R. Long;* A NOTE ON THE INFLUENCE OF THE LEWIS NUMBER ON FLAME STABILITY. *J. Menkes*	437
INDEX	451

Published quarterly. Annual subscription including postage—U.K. £5 5s. 0d.; U.S.A. $16.00. Combined subscription with FUEL*—U.K. £8 8s. 0d.; U.S.A. $25.00. Editorial Offices, Showroom, Binding and Trade Departments:* 4-5 Bell Yard, Temple Bar, London, W.C.2. *Publishing and Advertisement Offices:* 88 Kingsway, London, W.C.2. *Telephone:* Holborn 6900. *U.S.A. Distributors: Interscience Publishers Inc., 250 Fifth Avenue, New York 1, N.Y.*

BUTTERWORTHS SCIENTIFIC PUBLICATIONS

Experimental Study of a Reversed Jet Flameholder

G. A. AGOSTON, A. W. NOON and T. D. WITHERLY

Experiments and analyses were performed to contribute to a basic understanding of the holding of flame in a stream of a combustible gas mixture by a small gas jet directed upstream. The main stream, a mixture of natural gas and air, entered a cylindrical transparent test section at uniform velocity. A flameholding jet of air was directed counter to the stream along the axis of the test section. Observations of the flow field and flame behaviour were made by means of time-exposure photographs, high-speed motion pictures, and spark shadowgraphs. A pilot flame was delineated, and its significant time-averaged dimensions were noted as a function of jet and main-stream velocities. New evidence was obtained indicating the occurrence of recirculation. Transmission of flame from the pilot to the main stream is accomplished through a mixture continuously shedding from the pilot flame. Rough burning near a stability limit occurs when significant portions of the shedding mixture are not inflammable. The influence of non-uniform fuel concentration patterns in the main stream on flame stability limits was also investigated. Interpretation of the data leads to conclusions which conflict with a currently held mechanism for reversed-jet flame stabilization. A mechanism is proposed which is plausible in the light of current observations.

THE holding of flame in high-velocity, combustible streams such as in ramjets and afterburners is generally accomplished by bluff bodies. Such obstructions produce local low-velocity regions where reactions may proceed, thus providing a continuous source of ignition to the ambient stream. In recent years attention has been given to the possibility of employing reversed gas jets for the holding of flame. This novel mode of flame stabilization is of practical interest because of possibilities of attaining more stable burning, easier ignition, and lower drag during periods when afterburners are not in operation.

Experimental studies of reversed-jet flameholding by A. SCHAFFER and A. B. CAMBEL[1-3], R. H. EUSTIS and C. L. MRAZ[4], A. W. NOON[5], and A. E. NOREEN and W. T. MARTIN[6] have provided quantitative information on the influence of such operational variables as the composition, temperature and pressure of the main stream and the composition, temperature, mass velocity, diameter and orientation of the jet.

Schaffer and Cambel considered the mechanism of jet flameholding and proposed the concept of a critical zone controlling the maintenance of flame. Noreen and Martin have combined this concept with the homogeneous reactor theory of J. P. LONGWELL, E. E. FROST and M. A. WEISS[7] in relating their observations of maximum blowout velocity to the main-stream temperature, composition and pressure. The subject of flame

Presented at the Winter Meeting of the Western States Section of the Combustion Institute, 20 January 1958, Pasadena, California.

holding by reversed jets has been reviewed by S. S. PENNER and F. WILLIAMS[8] and by A. B. CAMBEL[9].

In the present work a study was made of the physical structure of the jet and flame, the phenomenon of unstable burning, and the mechanism of stable burning.

APPARATUS

A schematic diagram of the experimental apparatus is shown in *Figure 1*. Air (at about 140°F) supplied by a blower is passed through a 12 in.

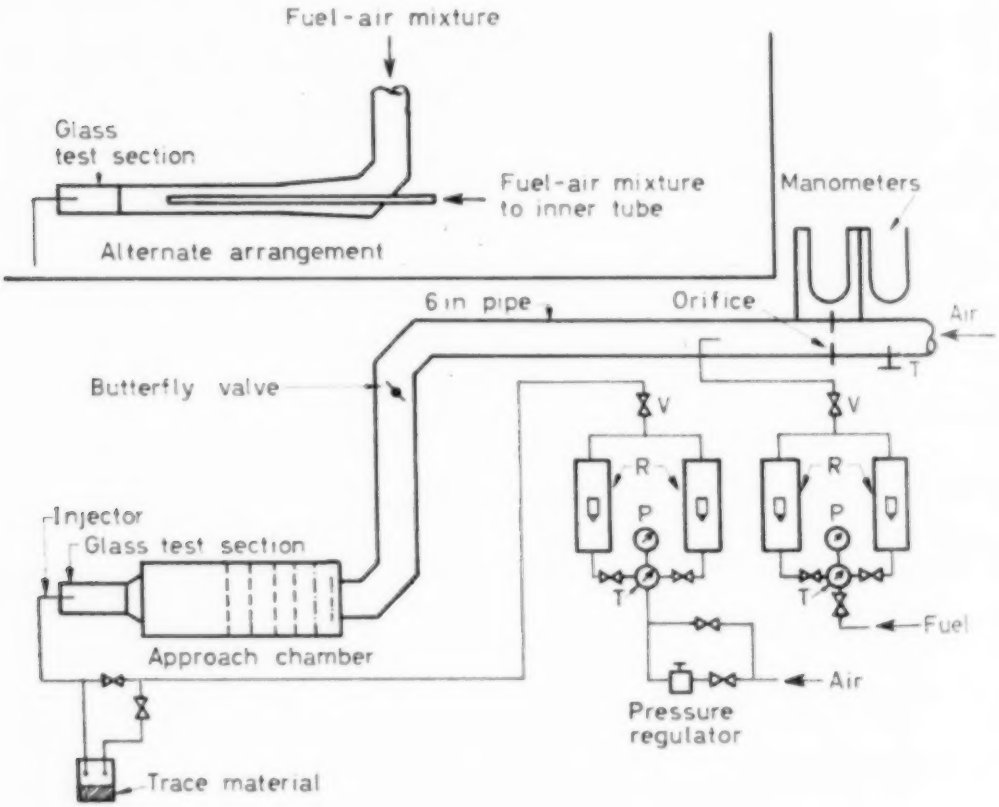

V Control valve
T Thermometer
R Flowmeter
P Pressure gauge

Figure 1. Apparatus

diameter approach chamber and a converging nozzle with a 2 in. throat. This chamber is designed to produce uniform, low-turbulence flow at the nozzle outlet. A glass (Pyrex) test section 2 in. in diameter and 6 in. long is fitted to the nozzle. Natural gas is introduced into the main air stream approximately 30 pipe diameters upstream of the approach chamber.

The air-jet injector mounted at the exit of the glass test section consists of a stainless steel tube (inside diameter 0·054 in.) surrounded by a tubular

water cooling jacket (outside diameter 0·25 in.) with forward and return annular passages. The tip of the injector is flat, with sharp edges, and the straight exit portion of the injector is 113 diameters long. The jet air (supplied by a compressor) is always close to room temperature at the injector exit.

For tests in which a non-uniform symmetrical fuel profile is desired, the approach chamber is replaced by a 2 in. pipe in which a smaller tube can be mounted coaxially (see alternate arrangement in *Figure 1*). The composition and flow rate of the mixture through the inner tube are regulated independently.

For purposes of tracing flow and colouring the flame for photography, particles of sodium chloride, magnesium or iron are introduced into the jet air before ejection (*Figure 1*). Motion pictures are taken with a Fastax camera. Shadowgraph pictures of flow detail are obtained with a point light source (10^{-7} sec) produced by a Liebessart spark gap[10].

RESULTS

Jet and flame structure

The principal structural features of an air jet and flame are illustrated in *Figure 2*. The air column issuing from the injector assumes a trumpet shape as it decelerates, penetrating the oncoming stream to a distance L. A correlation of the penetration L based on photographic measurements is presented in *Figure 3*, where d and D represent the inside diameter of the injector tube and test section respectively, V_s is the average velocity of the main stream, F/A represents the fuel/air weight ratio of the main stream, and G_s and G_j are the mass velocities (mass flow rate per unit cross section) of the main stream and jet, respectively. The jet penetration is essentially unaffected by variations in fuel/air ratio[6, 9].

In the tip region the air column disintegrates into a turbulent mass, evidence of which is given in the uneven, foamlike structure of the flame surface in *Figure 4*. This turbulent fluid spills over continuously in the form of a helix (*Figures 2* and *5*), which indicates that the tip is rotating around the injector axis. The frequency of rotation appears to increase with increasing G_j/G_s. Tests with luminous tracers prove that the helix is not twisting and that there is no general vortex flow in the main stream.

The apparent growth of the helix as it moves downstream reflects the spread of flame into the unburnt main gas stream. The time-averaged

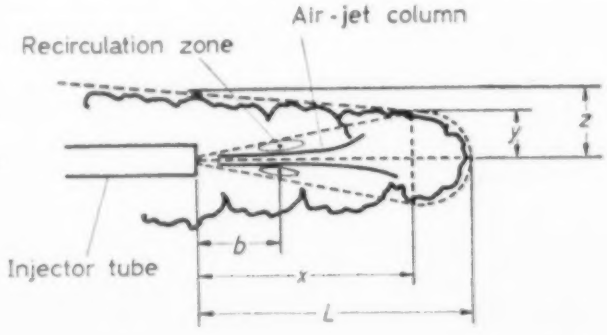

Figure 2. Jet and flame shape

shape of this flame envelope may be typified by a parabaloid (upper dash line in *Figure 2*) with the flame skirt radius at the injector tip represented by z. Since for given main-stream velocity V_s, and jet velocity at the injector tip V_j, the radius z is a measure of flame speed, z is expected to be a maximum when F/A is close to the stoichiometric value (about 0·0). Thus, when the F/A is increased, starting in the rich region and at, say, $V_s = 118$ ft sec^{-1}, the flame skirt becomes narrower (*Figure 6*) until finally the inflammability limit is reached. Although near the inflammability limit flameholding is intermittent (as is discussed below), z reaches a lower limiting value that is set by the maximum radius y of the pilot flame, the core of flame that remains when the flame skirt breaks away (*Figure 6*). When the flameholding limit is not determined by inflammability of the main stream, then z exceeds y at blowout.

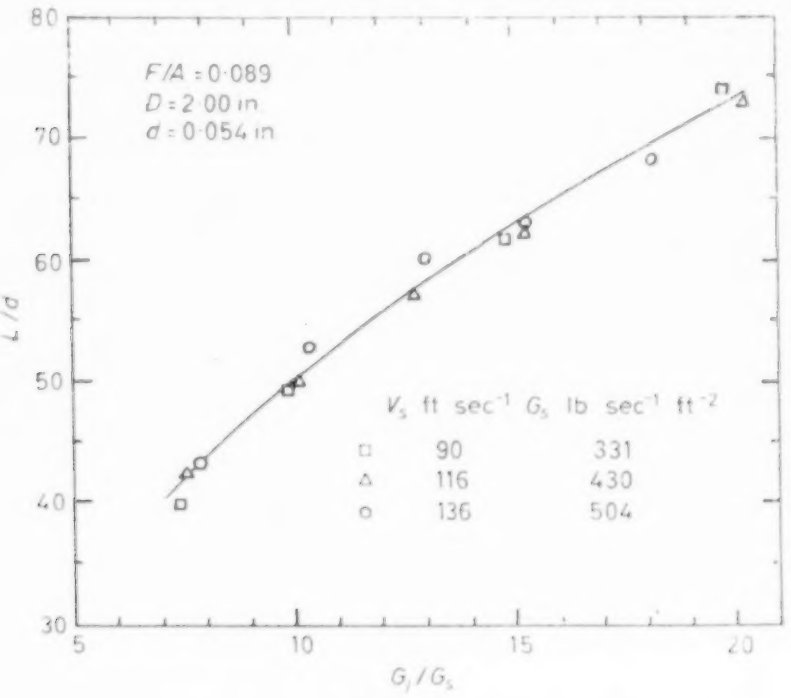

Figure 3

The shape of the pilot zone can be characterized by a cone with a rounded base specified by the dimensions L, y and x, where x is the axial position of the maximum radius of the pilot zone y (*Figure 2*). One measurement of y from a photograph of an isolated pilot flame is represented by the solid triangle in *Figure 7*. The remaining values of y and x in *Figure 7* represent the space coordinates of a small bead of sodium chloride at the tip of a fine wire (similar to earlier techniques[9, 11, 12]). When the bead touches the flame envelope at points upstream from the position described by x and y, the whole pilot zone and flame envelope become yellow in colour, indicating that the pilot zone has been entered. Downstream from x and y, the bead touching the flame envelope produces a yellow plume and sodium chloride is not swept into the pilot zone. The

plots indicate that the parameters x/L and y/L are independent of the mass velocity ratio: $x=0{\cdot}78L$ and $y=0{\cdot}18L$.

Values of the flame skirt radius z obtained from photographs are also presented in *Figure 7*. Three lines are obtained because the ratio z/L is evidently also a function of U/V_o, where U is the flame speed. On the basis of the above considerations none of the lines may cross $z/L=0{\cdot}18$.

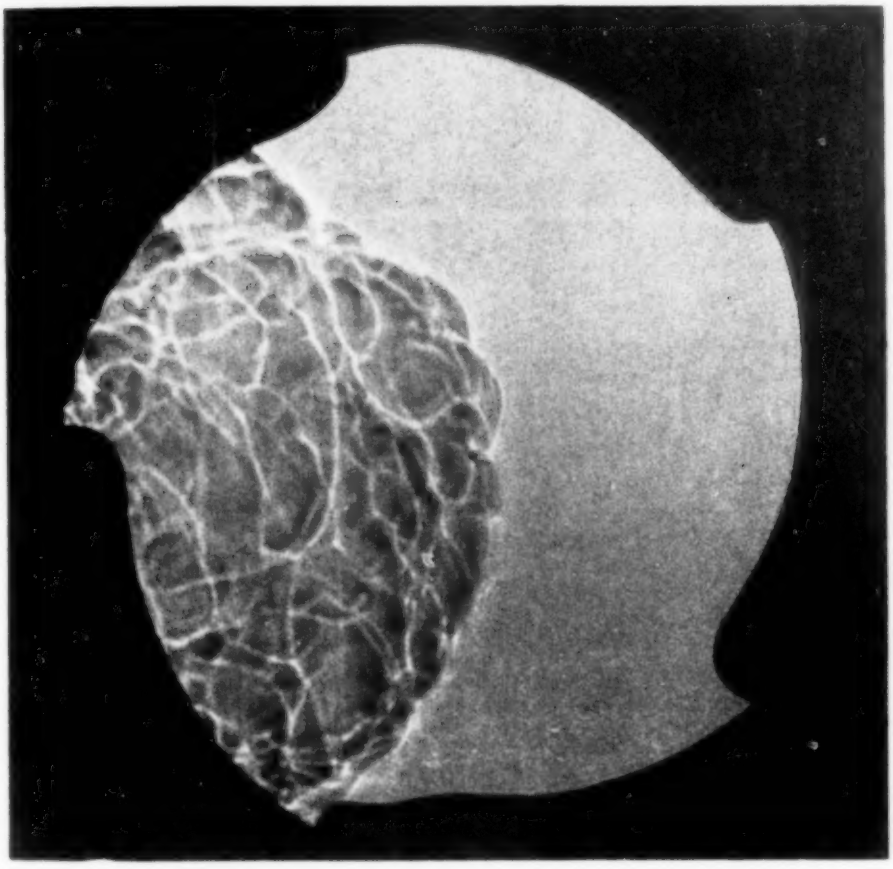

Figure 4. Shadowgraph of unconfined flame at its upstream tip

The location of a recirculation zone in the pilot flame is designated by distance b in *Figure 2*. Presumably the recirculation zone is toroidal with a distorted cross section as indicated. Experimentally the recirculation zone was identified as the region where tracer particles become appreciably detained in their travel (as long, sometimes, as one millisecond). In a plot of b/L versus G_j/G_o (*Figure 8*) a rather marked change in slope is apparent, a behaviour suggestive of two recirculatory flow régimes. In all cases the detained particles were observed in close proximity to the jet column. No indication was found of particle detention near the tip or in other regions of the pilot flame.

Further evidence of recirculating gases close to the jet column is presented in *Figure 6*. The surface of the air jet column is bordered by a thin purple layer (or sometimes by two coloured layers, e.g. a purple inner layer and an outer light blue layer), suggesting the presence of a thin

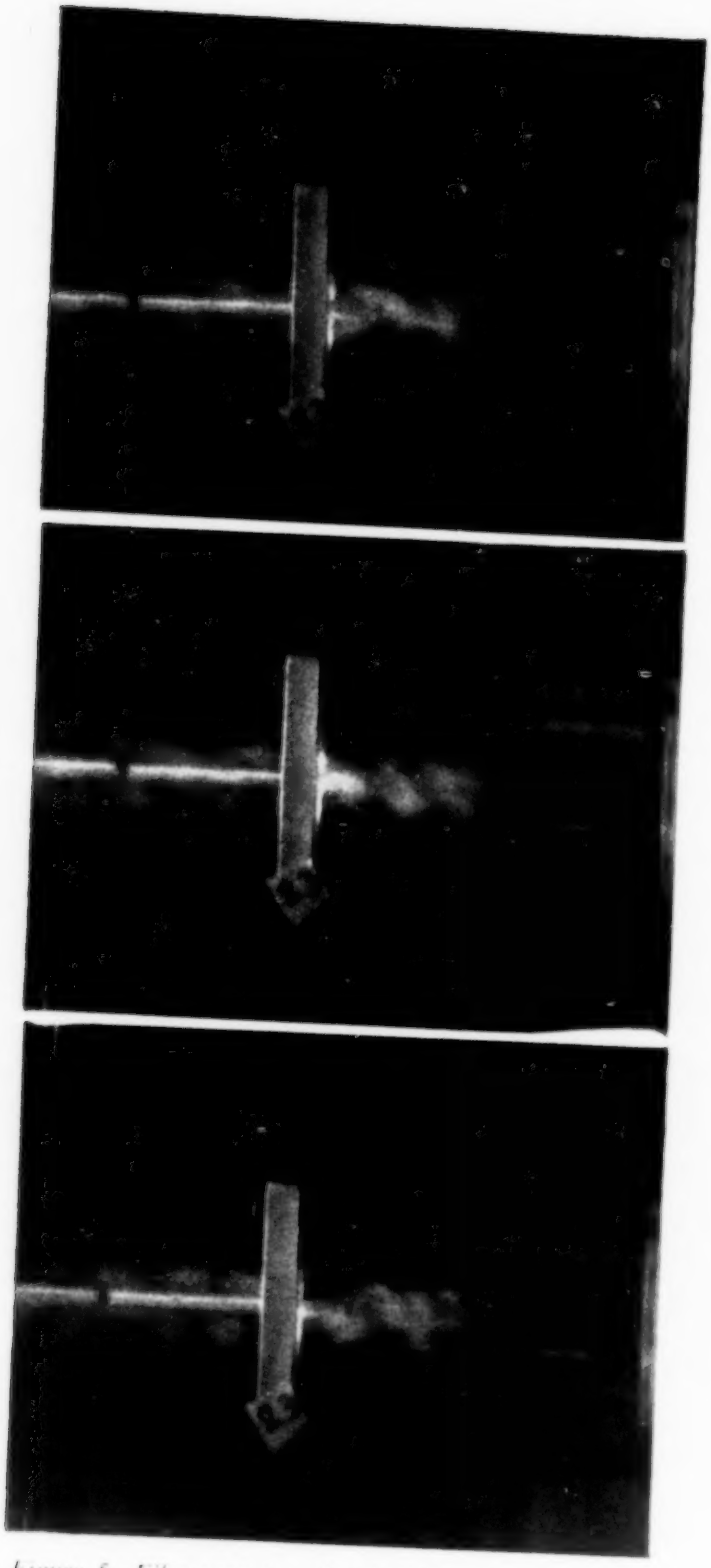

Figure 5. Film sequence showing helical structure of spillover fluid. V_j 945 ft sec^{-1}, V_a 126 ft sec^{-1}, G_j/G_a 9·6, F/A 0·088. Film speed 2 800 frames sec^{-1}. Tip rotating frequency 3 150 sec^{-1}. Additive iron powder (325 mesh)

reaction zone wherein jet air and unburnt fuel combine. Similar luminosity has been noted with propane as fuel[2, 3]. On the basis of the interpretation of the sodium chloride bead test mentioned above, only unburnt fuel from within the pilot flame zone can reach the jet column.

The green coloration near the rich limit indicates the presence of the C_2 radical (*Figure 6*). When the F/A is reduced, the green zone becomes

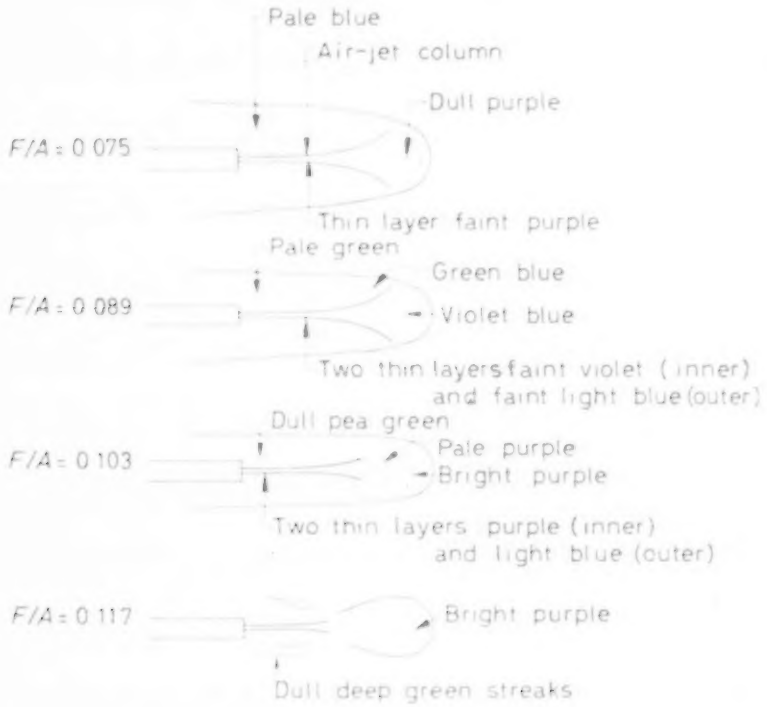

Figure 6. Flame patterns and colours for different main-stream fuel air ratios. V_j = 1025 ft sec^{-1}, V_j = 111 to 118 ft sec^{-1}, G, G = H

hinter and finally changes into a pale blue colour, characteristic of the CH radical, generally prominent in hydrocarbon flames when ample oxidizer is present. The change in colour in the downstream direction (e.g. green blue to pale green at F/A = 0·089) indicates an increase in fuel concentration at the flame envelope, as the flame spreads farther into the ambient stream.

Flame stability

The performance of a flameholding jet in a uniform gas stream may be characterized by a flameholding-limit curve, an example of which is given in *Figure 9*. Since the jet fluid is air in the present work, the lean limit (defined to be the portion of the curve to the left of the maximum) falls predominantly in the fuel-rich region. In *Figure 9* the vertical portion of the rich limit is defined by the upper inflammability propagation limit

which is taken to be $F/A = 0{\cdot}11$ (the reported value for natural gas is 0·10 at room temperature under non-turbulent conditions[13]).

In the region of the lean limit, combustion is smooth. Flame blowout occurs suddenly, without roughness, when the lean limit is traversed. When the F/A is increased from the lean limit and V_s is held constant

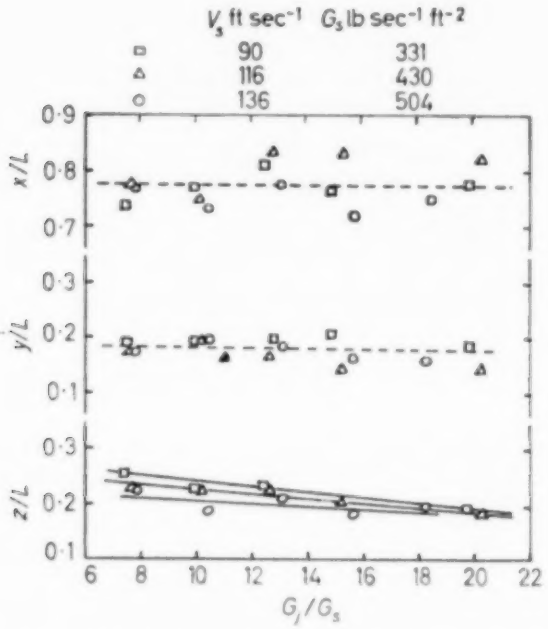

Figure 7. Flame dimensions as a function of mass velocity ratio. $F/A = 0{\cdot}089$. $D = 2{\cdot}00$ in. $d = 0{\cdot}054$ in.

(e.g. $V_s = 118$ ft sec^{-1}), an F/A is reached where roughness in burning becomes apparent, the rich limit of smooth burning. With further increase in F/A, the noise level rises to a maximum and then falls. When the inflammability limit is reached and traversed, rough burning continues with decreasing frequency until individual pops can be distinguished aurally. At $F/A = 0{\cdot}117$ the popping and shedding of flame fragments cease, leaving a rather stable isolated pilot flame. Motion pictures obtained during rough

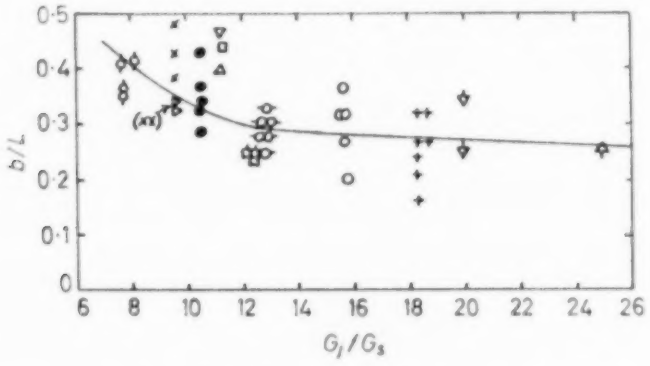

Figure 8. Location of recirculation zone as a function of mass velocity ratio. Symbols refer to individual reels of motion picture films. Sodium chloride was employed in all tests except those designated by × (magnesium powder) and ▷ (iron powder)

burning show that the full pilot flame is present continually and that ignition of the main stream occurs at random intervals. At very low popping frequencies it was observed that each pop is associated with an individual ignition by the pilot flame.

Effect of a non-uniform concentration pattern

Data obtained in tests in which the fuel concentration in the oncoming stream varied radially are presented here because they are used below in calculations performed to test concepts of the mechanism of flameholding. Approximately symmetrical fuel concentration patterns were obtained by

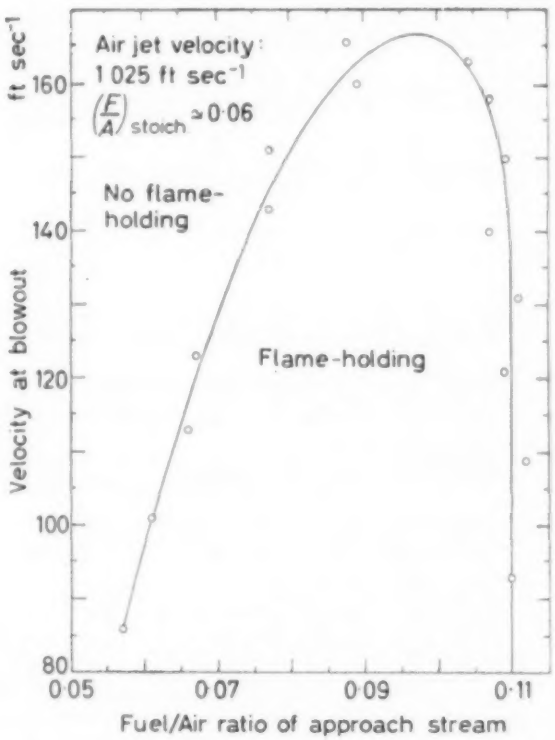

Figure 9. Flameholding-limit curve

joining two concentric streams (*Figure 1*, alternate arrangement), having different but uniform compositions, at a point usually 12 in. upstream from the injector. Blowout velocity observations were made only when the average velocities of the inner and outer streams were equal.

Blowout velocity data obtained with two inner tube sizes and three outer stream fuel/air ratios are presented in *Figures 10* and *11*, where $(F/A)_o$ and $(F/A)_i$ are the fuel/air mixtures of the outer and inner concentric streams, respectively, before joining. The solid data symbols, representing uniform mixtures (no inner tube present), are from the smooth curve of *Figure 9*. The positions of the solid diamond in *Figure 10* and the solid triangle and semicircle in *Figure 11* indicate that disturbances arising from the presence of the inner tube do not affect the blowout velocity noticeably.

In *Figure 11* the effect of varying the fuel concentration pattern (i.e. by changing the inner tube diameter) is demonstrated. When the diameter is

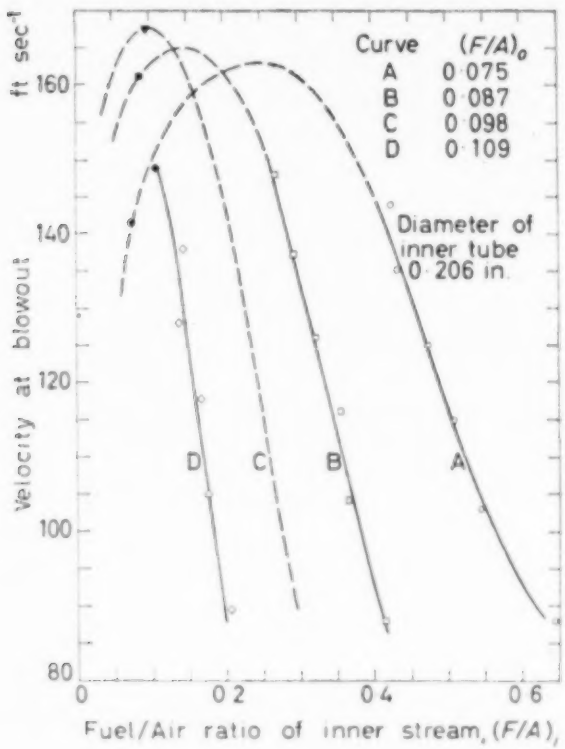

Figure 10. Flameholding limits (non-uniform fuel distribution)

increased, the area under the curve decreases, e.g. curve A (from *Figure 10*) and curve E. A family of curves representing all possible inner tube diameters and one value of $(F/A)_i$ has one common point (e.g. the solid

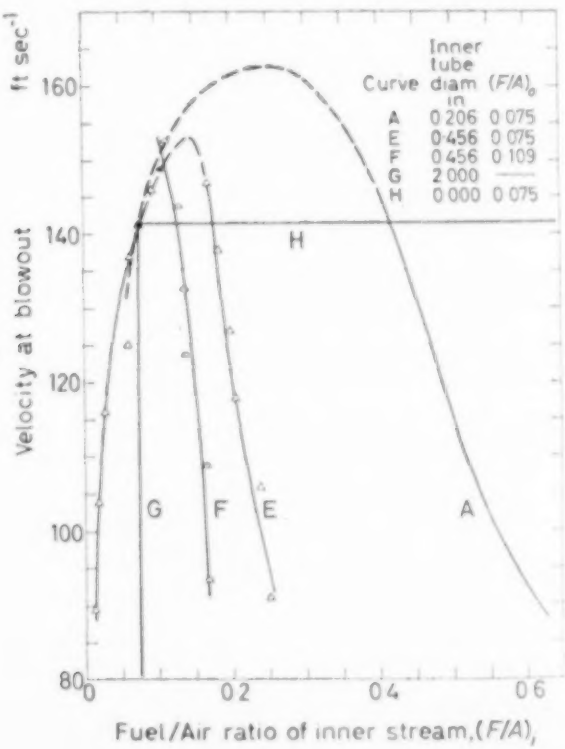

Figure 11. Flameholding limits (non-uniform fuel distribution)

triangle) designating a uniform main mixture, $(F/A)_a=(F/A)_i$. Lines G and H represent limiting conditions.

The portions of the curves exceeding the uniform mixture blowout velocities (solid symbols) represent operation which is benefited by local fuel enrichment. Curve C (*Figure 10*) was estimated to illustrate the one condition, $(F/A)_i=0{\cdot}098$, where the solid symbol is located at the maximum, and no benefit may be secured by local enrichment. The range of fuel/air ratios within which rough burning occurs, diminishes noticeably when the fuel pattern is made non-uniform in the above manner.

DISCUSSION

Unstable burning

A stable isolated pilot flame can be produced only when the flameholding limit is determined by the inflammability limit of the oncoming gas mixture; under this condition $z=y$ and the skirt breaks away. When the inflammability limit is not a factor, blowout of the pilot occurs before the flame skirt can become permanently detached (i.e. $z>y$). Intermittent ignition and flame detachment in the shedding helix result in the discontinuous transmission of flame to the ambient gas. Smooth burning occurs when the helical mass is able to transmit flame continually.

In the isolated pilot flame, it is believed that the spillover fluid which is mixed with ambient stream fluid in transit downstream is not inflammable. This fluid is not inflammable because most of the oxygen is consumed in reaction in the turbulent tip region of the flame. When F/A is reduced (within the non-inflammable range, e.g. 0·117 to 0·110) the probability of forming lean mixtures momentarily in the oscillating tip of the flame (and, hence, of forming inflammable gas zones in the helical mass farther downstream) increases, and therefore the popping frequency increases. When the inflammability limit is traversed (*Figure 9*), the occurrence of lean mixtures in the tip region continues to increase and isolated burning zones continue to be produced in the helical mass igniting the main stream. Upon further decrease in F/A, combustion becomes rougher because the frequency of the appearance of discrete inflammable zones increases. Ultimately, an F/A is reached where the roughness, or frequency, attains a maximum. The reason for this is that the frequency of inflammable-zone formation becomes so high that the inflammable zones begin to connect with one another resulting in fewer interruptions to flame propagation and consequently fewer ignitions. Finally, an F/A is reached where effectively a steady stream rather than isolated pockets of ignitable mixture is shed; this is the rich limit of smooth burning.

When the lean stability limit is approached by further decrease in F/A, no rough burning is experienced. The reason for this is that the F/A of the main stream is still rich and admixture of the necessary oxygen from the tip region fluid yielding a continuous stream of inflammable mixture is practically certain. At the lean limit, sudden, complete flame blowout occurs signifying extinction of the pilot itself.

In the current tests the region of rough burning appears to decrease when the stream velocity is increased to the maximum. This trend can be

explained by the associated decrease in F/A at the rich stability limit narrowing the region wherein the probability of forming non-inflammable mixtures is significant. The observed decrease in roughness accompanying higher temperatures in the main stream can be explained on the basis of increased inflammability.

In earlier tests with stabilizer jets composed of a stoichiometric mixture of natural gas and air, it was observed that the noise level decreased gradually as the lean limit is approached until only a pilot flame remains[5]. In this instance abrupt flame extinction without rough combustion occurs at the rich limit and the flameholding-limit curve is located largely on the LHS of the stoichiometric F/A value. The occurrence of rough burning near the lean limit can be explained on the basis of a deficiency of fuel (rather than of oxygen) in the helical mass.

Mechanism of flame stabilization

Schaffer and Cambel in their initial paper on reversed gas jets suggest that the holding of flame is dependent on the existence of a proper combination of temperature, composition and residence time in some particular region of the flame[1]. Such a critical zone probably consists of unburnt gases, recirculated gases and jet gas. One opinion is that this zone is homogeneously mixed and that it is located in the tip region of the flame[3, 6].

The present authors feel that the critical zone is, instead, a diffusion region bordering the upstream and outer portions of the toroidal recirculation zone. This type of critical zone resembles the 'ears' which border the recirculation zone in the wake of a bluff-body flameholder[1]. Reasons why the earlier concept is untenable become apparent in the following analysis, based on data for non-uniformly mixed streams.

Three specific questions are discussed here:

(*1*) Is the critical zone a thin region bounding the flame tip (i.e. at the forward stagnation point), whose ability to sustain a pilot flame is primarily dependent on the local F/A of the stream fluid at the tip?

(*2*) Is the critical zone essentially a homogeneous reactor?

(*3*) Is the critical zone located within the tip region of the flame?

The first question requires knowledge of F/A at blowout for the non-uniformly mixed main stream at the tip of the flame ($r = 0$). An affirmative answer is indicated if these values of F/A fall on the curve obtained for uniformly mixed streams (*Figure 9*).

In the calculation of F/A at the flame tip use is made of the following expression (based on equation 11 of ref. 14) which expresses the variation of fuel concentration C (mass of fuel per unit volume of gas mixture) with radial position r and time θ

$$\frac{C - C_a}{C_i - C_a} = \left(\frac{r_i}{r_a}\right)^2 + 2\left(\frac{r_i}{r_a}\right)^2 \sum_{n=2}^{n=\infty} e^{-\varepsilon z_n^2 \theta} \frac{J_1(r_i z_n) J_a(r z_n)}{(r_i z_n) J_a^2(r_a z_n)}$$

where r_i is the radius of the inner tube and r_o is the radius of the outer tube; C_i is the initial concentration in the inner tube and C_o is the initial concentration in the annular section; V_s is the main-stream velocity (assumed uniform); ε is the eddy diffusivity (assumed independent of r); and α_n corresponds to the roots of $J_1(r_o\alpha_n)=0$. On the basis of a measurement of eddy diffusivity performed in this investigation, the following relation is considered to apply for the present 2 in. duct: $\varepsilon\theta=0{\cdot}00013X$, where X is the distance (ft) between the inner tube and the tip of the jet. The eddy diffusivity determined is about two thirds of the value predicted from data reported for larger tubes[15]. Mixing is assumed to occur radially only.

The calculated points (*Figure 12*) representing data given in *Figures 10* and *11* do not fall on the original flameholding-limit curve (heavy line) of *Figure 9*. Refinement in the calculation to take into account the reduction in main fluid velocity near the tip (e.g. the local velocity is about 70 per cent of the main-stream value[6]) does not resolve the differences. For

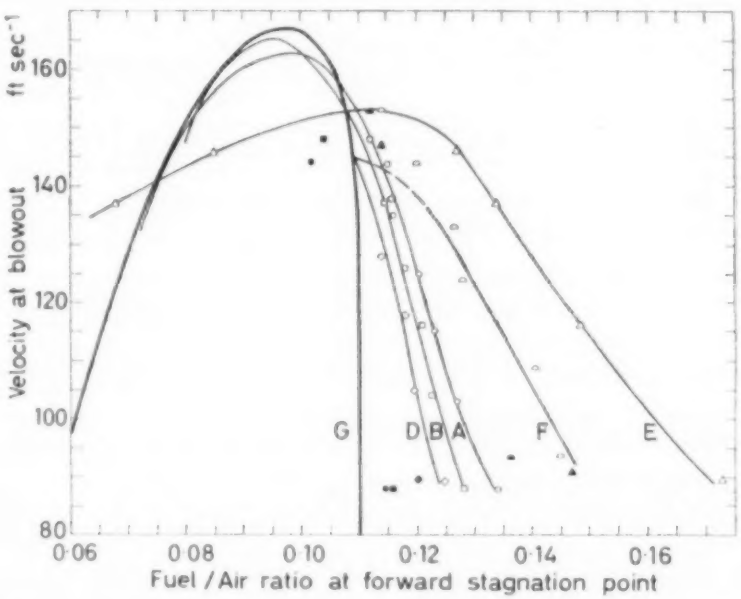

Figure 12. Flameholding limits (non-uniform fuel distribution) with symbols as identified in Figures 10 and 11

example, a liberal increase (50 per cent) in the value of $\varepsilon\theta$ yields no significant improvement in the location of all of the points (see solid symbols representing recalculated points in *Figure 12*); an increase of about 200 per cent is required to move line F over to the present position of line D. The trends shown in *Figure 12* (for example, curves A and E) suggest that as the concentration profile becomes flatter (i.e. the cross section of the inner tube increases from zero) departure from the original flameholding-limit curve initially increases. Evidently this departure reaches a maximum because the original flameholding-limit curve must again be reproduced when the concentration profile becomes uniform (i.e. the radii of the inner and outer tubes become equal). The failure of all of the points to fall on

the original curve (heavy line) indicates that the critical zone is not a thin region at the tip of the flame, dependent solely on the local F/A in the stream.

The question of whether a homogeneously mixed critical zone exists at the tip (or any other definite location) can be resolved by interpretation of the data represented by curves F and D in *Figure 12*. Since for a given blowout velocity, the F/A at the tip of the jet is greater when the larger inner tube is employed and the F/A at any radial position in the plane normal to the axis at the tip is likewise greater, the average concentration of fuel (burnt and unburnt) is higher in corresponding regions of the pilot flame. Furthermore, the F/A in the critical zone is estimated (by the method described in refs. 2, 3 and 8) to be rich. Therefore, increase in fuel concentration cannot itself lead to improved flameholding in a rich stream $(F/A)_{st}=0{\cdot}109$. If it can be shown that, at a constant blowout velocity (i.e. constant residence time in the critical zone), the unfavourable increase in fuel concentration is not offset by an increase in temperature, then the critical zone cannot be a homogeneous gas mixture.

An increase in F/A in the critical zone and recirculation zone (probably rich) is accompanied by a decrease in flame temperature. Furthermore, the temperature of the air jet is not expected to change significantly with increase in F/A of the main-stream fluid, because rich gases in contact with the air jet column presumably burn much as a diffusion flame (*Figure 6*), with the maximum temperature corresponding to the stoichiometric fuel concentration. Therefore, since compensating combinations of uniform temperature and uniform concentrations to yield a constant blowout velocity apparently do not exist, it is concluded that the critical zone is not a volume of homogeneously mixed reacting gases.

On the basis of sodium-D line temperature traverses, it has been suggested that the tip region is homogeneously mixed[3]. If this interpretation is correct, a non-homogeneous critical zone cannot be located in the tip region. Even if this region is at any moment not homogeneously mixed (a more likely condition in view of the present concept of rough burning), it appears improbable that a critical zone can be maintained continuously within the turbulent tip. These considerations, in addition to recent evidence obtained with flames stabilized by inert gases[9], lead to the conclusion that the critical zone is not situated in the tip region of the pilot flame. On the other hand, the suggested concept of a diffusion-type critical region bordering the recirculation zone does not appear to conflict with reported observations.

CONCLUSIONS

(*1*) A flameholding jet contains a pilot flame. The dimensions of the pilot flame are correlated for the system employed. A recirculation zone (apparently toroidal in shape) is located close to the jet column.

(*2*) Rough burning arises from the existence of non-inflammable zones in the shedding mixture which transmits flame to the ambient stream.

(*3*) Evidence is given which indicates that the concept of a homogeneously mixed critical zone in the tip of a flameholding jet is incorrect.

The existence of a thin unmixed zone at the forward stagnation point is found to be unlikely. A diffusion-type critical zone bordering the recirculation region is proposed.

The authors wish to acknowledge the sponsorship of the major portion of this programme by the Aeronautical Research Laboratory of the Wright Air Development Center [U.S.A.F. Contract No. AF 33(616)-3970]. The Stanford Research Institute supported the additional analytical work. The criticisms and suggestions offered by Drs Marjorie W. Evans, Robert H. Eustis, Anthony R. Kriebel, and others who read various portions of this manuscript are greatly appreciated.

Stanford Research Institute,
Menlo Park, California

(Received June 1958)

REFERENCES

[1] SCHAEFER, A. and CAMBEL, A. B. *Jet Propulsion*, 25 (1955) 284–287
[2] SCHAEFER, A. and CAMBEL, A. B. *Jet Propulsion*, 26 (1956) 576–578
[3] SCHAEFER, A. 'Aerothermochemical analysis of the opposing jet flameholder.' *Ph.D. Dissertation*, Northwestern University: Evanston, Ill., June 1957
[4] EUSTIS, R. H. and MRAZ, C. L. 'Investigation of jet flameholders.' *Wright Air Development Center Technical Note 56-316*, Part I, April 1956
[5] NOON, A. W. 'Investigation of jet flameholders.' *Wright Air Development Center Technical Note 56-316*, Part II, April 1957
[6] NOREEN, A. E. and MARTIN, W. T. Paper presented at the American Rocket Society 12th Annual Meeting, New York, 2 to 5 December 1957. *Paper No. 515-57*
[7] LONGWELL, J. P., FROST, E. E. and WEISS, M. A. *Industr. Engng Chem. (Industr.)* 45 (1953) 1629–1633
[8] PENNER, S. S. and WILLIAMS, F. *Appl. Mech. Rev.* 10 (1957) 229–237
[9] CAMBEL, A. B. 'A review of flame stabilization of gaseous jets.' *Selected Combustion Problems III*. Pergamon: London (in preparation)
[10] PRESCOTT, R. *Photogr. Engng* 3 (1952) 121–128
[11] NICHOLSON, H. M. and FIELD, J. P. *Third Symposium (International) on Combustion, Flames and Explosion Phenomena*, pp 44–68. Williams and Wilkins: Baltimore, 1949
[12] ZUKOSKI, E. E. and MARBLE, F. E. *Proceedings of the Gas Dynamics Symposium on Aerothermochemistry, 22–25 August 1955*, pp 205–210. Northwestern University: Evanston, Ill., 1956
[13] LEWIS, B. and VON ELBE, G. *Combustion, Flames and Explosions of Gases*, p 762. Academic Press: New York, 1951
[14] CARSLAW, H. S. and JAEGER, J. C. *Conduction of Heat in Solids*, p 178. Oxford University Press: London, 1947
[15] SHERWOOD, T. K. and PIGFORD, R. L. *Absorption and Extraction*, 2nd ed., p 44. McGraw-Hill: New York, 1952

On the Decomposition Flame of Liquid Ozone–Oxygen Mixtures in a Tube

R. SANDRI

A theory of flame propagation previously developed by the author is applied to a decomposition flame burning above a liquid ozone-oxygen mixture in a tube cooled with liquid oxygen at the outside. Neglecting heat losses to the wall, heat radiation and heat conduction along the glass tube, flame velocities are computed for pressures of 1, 2 and 10 atmospheres for mixtures containing 50, 75 and 100 per cent ozone. The results obtained for atmospheric pressure are in reasonably good agreement with the available experimental result.

THE decomposition flame of ozone is one of the simplest possible flames and is interesting also from a technological point of view. For these reasons, much experimental and theoretical investigation has been carried out in recent years which has widely clarified most aspects of the phenomenon. In particular, basic data have become available for the theoretical treatment of an experiment which presents the one-dimensional analogy to an ozone droplet 'burning'—i.e. evaporating and decomposing —in an oxygen atmosphere.

Dr A. G. STRENG, of the Research Institute of Temple University, was able to avoid detonation and to burn concentrated liquid ozone successfully in a glass tube of 9 mm diameter which was cooled by liquid oxygen at the outside. The flame was initiated above the liquid by means of a hot platinum wire. The burning velocity was determined in a preliminary manner and equalled, at atmospheric pressure and at approximately 90 per cent ozone concentration, approximately 0·4 cm/s. The flame, just above the liquid level, burned very much more intensely than the gaseous ozone flame[1, 2] primarily because of the much larger mass of ozone burning per second*.

A general theory of flame propagation has been developed by the author and has been applied to the decomposition flame of gaseous ozone–oxygen mixtures[1-6]. The results were found to be in good agreement with the experiments of B. LEWIS and G. VON ELBE[7] and A. G. STRENG and A. V. GROSSE[1, 2] and with the theoretical results of J. O. HIRSCHFELDER, C. F. CURTISS and D. E. CAMPBELL[8] and T. VON KÁRMÁN and S. S. PENNER[9, 10]. In the following, this theory is applied to the experiment described above.

Heat losses to the wall, heat radiation and heat conduction through the glass tube in a downward direction are considered negligible. Then, since no energy transport by diffusion through the surface of the liquid is possible, the heat conducted to the surface must increase the enthalpy of

*Private communication.

the substance from its initial value h_1 (enthalpy per gramme of liquid mixture at temperature of liquid oxygen, 90°K) to h_0 (gaseous mixture at surface temperature T_0). So we have

$$x_0 [\mathrm{d}T/\mathrm{d}x]^{x=0} = \rho_0 V_0 (h_0 - h_1) = \rho_1 V_1 (h_0 - h_1) \qquad \ldots . \quad [1]$$

Here, x is the coordinate parallel to the axis of the tube, x_0 is the heat conductivity of the gaseous mixture, ρ_0 is its specific mass and V_0 is the linear flame velocity in the gas at temperature T_0 while ρ_1 and V_1 are the corresponding values for the liquid.

At the hot boundary ($T = T_f$), we have

$$[\mathrm{d}T/\mathrm{d}x]^{x=\infty} = 0 \qquad \ldots . \quad [2]$$

In the theory referred to above, diffusion is accounted for indirectly by the assumption of linear decrease of ozone concentration with temperature near the hot boundary. Then, V_0 is calculated from the reduced energy equation

$$\zeta (\mathrm{d}\zeta/\mathrm{d}\eta + 1) = (1/V_0^2) F(\eta) \qquad \ldots . \quad [3]$$

where

$$\zeta = [\lambda/\rho_0 V_0 c_p (T_f - T_0)] [\mathrm{d}T/\mathrm{d}x]$$

$$\eta = (T_f - T)/(T_f - T_0)$$

$$F(\eta) = \lambda Q/\rho_0^2 c_p^2 (T_f - T_0)$$

Here, Q is the heat produced per unit of time and volume and c_p is the average heat capacity per gramme of the mixture at constant pressure. From equations 1 and 2 we then find the boundary conditions:

$$\text{for } \eta = 0 \quad (x = \infty) \qquad \zeta = 0 \qquad \ldots . \quad [2a]$$

$$\text{for } \eta = 1 \quad (x = 0) \qquad \zeta = \zeta_1 = (h_0 - h_1)/c_p (T_f - T_0) \qquad \ldots . \quad [1a]$$

In order to find V_0 without solving the differential equation 3, we integrate from $\eta = 0$ to $\eta = 1$ and obtain

$$\tfrac{1}{2}\zeta_1^2 + \int_0^1 \zeta \, \mathrm{d}\eta = (1/V_0^2) \int_0^1 F(\eta) \, \mathrm{d}\eta$$

The function $F(\eta)$ is zero in a large part of the interval and has a sharp peak for $\eta = \eta_m$. Under these circumstances, the eigenfunction ζ, which satisfies the differential equation 3 together with the boundary conditions 1a and 2a, approaches the broken line ABCD in *Figure 1*. We see that

$$\tfrac{1}{2}\zeta_1^2 + \int_0^1 \zeta \mathrm{d}\eta \doteq \tfrac{1}{2} (1 + \zeta_1 - \eta_m)^2$$

and therefore

$$V_0 \doteq [1/(1 + \zeta_1 - \eta_m)] \left[2 \int_0^1 F(\eta) \, \mathrm{d}\eta \right]^{1/2} \qquad \ldots . \quad [4]$$

This formula gives a very good approximation. In one of the numerical examples shown in *Table 1*, V_0 was determined by repeated numerical integration of equation 3 and was found to differ by only 1·5 per cent from the value obtained from equation 4.

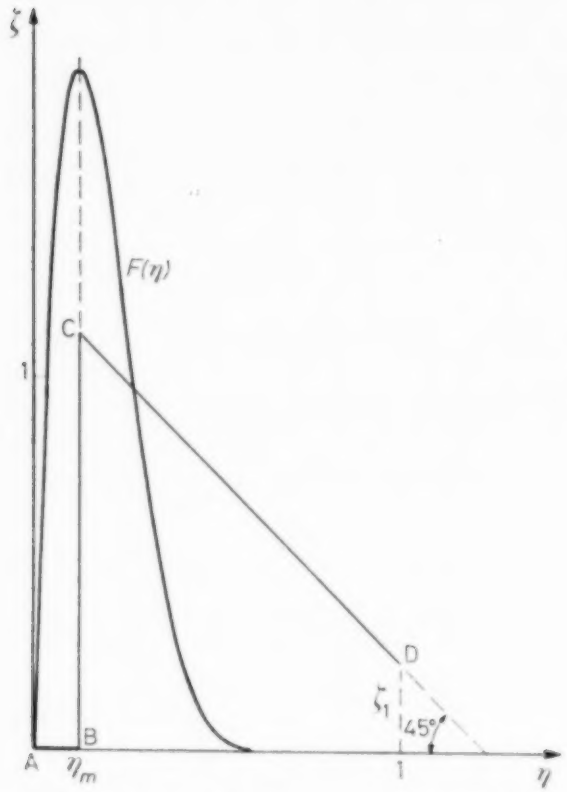

Figure 1. Solution of reduced energy equation

The value of the integral on the RHS has been determined in an earlier paper* of the author[4]

$$\int_0^1 F(\eta)\,d\eta = B\left[-(A+T_f)\,\mathrm{Ei}(-A/T_f) - \exp(-A/T_f)\right] \quad \ldots\ldots [5]$$

where $A = 12\,150^\circ$ and $B = 3{\cdot}23 \times 10^5 T_0^{\,2}(1+\zeta_1)^2/y_{30}(T_f - T_0)$.

Table 1. Flame velocities

Variable	$y_{30}=0{\cdot}50$			$y_{30}=0{\cdot}75$			$y_{30}=1{\cdot}00$		
p (atm)	1	2	10	1	2	10	1	2	10
T_s (°K)	150·5	160·5	187·5	156·5	167	198	161	172·5	206
T_f (°K)	1509	1508	1507	2029	2030	2031	2400	2414	2436
V_s (cm/s)	33·4	35·6	41·9	98·9	106	127	156	171	212
V_1 (cm/s)	0·0774	0·155	0·780	0·227	0·456	2·31	0·361	0·738	3·8

Tables of the 'exponential integral' Ei$(-x)$ are available. Further t was found

$$\eta_m = T_f^{\,2}/(A+T_f)(T_f - T_0) \quad \ldots\ldots [6]$$

Formula 5 has been derived under the simplifying assumption that

$$y_3 = y_{30}\eta$$

*The factor $(1+\zeta_1)^2$ does not appear in the paper quoted but has to be applied here because

$$34\,535 y_{30}/m_0 = c_p(T_f - T_0) + (h_0 - h_1)$$

and hence (considering equation 1a)

$$c_p = 34\,535 y_{30}/m_0(T_f - T_0)(1+\zeta_1)$$

where m_0 is the molecular weight of the unburnt mixture.

where y_3 is the relative concentration (molar fraction) of ozone and y_{30} is the initial value of y_3. Hence, substituting from equations 1a, 5 and 6 in 4, we obtain a first approximation V_{H0} for V_0. From this, an improved value V_0 of the flame velocity is found by means of the formula (derived in the paper quoted)

$$V_0 = \frac{V_{H0}}{1+0{\cdot}5y_{30}} \frac{\beta}{0{\cdot}94\beta - 0{\cdot}03 + 0{\cdot}06\,(\beta+0{\cdot}25)^{1/2}} \quad \ldots\ [7]$$

where

$$\beta = \frac{B\,(T_f - T_0)^2}{V_{H0}\,T_f} \exp\,(-A/T_f)$$

In this manner, values of V_0 were computed which are shown in *Table 1*. In calculating the enthalpy h_1 which is needed in equation 1a, it has been assumed that the heat of solution of liquid ozone in oxygen is zero and that no superheating occurs so that the top layer of the liquid boils at the condensation temperature T_0 of the vapour which was taken from Thorp's ozone bibliography[11]. The heat capacity of liquid ozone was assumed to be 0·45 cal/g°C*. The flame temperatures T_f were computed by thermodynamic methods, allowing for oxygen dissociation in the 'burnt' gas.

The evaporation velocity V_1 of the liquid is the velocity at which the surface of the liquid moves down. While V_0 is dependent on the pressure p only inasmuch as T_f and T_0 are dependent on it, V_1 is approximately proportional to p. For $y_{30}=0{\cdot}90$, at one atmosphere, we find by interpolation $V_1=0{\cdot}309$ cm/s which is in reasonably good agreement with the result found by Dr Streng (0·40 cm/s). The difference should be due chiefly to the fact that some heat is conducted from the flame to the liquid through the glass wall of the tube and to direct heat transfer by radiation from the flame to the liquid. Both influences tend to increase flame velocity. They have not been accounted for in the theory which deals with an idealized, purely one-dimensional process.

The author wishes to express his thanks to Dr J. W. Broughton of the National Research Council for helpful suggestions and to Dr A. V. Grosse for information on the experimental work carried out at the Research Institute of Temple University.

National Research Council of Canada,
Ottawa, Ontario

(*Received September 1958*)

REFERENCES

[1] STRENG, A. G. and GROSSE, A. V. *J. Amer. chem. Soc.* 79 (1957) 1517
[2] STRENG, A. G. and GROSSE, A. V. *Sixth Symposium (International) on Combustion*, p 264. Reinhold: New York, 1957
[3] SANDRI, R. *Canad. J. Chem.* 34 (1956) 313
[4] SANDRI, R. *Canad. J. Chem.* 34 (1956) 324
[5] SANDRI, R. *Canad. J. Chem.* 35 (1957) 474
[6] SANDRI, R. *Canad. J. Chem.* 36 (1958) 1210
[7] LEWIS, B. and VON ELBE, G. *J. chem. Phys.* 2 (1934) 283

*Private communication from Dr A. V. GROSSE, of Temple University (value found by Armour Research Foundation).

[8] HIRSCHFELDER, J. O., CURTISS, C. F. and CAMPBELL, D. E., *J. phys. Chem.* 57 (1953) 403
[9] VON KÁRMÁN, T. and PENNER, S. S. In *Selected Combustion Problems*, p 5. AGARD; Butterworths: London, 1954
[10] VON KÁRMÁN, T. *Sixth Symposium (International) on Combustion*, p 1. Reinhold: New York, 1957
[11] THORP, C. E. *Bibliography of Ozone Technology*, Vol. II, p 8. Armour Research Foundation of Illinois Institute of Technology: Chicago, 1956

Spectroscopic Studies on Temperature Gradients in Flames

R. H. TOURIN

The intensity distribution in the i.r. emission spectrum of a flame depends to a large extent on self-absorption within the flame. This self-absorption depends not only on the magnitude of the spectral absorption coefficients, but also on the temperature gradient along the optical path through the flame. Calculations were carried out to obtain estimates of the radiation contributions to the 4·3 micron emission band of carbon dioxide from zones of a flame at various temperatures, for typical temperature distributions encountered in practice. The calculations were based on Σ_u^+–Σ_g^+, Π_u–Π_g, *etc., vibrational transitions of the form* $0n^n1$–$0n^n0$ *(where* $n=0$, *1, 2 etc.), which have been shown to predominate in this spectral region, using measured emissivities of carbon dioxide. The temperature dependence of rotational energy distribution was accounted for in each vibrational transition. The calculated spectral contours were compared with measured spectra obtained with a special burner in which known temperature gradients could be set up at will. The results indicate that this technique may prove a useful tool in analysing temperature distributions within a flame.*

THE i.r. emission spectrum of a flame is affected considerably by self-absorption within the hot flame gases. At spectrum frequencies where the absorption is high, radiating zones on the far side of the flame from the measuring instrument contribute less to the observed radiation than zones nearer the detector.

Self-absorption in a flame depends largely on the temperature gradient along the optical path through the flame. Self-absorption in a flame can be analysed in terms of the distribution of the radiating molecular population among the vibrational and rotational energy states, at the temperatures in the flame temperature profile. This analysis is described in the next section of this paper. It enables us to interpret certain features of the i.r. emission spectrum of the flame in terms of the temperature profile. This is illustrated in the experimental section by an example based on experimental measurements made with a special burner in which known temperature profiles could be maintained. The measurements were made in the 4·3 micron emission band of carbon dioxide[1, 2].

Previous studies of this type are few. S. SILVERMAN[3] discussed the 4·3 micron carbon dioxide band briefly in relation to the vibrational population distribution. E. F. DALY and G. B. B. M. SUTHERLAND[4] analysed this emission, at temperatures below 700°K, in terms of the rotational distribution within the lowest excited vibrational state. The author[5] studied the emission of isothermal carbon dioxide at temperatures up to 1 273°K, and found that the 4·3 micron emission appeared to come chiefly from vibrational energy transitions of the form $0n^n1$–$0n^n0$ where $n=1$, 2, etc. This agrees with high resolution measurements at 773°K made by J. H. TAYLOR, W. S. BENEDICT, and J. STRONG[6]. In the present work, a detailed analysis

was undertaken, including vibration and rotation. It was found that a large number of vibrational levels must be included in order to interpret the emission spectrum of a flame with a strongly non-isothermal cross section.

THEORETICAL

Consider an i.r. spectrophotometer set up near a flame so that emission and absorption are measured along a common optical path through the flame. Imagine the path through the hot gas subdivided into n equal zones each isothermal, but differing in temperature, one from another. Consider frequencies $\nu_1, \nu_2, \ldots$ in the emission spectrum of the flame. At each frequency the emission is the sum of contributions from a number of vibration–rotation energy transitions, which we denote as $\omega_1, \omega_2, \ldots \omega_m$.

The emissivity at frequency ν_i of zone j, having temperature T_j, is

$$e_i(T_j) = e_i^1(T_j) + e_i^2(T_j) + \ldots + e_i^m(T_j) \qquad \ldots . [1]$$

where $e_i^k(T_j)$ is the contribution to the emissivity from the vibrational transition of frequency ω_k cm^{-1}. The components of zonal emissivity contributed by different vibrational states are additive, because there is no interaction between these states; a quantum of frequency ω_k, emitted by a molecule in the upper state of the transition corresponding to ω_k, can be absorbed only by a molecule in the lower state of the same transition.

Applying Kirchhoff's law, that emissivity equals absorptivity, and substituting emissivity for absorptivity in the Beer–Lambert absorption law, we get:

$$e_i^k(T_j) = 1 - \tau_i^k(T_j) = 1 - \exp[-\chi_i^k(T_j)] \qquad \ldots . [2]$$

where $\tau_i^k(T_j)$ is the transmittance, and $\chi_i^k(T_j)$ is proportional to the number of molecules present.

The spectral emission intensities can be written:

$$\begin{aligned} I_1 &= I_1(T_1) + I_1(T_2) + \ldots + I_1(T_n) \\ I_2 &= I_2(T_1) + I_2(T_2) + \ldots + I_2(T_n) \\ &\ldots \qquad \ldots \qquad \ldots \qquad \ldots \\ &\ldots \qquad \ldots \qquad \ldots \qquad \text{etc.} \end{aligned} \qquad \ldots . [3]$$

where I_i represents the flame emission observed at frequency ν_i, and $I_i(T_j)$ represents that portion of the energy radiated by zone j which reaches the exterior of the flame and so contributes to the observed emission. Each component $I_i(T_j)$ is given by

$$\begin{aligned} I_i(T_j) = I_i^b(T_j) \{ &[e_i^1(T_j)(1 - e_i^1\langle T_{j+1}\rangle) \ldots (1 - e_i^1\langle T_n\rangle)] \\ &+ [e_i^2(T_j)(1 - e_i^2\langle T_{j+1}\rangle) \ldots (1 - e_i^2\langle T_n\rangle)] \\ &\ldots \qquad \ldots \qquad \ldots \qquad \ldots \\ &\ldots \qquad \ldots \qquad \ldots \qquad \ldots \\ &+ [e_i^m(T_j)(1 - e_i^m\langle T_{j+1}\rangle) \ldots (1 - e_i^m\langle T_n\rangle)] \}. \end{aligned} \qquad \ldots . [4]$$

where $I_i^b(T_j)$ is the Planck blackbody function. The contributions of the vibrational transitions ω_1 to ω_m are denoted by the superscripts. In each set of square brackets $e_i^k(T_j)$ is the emissivity contribution from transition

ω_k, of zone j; $(1-e_i^k\langle T_{j+1}\rangle)$ is the transmittance contribution of zone $j+1$, adjacent zone toward the radiation-detecting instrument; $(1-e_i^k\langle T_{j+2}\rangle$ is the transmittance contribution of the next adjacent zone, etc. By the Beer–Lambert law, the product of these zonal transmittance contributions is the the transmittance contribution of the whole flame path which radiation from zone j traverses.

The emissivity contributions are calculable from equation 2, where

$$\chi_i^k(T_j)=n_0P_i^k(T_j)=n_0S(T_j)\rho_v^k(T_j)\rho_r^k(T_j,J\langle\nu_i\rangle) \quad \ldots\ldots [5]$$

The factor n_0 is proportional to the path length and to the concentration of the radiating chemical species. In this paper n_0 is assumed constant, i.e. there is no concentration gradient along the optical path.

The factors of the population function $P_i^k(T_j)$ are as follows. The factor $S(T_j)$ is the vibrational transition probability for emission. It is given by the expression (cf. L. PAULING and E. B. WILSON[7])

$$S(T_j)=A+B\sigma(\omega,T_j) \quad \ldots\ldots [6]$$

where A and B are the Einstein coefficients and $\sigma(\omega,T_j)$ is the radiation density. The remaining factors in $P_i^k(T_j)$ are the Boltzmann population factors of the upper state. For carbon dioxide, these are as follows: vibrational

$$\rho_v^k(T_j)=[g_v/Q_v(T_j)]\exp(-c_2G_0^k/T_j) \quad \ldots\ldots [7]$$

rotational

$$\rho_r^k(T_j,J\langle\nu_i\rangle)=[(2J+1)/Q_r(T_j)]\exp[-c_2B_eJ(J+1)/T_j] \quad \ldots\ldots [8]$$

In equation 7 g_v is the statistical weight for vibrational states; it equals unity for Σ vibrational states and equals two for all other vibrational states; $Q_v(T_j)$ is the vibrational partition function; G_0^k is the vibrational term value (G. HERZBERG[8]) for the upper state of transition ω_k and c_2 is the second radiation constant.

Equation 8 represents the rotational distribution function for a rigid linear molecule. The statistical weight is $2J+1$, where J is the rotational quantum number; $Q_r(T_j)$ is the rotational partition function; and $B_e=h/8\pi^2cI_e$, where I_e is the equilibrium moment of inertia of the rotating molecule. We write $J(\nu_i)$ explicitly in $\rho_r^k(T_j,J\langle\nu_i\rangle)$ because the J value for the rotational transition, within a vibrational transition ω_k, that produces a line at frequency ν_i in the observed spectrum is determined by the condition that the rotational transition frequency equals $|\nu_i-\omega_k|$. For P-branch lines

$$|\nu_i-\omega_k|=B_e[(J_{in}-1)J_{in}-J_{in}(J_{in}+1)]=2J_{in}B_e$$

so that

$$J_{in}^P=|\nu_i-\omega_k|/2B_e \quad \ldots\ldots [9]$$

Similarly, for R-branch lines

$$J_f^R=|\nu_i-\omega_k|/2B_e \quad \ldots\ldots [10]$$

where the subscripts in and f refer to the initial and final states respectively.

In applying equation 5, all the quantities but n_0 can be calculated from known molecular constants; n_0 is found as follows. The emissivity e_i

measured at frequency ν_i is the sum of contributions from a number of vibration–rotation transitions. It must be proportional to the overall sum of the initial state populations of these transitions, computed for each temperature zone, each population factor being multiplied by the appropriate transition probability. The proportionality constant is the concentration factor, n_0. The total population factor of one zone is $\sum_{k=1}^{m} P_i^k(T_j)$, and the grand total contributing to e_i must be the sum of these sums for all n zones. Summing equation 5 over k and j we get

$$\chi_i = n_0 \sum_{j=1}^{n} \sum_{k=1}^{m} P_i^k(T_j) \qquad \ldots . [11]$$

from which n_0 can be determined.

EXPERIMENTAL

As the first step in applying the above analysis, we took a case where the temperature profile was known. The measurements were obtained by G. A. HORNBECK and L. O. OLSEN[9], using the combustion facility at the National Bureau of Standards[10]. Unleaded gasoline was burned with air in a Jumo turbojet combustor. The combustor was mounted inside an Inconel pipe, eight inches in diameter. Secondary air, supplied by compressors, was mixed with the combustion products, in order to reduce the temperature of the effluent gases. The hot gas stream flowed through a twenty-foot length of Inconel pipe downstream of the burner and was discharged into an open stack.

The i.r. emission and absorption of the gas stream were observed through two sapphire windows mounted opposite one another in the twenty-foot pipe, on a horizontal line-of-sight through the gas. The measurements were made with specially adapted commercial i.r. equipment[9]. The optical path outside the hot gas stream was enclosed and flushed with dry nitrogen to minimize atmospheric absorption. The gas flow velocity was several hundred feet per second, and the mass flow about 4 lb/in^2 sec. The flow was fully turbulent. Temperature profiles were created by varying the heat transfer rates in different portions of the gas stream by means of baffle plates in the stream. Temperatures were measured with chromel–alumel thermocouples. Temperatures were read along the optical path, and the profiles plotted from these data. *Figure 1* shows the measured profiles on which the calculation was based. The detecting component of the i.r. spectrophotometer was located to the right, as indicated by the legend 'to receiver'. The optical path was divided into four equal zones and the temperatures averaged for each zone. In this way, we obtained *Figure 2*.

The emission spectra corresponding to the profiles of *Figure 1* are shown in *Figure 3*. This emission is due to vibration–rotation transitions of the carbon dioxide molecule in which the quantum number v_3 corresponding to the asymmetric stretching vibration, changes by unity. Eight transitions of this type are given in *Table 1*. The symbols in the first column are

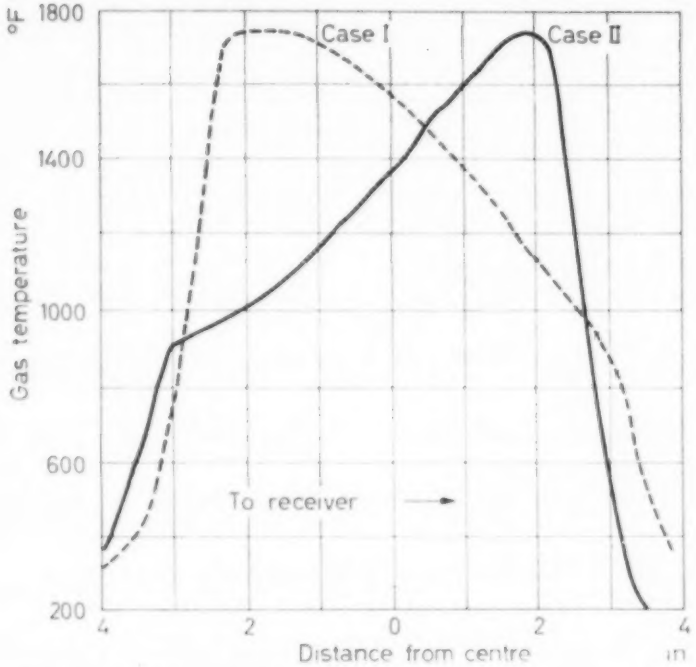

Figure 1. Asymmetric temperature profiles along the optical path

arbitrary. The last column of *Table 1* gives the frequencies of the band origins. These transitions are parallel-type; hence each band consists of a *P*-branch and an *R*-branch. These eight transitions include all those having upper state populations above 0·1 per cent at the temperatures in the profiles. It will be shown later that there are many additional transitions which contribute appreciably to the spectrum. Only eight were used in this calculation in order to keep the computation required within manageable proportions.

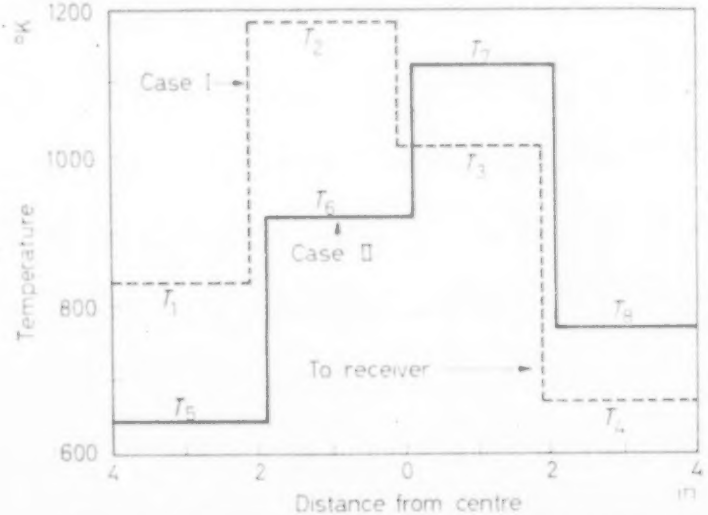

Figure 2. Averaged asymmetric temperature profiles

Table 1. Some vibrational energy transitions of carbon dioxide

Symbol	*Upper state* $v_1 v_2^l v_3$	*Lower state* $v_1 v_2^l v_3$	*Frequency* cm^{-1}
ω_1	$00^0 1$	$00^0 0$	2349
ω_2	$01^1 1$	$01^1 0$	2337
ω_3	$02^0 1$	$02^0 0$	2327
ω_4	$10^0 1$	$10^0 0$	2326
ω_5	$02^2 1$	$02^2 0$	2324
ω_6	$03^3 1$	$03^3 0$	2320
ω_7	$03^1 1$	$03^1 0$	2313
ω_8	$11^1 1$	$11^1 0$	2312

For comparison of calculated and measured spectrum data, we selected two frequencies $\nu_1 = 2\,326$ cm^{-1} and $\nu_2 = 2\,273$ cm^{-1}, corresponding to wavelengths of 4·3 and 4·4 microns respectively, in the spectra shown in *Figure 3*. The emission intensities at each frequency were calculated by the procedure described in the theoretical section.

Transition probabilities

The vibrational transition probabilities $S(T_j)$ were calculated from equation 6 using the value for A given by W. S. BENEDICT and E. K. PLYLER[11]. The dependence of $S(T_j)$ on frequency is small for the narrow frequency spread between ω_1 and ω_8. Hence $S(T_j)$ was calculated

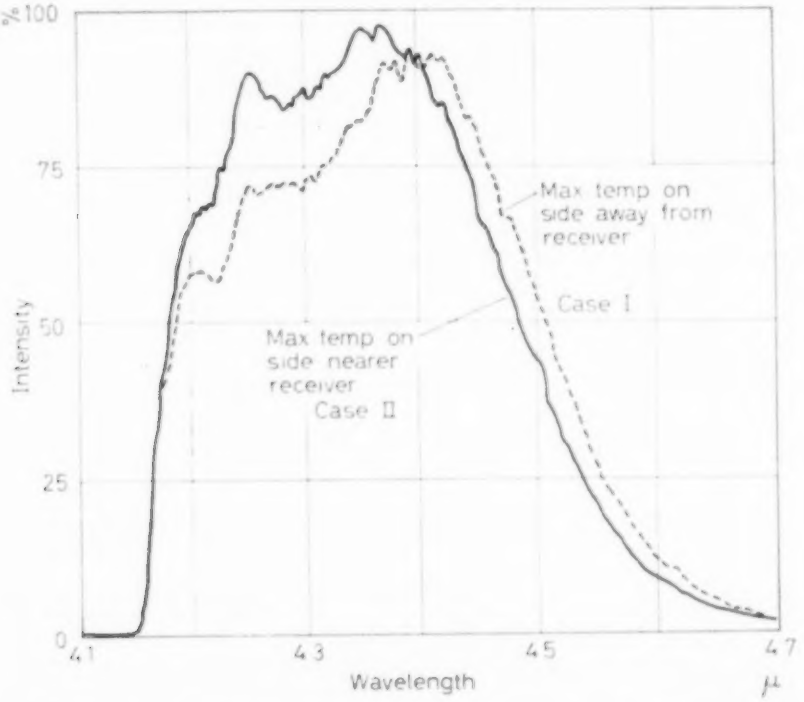

Figure 3. Emission from exhaust gases with asymmetric temperature profiles

for ω_4, and the same value used for all eight frequencies at each temperature. With this simplification, the transition probability becomes

$$S(T_j)=431\,[1+(e^{3\,345/T_j}-1)^{-1}] \qquad \ldots\ [12]$$

Vibrational population factors

The carbon dioxide vibrational population factors were previously calculated from equation 7, and plotted against temperature[3]. *Table 2* gives the complete set of vibrational population factors at the eight zonal temperatures. The vibrational energy distribution at several temperatures

Table 2. Populations of excited vibrational states

Vibrational transition	*Temperature °K*							
	643 T_5	671 T_4	769 T_8	830 T_1	922 T_6	1015 T_3	1125 T_7	1183 T_2
ω_1	0·29%	0·35%	0·59%	0·73%	0·94%	1·12%	1·33%	1·42%
ω_2	0·14	0·18	0·35	0·47	0·66	0·89	1·17	1·30
ω_3	0·032	0·043	0·093	0·15	0·235	0·345	0·49	0·57
ω_4	0·0075	0·011	0·028	0·047	0·087	0·14	0·21	0·25
ω_5	0·0178	0·0231	0·053	0·0785	0·130	0·185	0·262	0·303
ω_6	0·0089	0·0118	0·0332	0·0448	0·0930	0·149	0·232	0·291
ω_7	0·0071	0·0093	0·025	0·041	0·076	0·124	0·193	0·24
ω_8	0·0140	0·0186	0·0435	0·0673	0·107	0·156	0·233	0·274

is represented in *Figure 4*, where the relative population of each state is plotted at its frequency in cm^{-1}, measured from the ground state frequency. *Figure 4* shows that the molecular population is concentrated in the ground state at room temperature, but the population becomes redistributed more uniformly as the temperature increases. At high temperatures, there is no

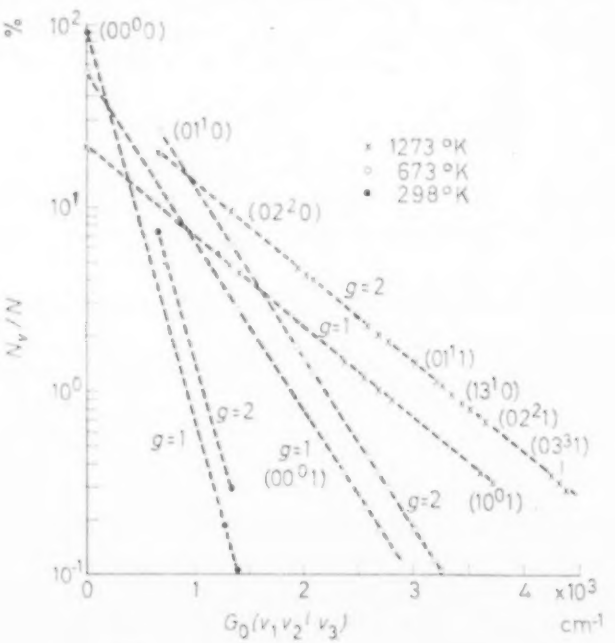

Figure 4. Vibrational energy distribution of carbon dioxide

concentration of population anywhere, but a large number of levels each have a small fraction of the population. The aggregate relative population of the upper states of the eight transitions, ω_1 to ω_8 at the lowest zone temperature, T_5 (643°K) is 0·51 per cent. At the highest zone temperature, T_2 (1 183°K), these same states have an aggregate population of 4·6 per cent.

Rotational population factors

The first step in computing values of $\rho_r^k(T_i, J\langle v_i\rangle)$ is to determine the proper J values. Substituting the value $B_e = 0{\cdot}391$ cm^{-1} for carbon dioxide into equations 9 and 10 we get:

$$J_i^R = J_m^P = 1{\cdot}28m|\nu_i - \omega_k| \quad \ldots\ [13]$$

where $m = -1$ for the P branch and $m = +1$ for the R branch. To be strictly correct, we should choose the J values in accordance with the vibrational symmetry species. Alternate rotational energy levels are missing in the Σ vibrational states of carbon dioxide, and only half as many rotational levels occur in the other vibrational states compared to the number that would be expected from the l-doubling. Neglect of these considerations may cause, at most, an error of one unit in any J value, and this can have only a negligible effect on the value of the rotational population factor. Further discussion may be found in Herzberg's books[5, 12].

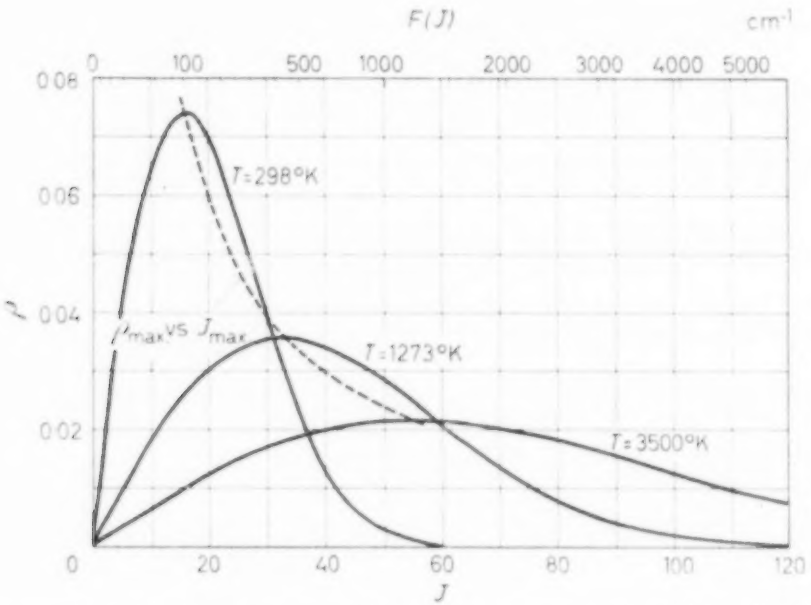

Figure 5. Rotational energy distribution function of carbon dioxide

The rotational distribution function, given by equation 8, is plotted in *Figure 5*. The spacing of the rotational levels is very close compared to the scale of the diagram, and the curves are plotted as continuous lines, although only the values at integral values of J have physical significance.

Molecular concentration factor

According to equation 11, the molecular concentration factor n_0 may be determined from a measurement of emissivity e_i at any spectral frequency ν_i, and the total relative population in the optical path. Computations of n_0 obtained from different frequencies should give the same result. This principle was applied in calculating n_0 from the Case I and Case II profiles for $\nu_2 = 2\,273\ \text{cm}^{-1}$. The results are summarized in *Table 3*. Values of n_0

Table 3. Determination of n_0

Frequency	*Profile*	*Measured emissivity*	X_i	P_i	$n_0 = \frac{X_i}{P_i}$	*Calculated emissivity*
ν_1	I	0·999	—	126	—	0·798
ν_1	II	0·988	—	106	—	0·741
ν_2	I	0·822	0·410	0·324	1·27	0·822
ν_2	II	0·786	0·496	0·228	2·18	0·257

cannot be calculated from the ν_1 data because the emissivities there are so close to unity that the exponent explodes towards $-\infty$ and cannot be determined accurately. The calculated emissivities in the last column of *Table 3* were obtained by assuming the value $n_0 = 1{\cdot}27$, calculated for Case I at ν_2, to be correct, and determining the other three values of e_i from equation 2. The two calculated values of n_0 agree as to order of magnitude. To get a better value of n_0, it would be necessary to take many vibrational states into account. This is discussed further below. We adopted the value $n_0 = 1{\cdot}72$, the average of the two values in *Table 3*.

Calculated intensities

Substituting the calculated values of n_0, $S(T_j)$, $p_i^k(T_j)$, and $p_i^k(T_j, J\langle\nu_i\rangle)$ into equation 5, and then substituting the results into equation 2, we get the emissivity contributions for equation 4. Upon substitution of these into equation 4, we get the effective zonal intensities, including self-absorption. These values are summarized in *Table 4*. The blackbody intensities $I_i^b(T_j)$ were read from a Thornton blackbody slide rule. The calculated effective zonal intensities of *Table 4* are in units of watt per unit area of radiating surface, per cm of spectral wavelength interval. The experimental values were measured as scale deflections in cm on *Figure 3*.

Substituting the values of $I_i(T_j)$ from *Table 4* into equation 3 we obtain the spectral emission intensities. The calculated and experimental spectral emission intensities are compared in *Table 5*. For comparison purposes the intensities have been normalized to unity for Case I profile at ν_1.

DISCUSSION

The normalized intensities in *Table 5* show good agreement as to order of magnitude between the calculated and measured values. This is as much as could be expected, in view of the small number of vibrational states included in the calculation, and the simplified zone subdivision used.

Table 4 indicates that the emission on the low frequency wing of the 4·3 micron band comes predominantly from high temperature zones in the profile, and *Figures 4* and *5* show that this emission is contributed largely by low *J*-value rotational transitions in vibrational transitions from highly excited vibrational states. There is a tendency to disregard contributions of highly excited vibrational states to i.r. emission spectra on the grounds that the relative populations of these states are negligible. However, it is necessary to be very cautious in discarding these 'negligible' quantities. In the first place, *Figure 4* shows that, as higher temperatures are approached, all the

Table 4. Effective zonal emission intensities

Temperature °K T_j	*Blackbody intensity* $I_i^b(T_j)$	*Effective zonal emissivity* $e_i^{eff}(T_j)$	*Effective zonal intensity* $I_i(T_j)$
(*a*) at 2326 cm^{-1} (ν_1):			
830	4560	0·210	958
1183	15800	0·575	9085
1015	9660	0·553	5344
671	1750	0·196	343
643	1400	0·0802	112
922	6910	0·327	2259
1125	13500	0·622	8397
769	3310	0·316	1046
(*b*) at 2273 cm^{-1} (ν_2):			
830	4460	0·0420	187
1183	15100	0·337	5089
1015	9290	0·159	1477
671	1740	0·0073	12·7
643	1410	0·00517	7·3
922	6710	0·174	1168
1125	12900	0·272	3509
769	3250	0·0244	79·3

individual state populations become negligible compared to unity, but the sum of many such small quantities can be appreciable. Secondly, the effect of rotation must be taken into account. For the lower, more populous vibrational states the product $\rho_{v_i}^b(T_j)\,\rho_r^b(T_j, J\langle v_i\rangle)$ is small at spectrum frequencies away from the fundamental, because of the high *J* value, which makes $\rho_r^b(T_j, J\langle v_i\rangle)$ very small. As an extreme example,

Table 5. Calculated and experimental intensities

Profile	*Frequency*	*Normalized intensities* *Calculated*	*Observed*
I	ν_1	1·0	1·0
II	ν_1	0·75	1·2
I	ν_2	0·43	1·3
II	ν_2	0·30	1·3

when the above treatment is followed through for a much lower frequency, $\nu_4 = 2\,174\ cm^{-1}$, using the same eight transitions as before, we find that the calculated emission is only 2×10^{-5} times its value at $\nu_3 = 2\,222\ cm^{-1}$, while the observed ratio is about 0·5. The reason for this discrepancy is that at the low frequency end of the band, the J values in the transitions ω_1 to ω_8 are very large and consequently the values of $p_r^k(T_j, J\langle\nu_i\rangle)$ are extremely small. *Table 6* shows the effect of high J values on the overall population at one temperature. As we go from ω_1 to ω_8, the vibrational population declines by a factor of 0·056, but the rotational population increases by

Table 6. Population factors at 2173 cm⁻¹

State $v_1 v_2^l v_3$	*Vibrational factor* $p_v^k\ (T = 830°K)$	*Rotational level* J	*Rotational factor* $p_r^k\ (830°K,\ J)$	*Population factor* $p_v^k\ p_r^k$
$00^0 1$	0·0073	225	$0{\cdot}660 \times 10^{-13}$	$0{\cdot}00224 \times 10^{-12}$
$01^1 1$	0·0047	210	$0{\cdot}518 \times 10^{-13}$	$0{\cdot}113 \times 10^{-12}$
$02^0 1$	0·000785	197	$0{\cdot}177 \times 10^{-11}$	$0{\cdot}646 \times 10^{-12}$
$10^0 1$	0·000673	196	$0{\cdot}229 \times 10^{-11}$	$0{\cdot}717 \times 10^{-12}$
$02^2 1$	0·0015	193	$0{\cdot}500 \times 10^{-11}$	$3{\cdot}49 \times 10^{-12}$
$03^1 1$	0·00047	188	$0{\cdot}178 \times 10^{-11}$	$3{\cdot}90 \times 10^{-12}$
$03^1 1$	0·000448	180	$0{\cdot}125 \times 10^{-9}$	$26{\cdot}0 \times 10^{-12}$
$11^1 1$	0·00041	178	$0{\cdot}202 \times 10^{-9}$	$38{\cdot}6 \times 10^{-12}$

3×10^3, because of the decrease in J value. The overall effect is an increase in population by $1{\cdot}7 \times 10^4$. Hence the low frequency wing of the emission band must come from low J lines of more highly excited vibrational states. If an adequate number of vibrational transitions is taken into account, it should be possible to predict the spectral intensity distribution within an uncertainty of a few per cent, and by working backward from an observed spectrum to determine an unknown temperature profile.

The analysis in this paper was developed to gain insight into the effect of temperature gradients on the i.r. emission spectra of flames. The procedure is somewhat cumbersome for practical flame studies, although the work can be speeded up by the use of computors. Recent studies by G. A. HORNBECK[13] indicate that a much simpler procedure is possible through the aid of some empirical relationships, and the profile may be determined from a simple set of linear algebraic equations, or from prepared charts.

The author is indebted to George A. Hornbeck, for the experimental data upon which this work was based, and for many stimulating discussions. The vibrational and rotational population factors were computed by Paul M. Henry. This research was supported in part by the U.S. Air Force, through the Geophysics Research Directorate, Bedford, Mass.

Warner & Swasey Research Corpn,
New York, N.Y.

(Received September 1958)

REFERENCES

[1] ELLIS, J. W. *Phys. Rev.* 26 (1925) 469
[2] PLYLER, E. K. *J. Res. nat. Bur. Stand.* 40 (1948) 113
[3] SILVERMAN, S. *J. opt. Soc. Amer.* 39 (1949) 275
[4] DALY, E. F. and SUTHERLAND, G. B. B. M. *Third Symposium (International) on Combustion, Flames and Explosion Phenomena*, p 530. Williams and Wilkins: Baltimore, 1949
[5] TOURIN, R. H. *Symposium on Molecular Structure and Spectra*, Paper No. E1, Ohio State University, 1957
[6] TAYLOR, J. H., BENEDICT, W. S. and STRONG, J. *J. chem. Phys.* 20 (1952) 1884
[7] PAULING, L. and WILSON, E. B. *Introduction to Quantum Mechanics*. McGraw-Hill: New York, 1935
[8] HERZBERG, G. *Infrared and Raman Spectra of Polyatomic Molecules*. Van Nostrand: New York, 1945
[9] HORNBECK, G. A. and OLSEN, L. O. *W.A.D.C. tech. Rep. No. 57-516*. Dayton, Ohio, 1957
[10] *Misc. Publ. nat. Bur. Stand.* 198 (1949) 4 and 18
[11] BENEDICT, W. S. and PLYLER, E. K. *Circ. U.S. Bur. Stand. No. 523* (1954) 57
[12] HERZBERG, G. *Spectra of Diatomic Molecules*, 2nd ed. Van Nostrand: New York, 1950
[13] HORNBECK, G. A. Private communication, 1957

Speed of Flame in Slowly Moving Clouds of Cork Dust

R. H. ESSENHIGH and D. W. WOODHEAD

Flame speeds in cork-dust clouds falling freely in a vertical tube 17 ft long, and either 2 or 3 in. in diameter, were measured as a function of the dust concentration by a photographic method. At the top of the tube, cork dust of two levels of fineness was delivered by a mechanical feeder; except for the dust chute the top was closed, and the bottom could be closed or open as desired. With ignition at the bottom when open the flame travelled up the tube at a constant speed in the approximate range of 40 to 100 cm/sec. The lower limit of inflammability, and the flame speed at that limit, were both found to be independent of dust fineness and of tube diameter within the ranges examined. The flame speed increased with dust concentration up to a maximum whose value increased with fineness and tube diameter. The concentration that gave the maximum flame speed was, for the coarser dust sample, about four times that of the estimated stoichiometric, and for the dust sample with fines, about seven times. The flame length was found to vary linearly with the burning time.

Observations were also made of: (i) a flame propagation downwards, also in 'open-to-closed' conditions, that was found to be steady and often to move even more slowly than the falling dust (about 45 cm/sec), and (ii) a more rapid explosion flame ('closed-to-open' conditions) in both upward and downward directions. The latter flame accelerated rapidly, usually to above 2 m/sec, and tended to be oscillatory.

OF more than 200 industrial dusts, including organic materials (both natural and synthetic) and metals, that have been reported[1] as having been tested for inflammability, more than three quarters were found to be either mildly or dangerously explosive. As modern manufacturing methods have increased the production of dusts, either as a stage in manufacture or as a waste product, so also has the industrial explosion hazard increased.

Because of this increasing hazard, research on the prevention and suppression of dust explosions[2–5] in industry is in progress at the Safety in Mines Research Establishment on behalf of H.M. Factory Inspectorate. The chief obstacle hampering the development of suitable precautionary measures has been found to be a lack of data on the characteristics of flames in dust clouds; quantitative information on the speed of inflammation is particularly sparse. Only three investigations of stationary flames have been reported[6–8] in which flame speed was measured at different dust concentrations; of investigations of moving flames (the more important from the practical point of view of industrial dust explosions) seven papers have been found [3, 7, 9–13] but recording only few values of speed of flame.

The counterparts of flames in gases, as propagated in various conditions, are found also in dust clouds, and thus fall into three groups: (*1*) stationary flames in moving clouds, as in a pulverized fuel furnace; (*2*) moving flames in stationary clouds (to be termed 'steady propagation flames'); and (*3*) explosion flames, moving flames in moving clouds. Industrial fuels for

REFERENCES

[1] ELLIS, J. W. *Phys. Rev.* 26 (1925) 469
[2] PLYLER, E. K. *J. Res. nat. Bur. Stand.* 40 (1948) 113
[3] SILVERMAN, S. *J. opt. Soc. Amer.* 39 (1949) 275
[4] DALY, E. F. and SUTHERLAND, G. B. B. M. *Third Symposium (International) on Combustion, Flames and Explosion Phenomena*, p 530. Williams and Wilkins: Baltimore, 1949
[5] TOURIN, R. H. *Symposium on Molecular Structure and Spectra*, Paper No. E1. Ohio State University, 1957
[6] TAYLOR, J. H., BENEDICT, W. S. and STRONG, J. *J. chem. Phys.* 20 (1952) 1884
[7] PAULING, L. and WILSON, E. B. *Introduction to Quantum Mechanics*. McGraw-Hill: New York, 1935
[8] HERZBERG, G. *Infrared and Raman Spectra of Polyatomic Molecules*. Van Nostrand: New York, 1945
[9] HORNBECK, G. A. and OLSEN, L. O. *W.A.D.C. tech. Rep. No. 57-516*. Dayton, Ohio, 1957
[10] *Misc. Publ. nat. Bur. Stand.* 198 (1949) 4 and 18
[11] BENEDICT, W. S. and PLYLER, E. K. *Circ. U.S. Bur. Stand. No. 523* (1954) 57
[12] HERZBERG, G. *Spectra of Diatomic Molecules*, 2nd ed. Van Nostrand: New York, 1950
[13] HORNBECK, G. A. Private communication, 1957

Speed of Flame in Slowly Moving Clouds of Cork Dust

R. H. ESSENHIGH and D. W. WOODHEAD

Flame speeds in cork-dust clouds falling freely in a vertical tube 17 ft long, and either 2 or 3 in. in diameter, were measured as a function of the dust concentration by a photographic method. At the top of the tube, cork dust of two levels of fineness was delivered by a mechanical feeder; except for the dust chute the top was closed, and the bottom could be closed or open as desired. With ignition at the bottom when open the flame travelled up the tube at a constant speed in the approximate range of 40 to 100 cm/sec. The lower limit of inflammability, and the flame speed at that limit, were both found to be independent of dust fineness and of tube diameter within the ranges examined. The flame speed increased with dust concentration up to a maximum whose value increased with fineness and tube diameter. The concentration that gave the maximum flame speed was, for the coarser dust sample, about four times that of the estimated stoichiometric, and for the dust sample with fines, about seven times. The flame length was found to vary linearly with the burning time.

Observations were also made of: (i) *a flame propagation downwards, also in 'open-to-closed' conditions, that was found to be steady and often to move even more slowly than the falling dust (about 45 cm/sec), and* (ii) *a more rapid explosion flame ('closed-to-open' conditions) in both upward and downward directions. The latter flame accelerated rapidly, usually to above 2 m/sec, and tended to be oscillatory.*

Of more than 200 industrial dusts, including organic materials (both natural and synthetic) and metals, that have been reported[1] as having been tested for inflammability, more than three quarters were found to be either mildly or dangerously explosive. As modern manufacturing methods have increased the production of dusts, either as a stage in manufacture or as a waste product, so also has the industrial explosion hazard increased.

Because of this increasing hazard, research on the prevention and suppression of dust explosions[2–5] in industry is in progress at the Safety in Mines Research Establishment on behalf of H.M. Factory Inspectorate. The chief obstacle hampering the development of suitable precautionary measures has been found to be a lack of data on the characteristics of flames in dust clouds; quantitative information on the speed of inflammation is particularly sparse. Only three investigations of stationary flames have been reported[6–8] in which flame speed was measured at different dust concentrations; of investigations of moving flames (the more important from the practical point of view of industrial dust explosions) seven papers have been found [3, 7, 9–13] but recording only few values of speed of flame.

The counterparts of flames in gases, as propagated in various conditions, are found also in dust clouds, and thus fall into three groups: (*1*) stationary flames in moving clouds, as in a pulverized fuel furnace; (2) moving flames in stationary clouds (to be termed 'steady propagation flames'); and (3) explosion flames, moving flames in moving clouds. Industrial fuels for

stationary flames (type 1) are generally limited to coal and peat, but explosion flames (type 3) can involve also a wide variety of other industrial materials. Much of the earlier work was carried out in explosion tubes with one end open and with the source of ignition at the closed end. Such 'closed-end ignition' conditions invariably cause a rapid explosion flame (type 3); the pressure generated in the hot combustion products is relieved by expansion, thus setting into motion the unburnt dust cloud ahead of the flame. Furthermore, as this motion usually becomes rapid, it is then difficult to measure either the burning velocity relative to the dust cloud or the dust concentration. Although such a system most nearly simulates what happens in practice, flame speed measurements require, in the first instance, a system such that the propagation of the flame causes the minimum disturbance to the unburnt cloud ahead of the flame. This problem first occurred during gas explosion investigations, and it was solved for those systems by the simple expedient of igniting the gas mixture at the *open* end of a horizontal tube, so that expansion occurs in the opposite direction to that of travel of the flame ('open-to-closed' propagation giving the well known 'uniform movement' of flame). There are difficulties in applying this system to dusts as, strictly speaking, a stationary dust cloud cannot exist. The chief reason for the sparseness of the data on flame speeds is undoubtedly the difficulties of experiment, in particular, that of obtaining a uniform and controllable dust cloud. However, a dust cloud falling under gravity in still air, which is the nearest practical approach to the ideal, is a reasonably good approximation, and this has now been achieved by delivering dust continuously at a known rate into the top of a vertical tube from a mechanical feeder[14]. This system is a development of that of E. JONES and A. G. WHITE[13], whose vertical tube was surmounted by a carrier of gauze that was charged with dust and caused to vibrate.

In the present paper, therefore, we report observations of flame speeds in clouds of cork dust which, chosen as a representative industrial dust having the additional properties of high inflammability and high dispersability, was dispersed in the above vertical tube system. With such a controllable system it has also been possible to discern appreciable detail of flame characteristics and structure not previously reported. For comparative purposes some measurements were first carried out with rapid explosion flames. In the subsequent and more detailed experiments on the slowly moving dust clouds, the chief dependent variable investigated was flame speed in relation to the dust concentration; three sets of such measurements were made, at two levels of fineness and two diameters of the vertical flame tube. These results have indicated the influence of (*i*) fineness, for a given flame tube diameter, and (*ii*) flame tube diameter, at a single fineness.

EXPERIMENTAL METHOD

Apparatus

The vertical tube apparatus is shown diagrammatically in *Figure 1*. Full details of the construction and calibration of the system were given in a previous report[14]; it consisted essentially of a vertical tube of Pyrex glass about 17 ft long and either 2 or 3 in. in diameter, into the top of which

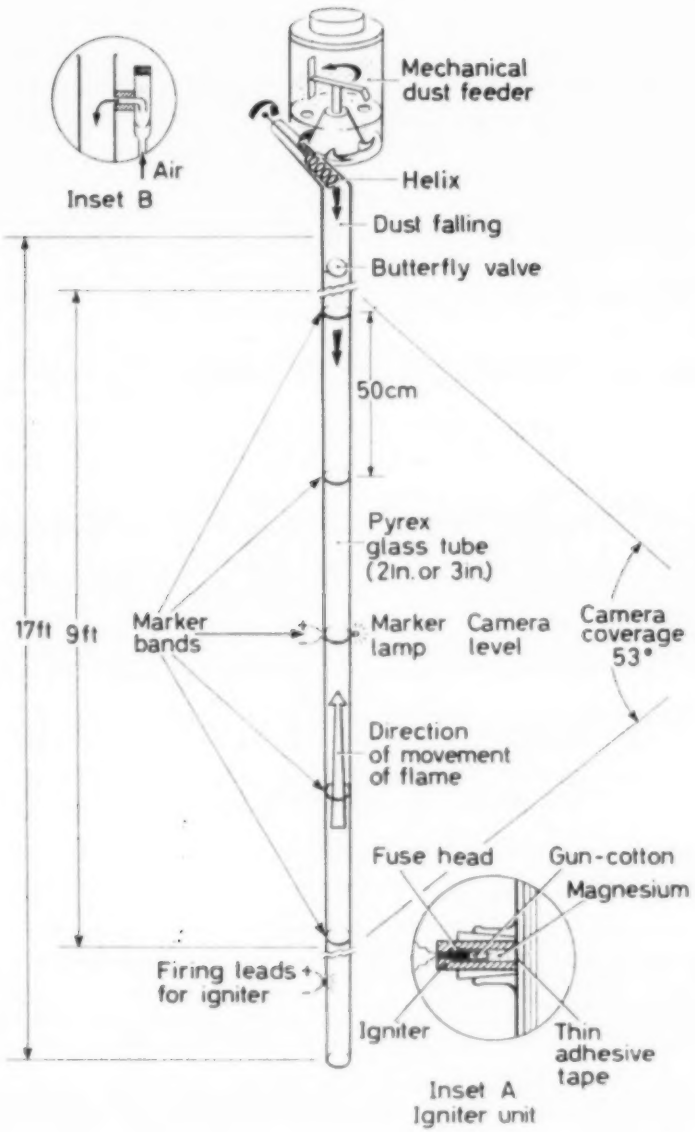

(Crown Copyright: S.M.R.E.)

Figure 1. Dust feeder and flame tube

the dust was delivered continuously from a feeder at a known rate. The cork dust was found to disperse satisfactorily in this system and to form in the tube a cloud of reasonably uniform density falling with a uniform terminal velocity (V_c) that has been shown[14] theoretically and experimentally to vary with the concentration (D) according to the relation

$$V_c = K_0 . D^m \qquad \ldots . [1]$$

where K_0 and m were empirical constants determined experimentally; their values (see *Table 1*) varied with tube diameter and dust fineness.

The dust cloud concentration was measured, after establishing steady state conditions in the system, by simultaneously closing valves at the top and the bottom of the tube and then weighing the settled dust. The cloud may be considered to behave as a continuous moving porous piston whose

action, in accordance with Darcy's equation, was to reduce the pressure at the top of the tube slightly below atmospheric pressure. Measurement of the pressure drop confirmed a derived prediction that this was proportional to the cloud concentration; further measurements, in showing a linear variation of pressure up the tube, indicated that the dust cloud distribution was reasonably uniform. This was subsequently confirmed in the flame speed experiments, reported below, by the uniformity in the flame speed observed in the steady propagation tests. The relation between pressure drop and cloud concentration was used in calibrating the system.

Table 1. Dust characteristics

		Cumulative fraction of dust sample, per cent		
		C	*D*	*E*
(1) Sieve size				
Sieve: B.S.	*Size: micron*			
Through 240 *mesh*	66	32	0	0
Through 120 *mesh*	124	42	5	8
Through 60 *mesh*	251	81	48	45
Through 30 *mesh*	500	100	100	100
(2) Constants (equation 1)				
c.g.s. units				
K_u		96	40	17
m		0·14	0	−0·10

For the flame speed experiments, the lower valve was removed, but the upper (butterfly) valve was retained (see *Figure 1*) to shield the dust feeder from flame. To ignite the dust several devices were tried, such as an electrically heated coil, a single spark, a continuous spark, a blackpowder fuse and other powder flashes of various types. Since preliminary tests indicated that the speed of the steady propagation flames was independent of the method of ignition, the igniter adopted for the majority of the experiments was the magnesium powder flash illustrated in *Figure 1* (inset A); the electrically fired fuse head ignited the short length of guncotton yarn, and this in turn ignited the stemming of magnesium powder. This igniting device was effective and consistent.

Figure 1 also shows (inset B) an alternative method of dust feed used in the preliminary explosion tests with closed-end ignition at the bottom of the tube; the dust feeder would have obstructed the expanding dust cloud. The dust, resting on a fine-mesh sieve in the side tube shown, was carried into the main tube on a steady air stream.

Methods of measurement

The moving flames in the vertical tube were recorded photographically with a revolving-drum camera which covered roughly a central 9 ft length of the flame tube. The camera was of conventional design in which a moving image was recorded on a moving paper to generate a distance/time trace as in *Figures 2*, *3*(a) and (b), and *4*. The lens was a Dallmeyer Super-

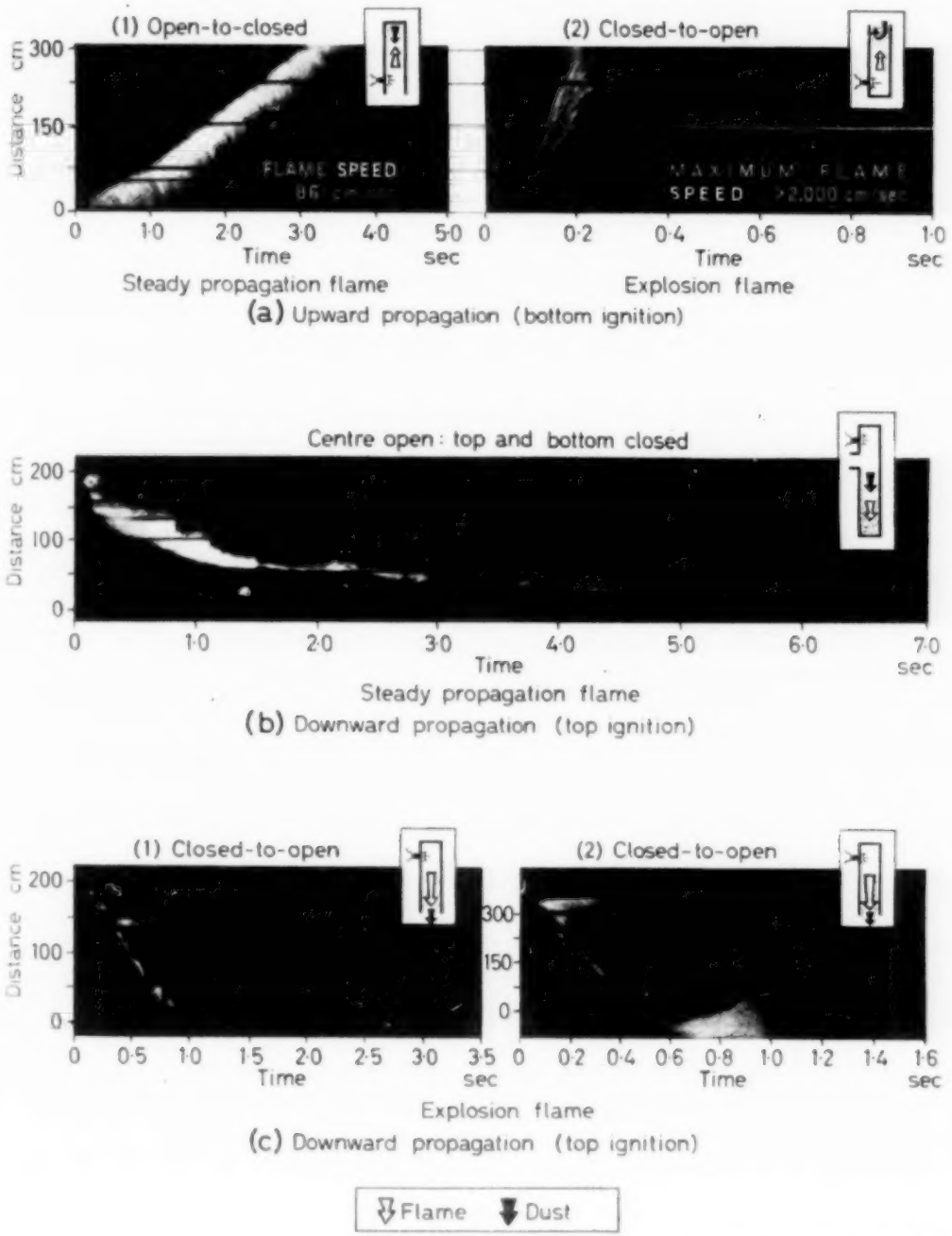

(Crown Copyright: S.M.R.E.)

Figure 2. Flame speed traces. Steady propagation and explosion flames (types 2 and 3). Upward and downward propagation

ix (*f* 1·9) of 7·6 cm focal length and a cover-angle of 53°. The camera drum, 9·2 cm wide and 40 cm circumference, carried Ilford B.P.1 (a high-contrast recording paper); the drum was mounted with its axis vertical so that the motions of the flame image and the recording paper were at right angles to each other. The peripheral drum speed was either 3 or 4·5 cm/sec according to the speed of the flame: these data provided the time base.

For the vertical distance calibrations, five marker bands of black adhesive tape were attached to the flame tube at 50 cm intervals (see *Figure 1*); these appeared on the records as black bands across the flame trace. The central band of tape carried a pea lamp as a marker to give a horizontal baseline on the record independently of the edge of the recording paper. This was necessary in case the paper was squint on the drum.

Dust characteristics

The cork dust was divided into five samples labelled A to E. All five were used in the initial investigation[14] of the physical behaviour of the dust cloud, but only the last three (C, D and E) were used in the present inflammation experiments. For consistency between the two parts of the investigation this nomenclature is retained. Samples D and E were nominally the same and differed from sample C by the removal of their fines through an 80-mesh sieve. Samples C and D were inflamed in the 3 in. tube and sample E in the 2 in. tube. Their fineness characteristics are given in *Table 1*.

The mean percentage results of an ultimate chemical analysis of the cork dust were C : 60·5, H : 7·1, and O : 32·4, giving an approximate empirical formula $C_2H_2O_2$. Since the ash and moisture contents were 3·2 and 3·8 per cent respectively, the corresponding stoichiometric concentrations of the dry ash-free and of the 'as received' materials were 0·14 and 0·15 g/l.*.

GENERAL BEHAVIOUR OF MOVING FLAMES

Flame speed

In the vertical tube system described, both steady propagation flames (type 2, open-end ignition) and explosion flames (type 3, closed-end ignition) were obtained, giving 'open-to-closed' and 'closed-to-open' propagation respectively. With a vertical tube system there are additionally two variants of each of these, namely upward and downward propagation. *Figure 2* shows the typical flame speed traces recorded by the revolving-drum camera for both variants of both types of flame. The diagram attached to each trace indicates the closed end, the position of the ignition source, the direction of travel of the flame (white arrow), and the motion of the dust cloud (black arrow).

The two traces in *Figure 2*(a) show the differences between the steady propagation flame and the explosion flame when both are in upward propagation. The striking difference in speed by a factor of more than 20 (86 cm/sec and above 2 000 cm/sec respectively) emphasizes the effect of thermal expansion in the latter case, though turbulence in the explosion flame might accelerate the reaction and hence the flame speed. This opinion was expressed by H. M. CASSEL *et al.*[7] in discussing their results with aluminium dust.

*The value of the stoichiometric concentration was given previously as 0·25 g/l. (*Report of the Fire Research Board 1953*); this was calculated on the assumption that cork approximated to a pectin or a pentosan (both carbohydrates), the ultimate analysis given above not then being available. Suberic materials, however, are not of definite or constant chemical composition, but vary with location and age; I. RIBAS-MARQUES[15] (quoting findings of Fierz-David and Ulrich) describes cork as 'a wood, that is, a mixture of cellulose and lignin, impregnated with wax and polymerized fatty acids'.

In downward propagation the explosion flame [*Figure 2*(c)] is again about 20 times or more faster than the steady propagation flame [*Figure 2*(b)], though in both cases the speeds are lower than the same type in upward propagation. This suggests that, if propagation is primarily a thermal phenomenon, then it is significantly aided in upward propagation by convection.

The orders of magnitude of the results obtained in these preliminary experiments are shown in *Table 2* where the results are compared with those obtained with other materials by other investigators. F. KISLIG's results[9] have been classified as upward explosion flames; although he claimed that his flames were in slowly moving clouds, he actually used central ignition and recorded (with a cine camera) the flame as it moved with the cloud to the open end of the tube. The data on speeds of stationary flames in coal given by A. DE GREY[20], and widely reproduced[21–28], have not been included as these were claimed as based on the dozen or so experimental values obtained by J. TAFFANEL and A. DURR for a single coal[6]. Although de Grey's curves may be qualitatively correct, quantitatively they should be treated with reserve[29]. The comparatively high explosion speeds in horizontal propagation can probably be ascribed to the large scale of all those experiments.

Flame characteristics

In addition to the manifest characteristics of the flame traces of *Figure 2* (for example, the constant speed of the steady propagation flame and the variable speed of the explosion flame), there are several individual features of interest.

(*i*) In the steady downward propagation flame [*Figure 2*(b)] the final flame speed was about 12 cm/sec relative to the tube. As the terminal velocity of the cloud was of the order of 40 to 50 cm/sec the dust was therefore moving downwards faster than the flame, and it must also have been falling counterflow to the combustion products. As the fresh oxygen was supplied from below, this presents the unusual circumstances of a moving flame that is being supplied by fuel and by oxygen from opposite sides.

(*ii*) The first of the two downward explosion flames in *Figure 2*(c) shows one that towards the end of its travel became oscillatory. This has been reported previously by Cassel *et al.*[7] though they found it in steady downward propagation flames in aluminium dust clouds and not in their explosion flames. Oscillations in the latter are a result either of cooling or of a pressure relief behind the flame front. The pulsation observed in the large-scale horizontal explosion galleries used for testing the inflammability of coal dust and stone dust mixtures[30] may be associated with cooling behind the flame front, though the effect may be concerned also with the pressure waves that travel up and down the gallery by alternate reflection from each end[31]. Another phenomenon also reported to occur in a very long gallery (for example, in a coalmine roadway) was a spasmodic progress of the flame. This has been attributed[32] to a process by which the flame blast, growing excessively intense, picked up too much dust and

Table 2. Values of flame speed

Flame type	*Investigator*	*Fuel*	*Speed range m/sec*
1. Stationary (*moving cloud*)	TAFFANEL *and* DURR[6]	*Coal*	7 *to* 16
	CASSEL *et al.*[7]	*Aluminium*	*About* 0·21*
	LONG[8]	*Coal*	0·04 *to* 0·28*
	BURGOYNE *and* LONG[17]	*Coal*	0·03 *to* 0·1*
	HATTORI[18]	*Coal*	0·1 *to* 0·5*
	GHOSH *et al.*[19]	*Coal*	0·6 *to* 1·2*
2. Steady propagation (*'stationary' cloud*)			
(i) *Upward*	ESSENHIGH *and* WOODHEAD	*Cork*	0·35 *to* 1·1
(ii) *Downward*	CASSEL *et al.*[7]	*Aluminium*	*Up to* 1·0
	ESSENHIGH *and* WOODHEAD	*Cork*	0·12
3. Explosion (*moving cloud*)			
(i) *Upward*	CASSEL *et al.*[7]	*Aluminium*	100 *to* 150 (*1-in. tube*) 5 *to* 10 (*2-in. tube*)
	KISLIG[9]	*Aluminium* *Lignin*	7 *to* 16 2
	ESSENHIGH *and* WOODHEAD	*Cork*	20
(ii) *Downward*	ESSENHIGH *and* WOODHEAD	*Cork*	2·7 *and* 8
(iii) *Horizontal*	MASON[16]	*Coal*	250 *and* 520
	RICE *et al.*[11]	*Coal*	1 400
	BROWN[3]	*Cork*	330
	HARTMANN[12]	*Cork*	370
		Aluminium, magnesium	1 070
	BROWN *and* WILLIAMS[13]	*Aluminium*	330

*Burning velocity

so caused the flame to choke; then, with the intensity of the blast from the choked flame reduced, dust fell out of suspension and allowed the flame to resume its course. This explanation of flame oscillation may be valid at high concentrations close to the upper limit or when the incombustible content of a particular dust is high, for instance owing to the presence of stone dust. (Unlike mixtures of a combustible gas with air, the oxygen content of a dust cloud is sensibly independent of the combustible content; that is, the calorific value of a cloud remains constant once the stoichiometric concentration has been exceeded.)

(*iii*) Another type of flame examined (but not photographed) was that produced by central ignition (as used by Kislig[9]) but with both ends of the tube open wherein two flames travelled in opposite directions away from the point of ignition. If the dust cloud was initially moving at a high enough speed, both flames could actually be carried downstream from the point of ignition. The two flame speeds relative to the tube would be different since one flame would be burning with the dust stream and the other against it. This result was observed, and it was observed also that, more often than not, the flame moving against the oncoming dust cloud, after first being carried some distance downstream would accelerate and, causing a reversal of the falling cloud, would then travel back up the tube as an explosion flame, eventually blowing the dust cloud out of the top of the tube. This ability of a dust explosion to reverse the ventilation or conveying air current is commonplace in coalmine and factory disasters, and has been demonstrated experimentally[33]. The explanation may in part be that the hot combustion gases between the two flames have so much greater viscosity, because of their temperature, that their resistance to flow causes the retardation of the ventilation current and allows one of the flames to progress upstream with increasing speed. When taking precautions against explosion, it is a reasonable assumption that, in the event of an ignition, the flame may cause reversal of the ventilation or conveying air current; this consideration may affect the choice of location of relief panels.

STEADY PROPAGATION FLAMES

For the more detailed quantitative determinations of flame speed, the steady upward propagation flames ('open-to-closed' or type 2) were chosen for investigation.

Flame structure

The records obtained by the revolving-drum camera (*Figures 2, 3* and *4*) were taken primarily to determine the flame speed, this being derived directly from the slope of the trace; on closer examination, however, the traces were found to reveal a number of detailed points of flame structure as described below.

(*i*) At very low dust concentrations the trace obtained was like that in *Figure 3*(a) which, by comparison with the trace in *Figure 3*(b), obtained at a higher dust concentration, is seen to be thin. Such thin flames were found to occur over the concentration range from the low limit at 0·05 g/l. to about 0·1 g/l. This range was common to all three dust samples and

therefore independent of both fineness and tube diameter. The length of the thin flames (that is, the vertical section of the flame trace) was about 10 cm [*Figure 3*(a)], compared with 50 to 100 cm for the thick flames obtained at higher concentrations [*Figure 3*(b)]. The thin flames had the shape of an inverted cone with a convex base and were quite unlike the

(a) Thin flame speed trace

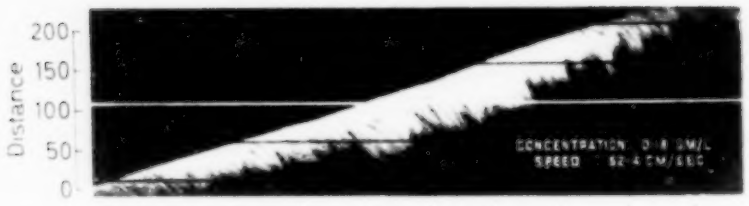

(b) Thick flame speed trace

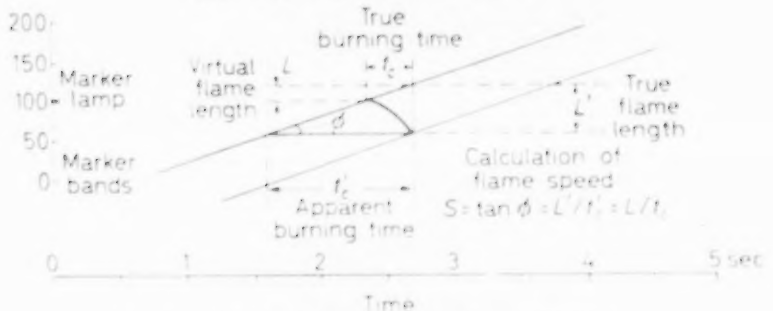

(c) Thick flame speed trace (diagrammatic)

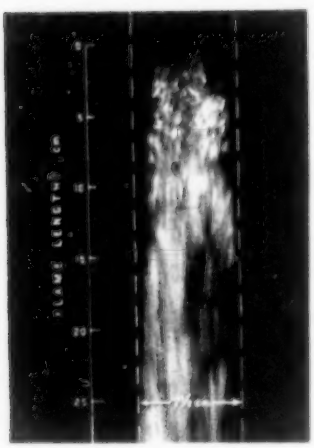

(d) Photograph of flame (exposure 1/100 second)

Figure 3. Flame structure. Steady upward propagation flames

thick flames which were comparatively long cylinders with convex fronts; the former may be characteristic of burning volatile matter rather than of burning solids.

(*ii*) Occasionally in the region of thin flames, groups of particles (or particle residues) continued to burn, possibly as random local agglomerates capable of maintaining their temperature (and hence reaction) despite a high radiative heat loss; such incandescent agglomerates may have caused the occasional trail behind the flame front exemplified in *Figure 3*(a). This possibly explains a phenomenon reported by Kislig[7] who observed, on single exposures of his cine film, isolated patches of flame separate from

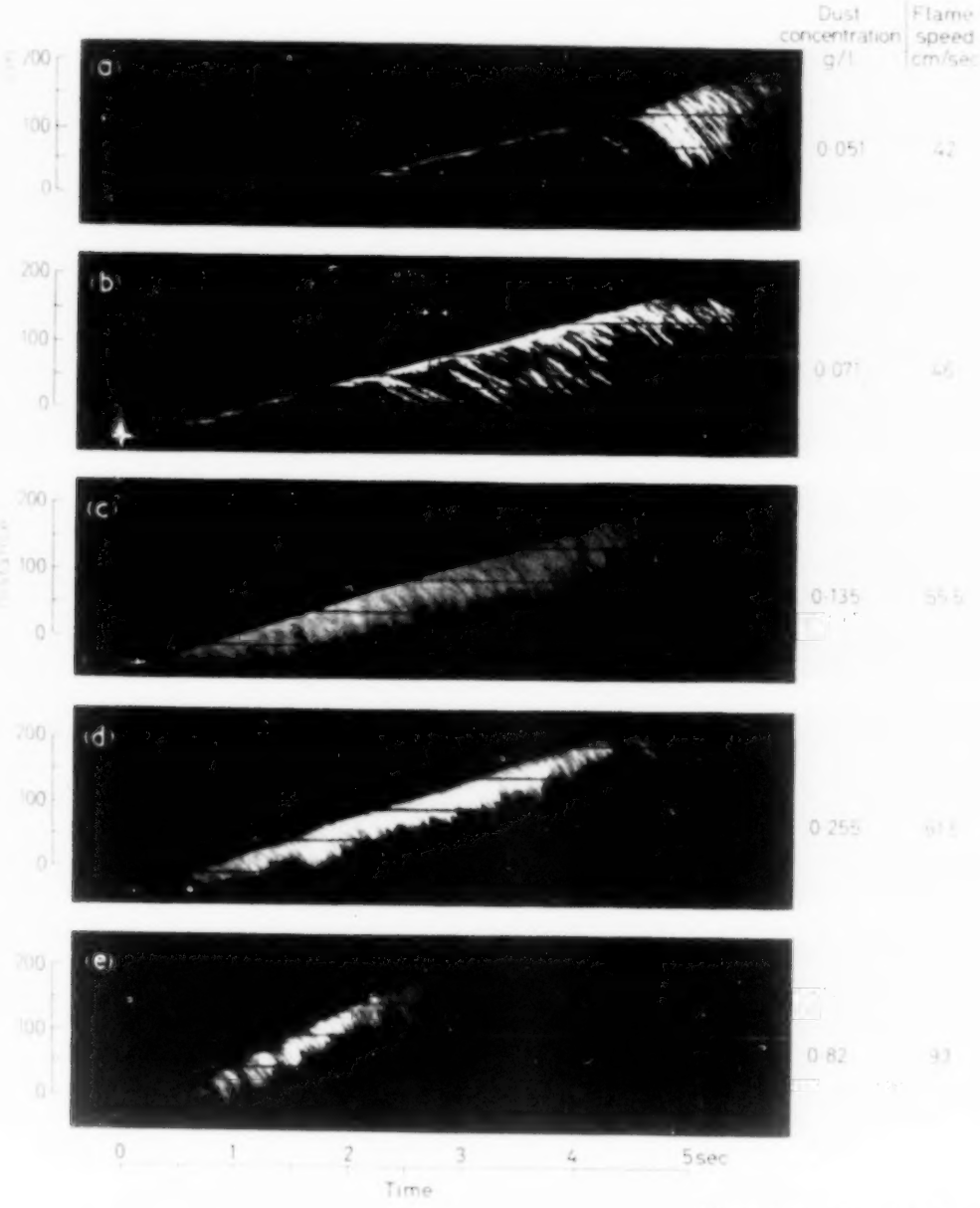

(Crown Copyright: S.M.R.E.)

Figure 4. Flame speed traces with increasing dust concentration. Steady upward propagation: dust sample D

the flame front; he believed this effect to be caused by dust after detachment from the walls of the tube. Though this explanation is admissible, a more likely one is indicated in *Figure 4*(b). On this trace of a thin flame two vertical lines are shown spaced 0·1 sec apart; it is clear that a time exposure of that duration (or less) would show two isolated patches of flame and it would not be apparent from cine records that both patches had their origins in the flame front. Hence, in any work on dust flames in which a single observation window or a recording photocell is used, traces that purport to indicate the passage of two or more flames past the observation point should be interpreted with care.

(*iii*) In the transition from thin flames to thick the number of trails suddenly increased as the dust concentration rose above 0·1 g/l., and the traces became as shown in *Figure 3*(b). Such thicker flames were maintained at all concentrations exceeding about 0·11 g/l. though, as the series of records in *Figure 4* shows, the length of the trace decreased steadily as the dust concentration rose. These traces, unlike the thin flame traces, show appreciable structure. The leading edge was mostly quite regular; the trailing edge was less so, but the boundary although variable was well defined and could be drawn in with reasonable accuracy by eye. Also, although the traces were dense, it was possible to follow the curved track of groups of burning particles as they were accelerated down the tube owing to thermal expansion. This type of rearward motion of incandescent products of combustion is a new demonstration in respect of the flame in a dust cloud, except in that a similar observation has been made indirectly in the study of the results of dust explosions in coalmines. For example, F. V. TIDESWELL[34] has noted that '. . . when the flame is moving steadily, or accelerating, this coked dust is thrown back by the flame and deposited consistently on surfaces facing in the direction the flame has gone'. There seems to be no reason to doubt the occurrence of a corresponding but often unobserved motion of hot gas behind the flame front in gas in accordance with the hydrodynamic theory of deflagration and detonation; here the effect may escape detection by direct photography owing to an absence of structure. In gaseous detonation, when particles are torn from the walls of the containing tube and promptly rendered incandescent, there is clearly always an initial *forward* motion which is followed by a reversal as the products of the explosion cool.

The leading edge, the trailing edge, and the particle track, have been represented diagrammatically in *Figure 3*(c) from which it is evident that there are four quantities to be measured, two of length and two of time. The vertical width of the trace is the actual flame length (L') that would be measured using a short time exposure on a still-plate camera; the true mean burning time of the particles (t_c) is the horizontal projection of the curved particle track; the horizontal width of the trace is the apparent burning time (t_c'); finally the virtual flame length (L) is the length the flame would have had if there had been no thermal expansion. If the thermal expansion factor is M, then by definition we have

$$M = L'/L = t_c'/t_c \qquad \ldots\ldots[2]$$

and the flame speed (S) is given by

$$S = L/t_c = L'/t_c' \quad \ldots . [3]$$

(*iv*) When the curved particle tracks were being drawn in on the original records, for measurement of the true burning times, they were observed to be horizontal, or nearly so, at the start of the combustion. As the particles were known from equation 1 to be falling into the flame at about 50 cm/sec, the inference was that the particles were brought to rest as they entered the flame. To see whether this conclusion could be substantiated, four snapshots of 1/25, 1/50, 1/75 and 1/100 sec exposure were taken of the nose of the flame. *Figure 3*(d) is a print of the exposure at 1/100 sec and in it can be clearly seen the typical 'granular' appearance of dust flames caused by incandescent groups of particles. This exposure shows that since the particle groups in the nose of the flame are sharply defined, they must be stationary or nearly so, a condition that is in marked contrast to the particle groups lying more deeply and which appear as blurred streaks. As the other three snapshots (not reproduced) also show areas

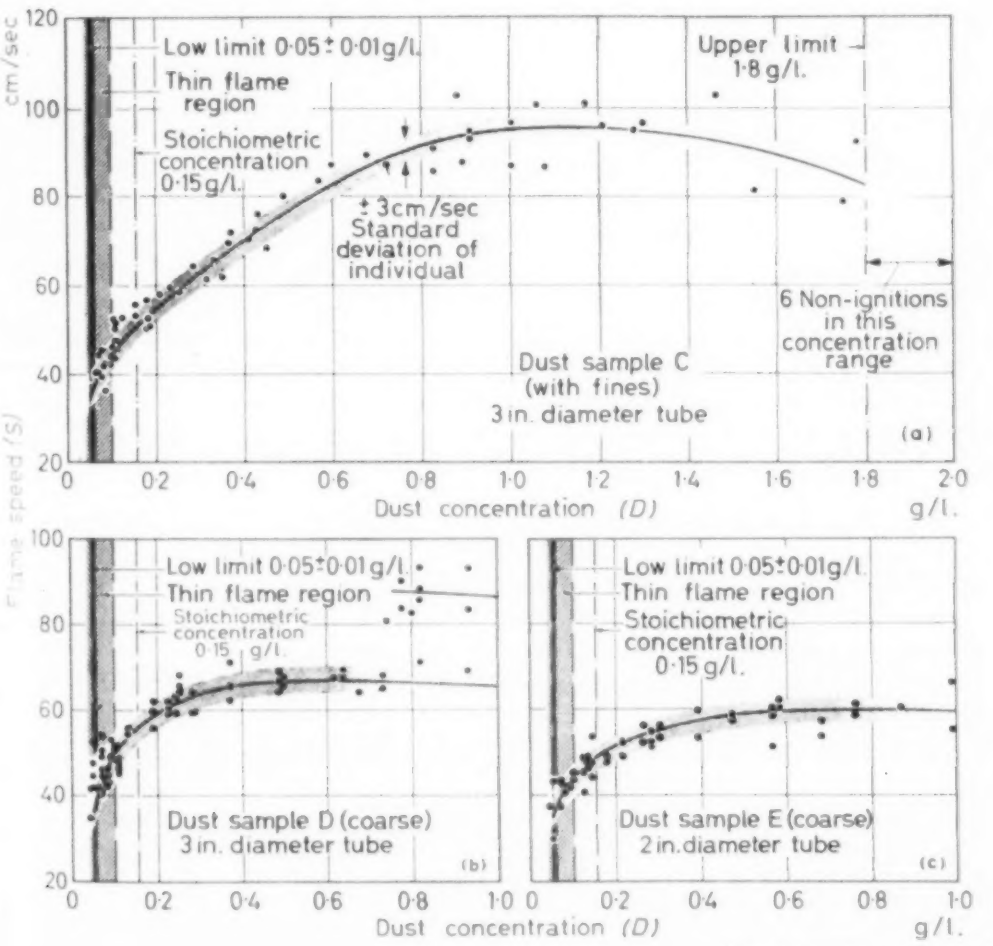
Flame speed (S) cm/sec
Low limit 0·05 ± 0·01 g/l.
Thin flame region
Stoichiometric concentration 0·15 g/l.
± 3 cm/sec Standard deviation of individual
Upper limit 1·8 g/l.
6 Non-ignitions in this concentration range
Dust sample C (with fines) 3 in. diameter tube
(a)
Dust concentration (D) g/l.
Low limit 0·05 ± 0·01 g/l.
Thin flame region
Stoichiometric concentration 0·15 g/l.
Dust sample D (coarse) 3 in. diameter tube
(b)
Low limit 0·05 ± 0·01 g/l.
Thin flame region
Stoichiometric concentration 0·15 g/l.
Dust sample E (coarse) 2 in. diameter tube
(c)
Dust concentration (D) g/l.

(Crown Copyright: S.M.R.E.)

Figure 5. Variation of flame speed with dust cloud concentration

of clear definition in the nose of the flame which narrow with lengthening exposure, the original conclusion is confirmed that the particles were brought to rest as they entered the flame, prior to undergoing rapid acceleration to the rear.

Flame speed and dust concentration

The flame speed was measured as a function of dust cloud concentration with the results shown graphically in *Figures* 5(a), (b) and (c), for samples C and D in the 3 in. tube and sample E in the 2 in. tube respectively. The shaded band on either side of the mean line up to a concentration of about 0·6 g/l. represents a range of ±3 cm/sec, which was the calculated value of the standard deviation of the individual; above that concentration there was a wider scatter. With sample D, in the 3 in. tube and only at the higher concentrations, the observations of flame speed tended to lie above the smooth curve as it has been drawn in *Figure* 5(b); a possible discontinuity in the speed/concentration relationship is recorded tentatively together with the observation that in some instances the flame would travel up a central region, thereby failing to fill the complete cross section of the tube.

As the curves show, the low limit and the minimum flame speed are independent of fineness and of tube diameter. The low limit can be stated as 0·05 ± 0·01 g/l. and the minimum flame speed for steady upward propagation as 35 ± 1 cm/sec (see below). The factors of fineness and tube diameter become important at higher concentrations, the curves showing clearly that flame speed rises with tube diameter (contrary to the results of Cassel *et al.* in *Table 2*) and with fineness. The upper limit was determined only for sample C and found to be about 1·8 g/l. [*Figure* 5(a), 3 in. tube]; with the samples without fines, D and E, the appearance and behaviour of the flame at the highest concentration examined gave indications that the upper limit for these samples would not be much above 1·0 g/l. Comparable values of the upper limit of fine coal dust have been given as 1·25 g/l.[35] and 0·9 g/l.[36].

The general shape of the curves and the positions of the maxima are of interest. The shape can be compared with those of four other curves given in various other papers[8, 20, 35, 37], three of which have been discussed elsewhere[38]; two of them relate to flame speed and two to inflammability as measured by the incombustible additive for extinction. The flat curves of *Figure* 5 are similar both to Long's curve of burning velocity[8] and to one of stone-dust content[35]; their shape is in contrast to a sharply peaked velocity extinction curve[37] and to the velocity curves of de Grey[20]. The concentrations for the maximum speeds were about 1·1 g/l. for sample C and 0·6 g/l. for samples D and E; thus, the 'optimum' concentrations were about seven times the stoichiometric value for the sample with fines and only four times for the two coarser samples. Since the maximum speed also was higher when the fines were present, it appears that, as the dust concentration and the flame speed rise, so does the proportion of fines being burnt.

Flame length and burning time

Values of flame length and burning time were calculated from the flame speed traces [see *Figure 3*(c)], and the pairs of values (real and apparent) of the two quantities were first plotted against each other to determine the expansion factor M (see equation 2). This was found to be reasonably constant for a given dust sample and the values are recorded, with certain other constants, in *Table 3*. The true flame length (L') and the apparent

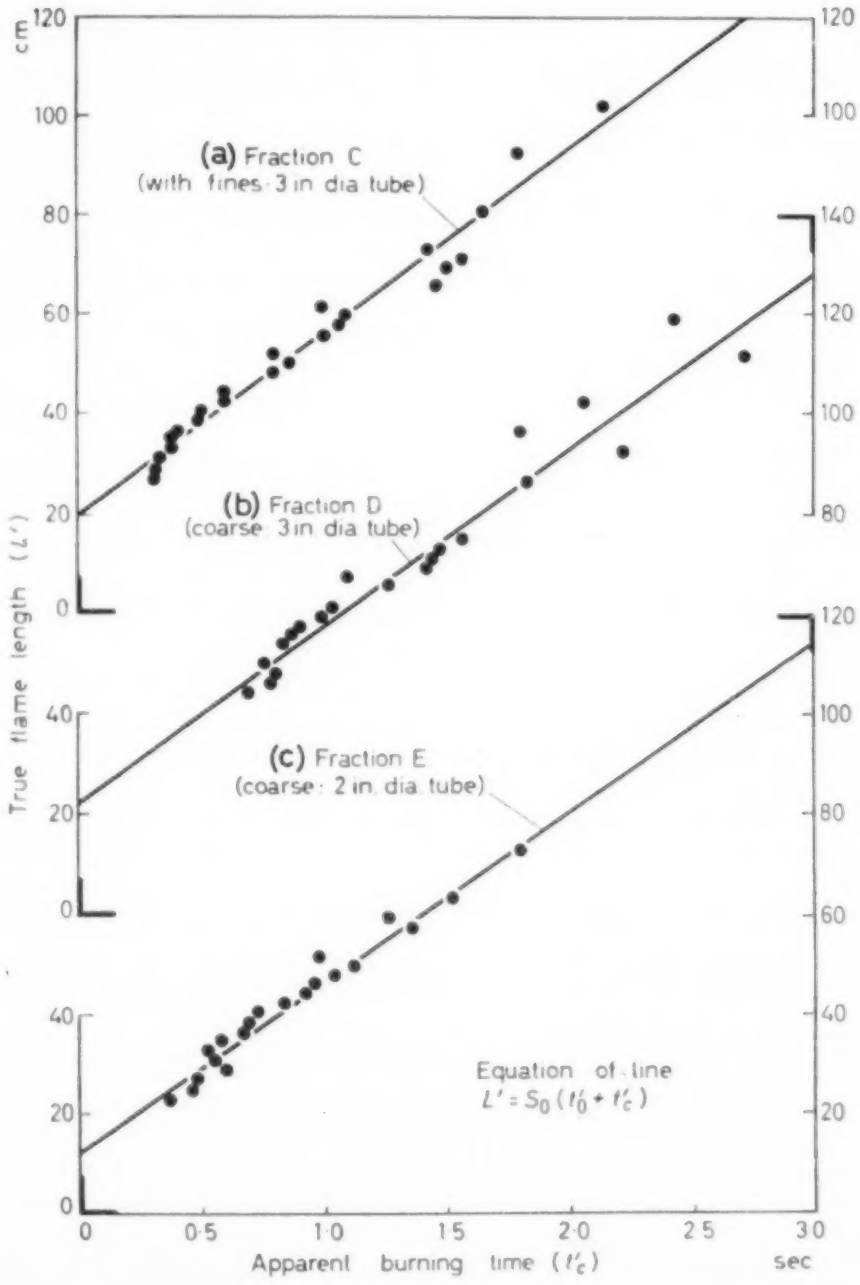

(Crown Copyright: S.M.R.E.)

Figure 6. Variation of true flame length with apparent burning time

burning time (t_c') were then plotted and found to be related linearly with an intercept in L' at zero time [*Figures* 6(a), (b) and (c)]. The equation can therefore be written

$$L' = S_u (t_u' + t_c') \quad \ldots . [4]$$

where S_u and t_u are constants having the values (determined experimentally) given in *Table 3*.

Table 3. Combustion constants (c.g.s. units)

Dust sample	*Tube diameter in.*	*Expansion factor M*	*Limit burning time t_u sec*	*Limit flame speed S_u cm/sec*
C (with fines)	3	3·42	0·52	36
D	3	3·53	0·64	34
E	2	3·10	0·35	35

The significance of t_u is not clear, but the limit flame speed (S_u) probably has a real meaning. Combining equations 2, 3 and 4 we have

$$S = S_u (1 + t_u/t_c) \quad \ldots . [5]$$

Hence, the flame speed is inversely proportional to the burning time. At the limit, however, when the burning time is infinitely long, the flame speed still has a finite value S_u (about 35 cm/sec) which is presumably the lowest speed at which a flame can propagate under the conditions stated; if the speed falls below this value for any reason, then the flame will be extinguished.

CONCLUSIONS

An experimental system, whereby cork dust was fed mechanically into the top of a vertical glass tube 17 ft long and either 2 or 3 in. in diameter, and allowed to fall under gravity, produced a dust cloud suitable for the investigation of moving flames under various conditions. The following conclusions are drawn.

(*1*) With open-end ignition and the other end closed, the flame traversed the tube at a steady speed in contrast to the accelerating flame obtained by closed-end ignition. In the latter conditions the flame speed reached a value more than 20 times that obtained in the former.

(*2*) In upward propagation the flames of both the steady propagation and explosion types travelled five or ten times faster than the same flame type in downward propagation. This observation suggests that, on a thermal theory of flame propagation and as in gas and vapour explosions, the heat transfer is significantly aided in upward propagation by convection additionally to conduction and radiation, the latter now regarded as of special importance in dust explosions[7].

(*3*) In steady upward propagation flames, the flame speed continued to rise with dust concentration well above the stoichiometric (at 0·15 g/l).

With two levels of fineness, and two tube diameters, the optimum concentration at which the flame speed maximum occurred appeared to be the same in a 2 in. and a 3 in. tube, but it increased with fineness, being four times greater than the stoichiometric for the sample D without fines and seven times for the sample C with fines. It appeared that with rising concentration the proportion of burning fines also rose.

(*4*) The low limit of inflammability (at 0·05 g/l.) and the limiting flame speed at that limit (35 cm/sec) both appeared to be independent of fineness and tube diameter within the ranges studied. The upper limit (at 1·8 g/l.) was measured only for the dust with fines (sample C).

(*5*) At low dust concentrations a narrow range was found (from the low limit at 0·05 up to 0·1 g/l.) in which the flame length was always slight (about 10 cm) compared with the length (50 to 100 cm) in the rest of the concentration range. It appeared that in the thin flame region the material burning was mainly the volatile matter of the cork dust. From the reaction zone of both thin and thick steady propagation flames, all incandescent material is projected in the rearwards direction in uniform fashion at a rising velocity.

(*6*) In the thick flame region, measurements of flame length (L) and burning time (t_c) showed these to be linearly related as expressed by the equation

$$L = S_u (t_u + t_c)$$

S_u and t_u are constants; S_u is the limiting flame speed that must be attained if propagation is to continue.

The authors wish to thank especially Mr L. P. Barbero, B.Sc., for assistance in the building of apparatus and in the experimental observations; other help was given by Messrs A. J. Beal and J. Seager, B.Sc. Acknowledgement is due to the Director of the Joint Fire Research Organization and to the Ministry of Power for permission to publish this paper.

Safety in Mines Research Establishment,
Buxton, Derbyshire

(*Received September 1958*)

REFERENCES

Factory Department, Ministry of Labour and National Service. *Inflammability of Dusts* (Form No. 830) (February 1953). Her Majesty's Stationery Office, London

BROWN, K. C. 'A review of the present methods of testing industrial dusts for inflammability.' *Saf.-i.-Mines Res. Rep. No. 21* (April 1951)

BROWN, K. C. 'Dust explosions in factories: the protection of elevator casings by pressure relief vents.' *Saf.-i.-Mines Res. Rep. No. 22* (April 1951)

BROWN, K. C. and WOODHEAD, D. W. 'Dust explosions in factories: closed-circuit test apparatus.' *Saf.-i.-Mines Res. Rep. No. 86* (December 1953)

BROWN, K. C. and WILDE, D. G. 'Dust explosions in factories: protection of plant by hinged explosion doors.' *Saf.-i.-Mines Res. Rep. No. 119* (September 1955)

TAFFANEL, J. and DURR, A. *Fifth series of experiments on the inflammation of dusts* (August 1911). Comité Central des Houillères de France: Paris

CASSEL, H. M., DAS GUPTA, A. K. and GURUSWAMY, S. 'Factors affecting flame propagation through dust clouds.' *Third Symposium on Combustion and Flame, and Explosion Phenomena, Wisconsin, 1948*, p 185. Williams and Wilkins: Baltimore, 1949

LONG, V. D. 'Flame propagation in suspensions of coal dust in air.' *Thesis*. Imperial College of Science and Technology: London, November 1956

[9] KISLIG, F. 'Contribution to knowledge of dust flames.' *Thesis*. Eidgenössische Technische Hochschule, Zürich. Rosch, Vogt: Bern, 1950
[10] MASON, W. 'Coal dust explosions.' *Trans. Instn Min. Engrs, Lond.* 68 (1924-25) 497
[11] RICE, G. S., JONES, L. M., EGY, W. L. and GREENWALD, H. P. 'Coal dust explosion tests in the experimental mine, 1913 to 1918 inclusive.' *Bull. U.S. Bur. Min. No. 167* (1922)
[12] HARTMANN, I. 'Recent findings on dust explosions.' *Chem. Engng Progr.* 53 (1957) 107-M
[13] BROWN, K. C. and WILLIAMS, H. L. *Prevention of the Propagation of Flame in Aluminium Dust Explosions*. Her Majesty's Stationery Office: London, 1951
[14] BROWN, K. C. and ESSENHIGH, R. H. 'Dust explosions in factories: a new vertical tube test apparatus.' *Saf.-i.-Mines Res. Rep. No. 165* (1959)
[15] JONES, E. and WHITE, A. G. 'Gas explosions and dust explosions: a comparison.' *Dust in Industry*, p 129. (Conference Leeds, September 1948). Society of Chemical Industry: London, 1948
[16] RIBAS-MARQUÈS, I. 'Study on the chemical constitution of cork.' *Chim. et Industr.* 68 (No. 3) (1952) 333
[17] BURGOYNE, J. H. and LONG, V. D. 'Some measurements of the burning velocity of coal-in-air suspensions.' *Conference on Science in the Use of Coal, Sheffield, April 1958*, Paper No. 28
[18] HATTORI, H. 'Flame propagation in pulverized coal-air mixtures.' *Sixth (International) Symposium on Combustion*, p 590. Reinhold: New York, 1957
[19] GHOSH, B., BASU, D. and ROY, N. K. 'Studies in pulverized coal flames.' *Sixth (International) Symposium on Combustion*, p 595. Reinhold: New York, 1957
[20] DE GREY, A. 'Experiments on coal dust combustion of pulverized coal.' *Rev. Métall.* 19 (1922) 645
[21] KREISINGER, H. Discussion on paper by J. C. HOBBS and L. W. HELLER: 'Pulverized fuel for a large boiler.' *Proc. Engrs' Soc. W. Pa* 39 (1923) 244
[22] HASLAM, R. T. and RUSSELL, R. P. *Fuels and their Combustion*, p 448. McGraw-Hill: New York, 1926
[23] CRAIG, O. 'Discharge temperatures from pulverizers.' *Trans. Amer. Soc. mech. Engrs* 61 (1939) 369
[24] TRINKS, W. *Industrial Furnaces*, Vol. II. (2nd edn). Wiley: New York, 1944
[25] DE LORENZI, O. *Combustion Engineering, 1947*, p 8 (sect. 3). Combustion Engineering: New York, 1947
[26] SMITH, M. L. and STINSON, E. W. *Fuels and Combustion*, p 258. McGraw-Hill: New York, 1952
[27] SPIERS, H. M. *Technical Data on Fuel* (5th edn), p 410. British National Committee, World Power Conference: London, 1950
[28] International Combustion Ltd. 'Coal milling and pulverized fuel firing.' *Publication No. W/513*
[29] ORNING, A. A. *Chemistry of Coal Utilization*, Vol. II, p 1549. Chapman and Hall: London, 1947
[30] WHEELER, R. V. 'Coal dust explosions, Eskmeals, 1923.' *Saf.-i.-Mines Res. Pap. No. 3* (1924)
[31] SHAW, S. K. and WOODHEAD, D. W. 'Igniters for experimental coal dust explosions.' *Saf.-i.-Mines Res. Rep. No. 69* (1953)
[32] MASON, T. N. and WHEELER, R. V. 'Inflammation of coal dusts: effect of the presence of firedamp.' *Saf.-i.-Mines Res. Pap. No. 64* (1931)
[33] Mining Association of Great Britain. *Record* of experiments carried out during 1908 and 1909 at the Altofts Experiments Station, p 19. Colliery Guardian: London, 1910
[34] TIDESWELL, F. V. 'Methods of examination following a colliery explosion.' *Trans. Instn Min. Engrs, Lond.* 112 (No. 3) (1952-53) 157
[35] Safety in Mines Research Board. *Fourteenth Annual Report 1935*, p 19. Her Majesty's Stationery Office: London, 1936
[36] CYBULSKI, W. B. 'Experiments to determine the explosion limits of coal dust.' *Eighth International Conference of Directors of Safety in Mines Research, Dortmund–Derne, 1954*, Paper No. 41
[37] Ministry of Fuel and Power. *33rd Annual Report on Safety in Mines Research 1954*, p 21. Her Majesty's Stationery Office: London 1955
[38] ESSENHIGH, R. H. and PERRY, M. G. 'Combustion and gasification: a review.' *Conference on Science in the Use of Coal, Sheffield, April, 1958*

Confined Jets and Recirculation Phenomena with Cold Air

R. CURTET

An approximate theory of confined jets established by A. Craya and R. Curtet is developed, allowance for wall effect being made when studying the mixing of a jet with a surrounding stream enclosed in a duct. Two-dimensional and axisymmetric conditions are considered. Experimental results are given: these show two distinct régimes can be identified, and the creation of recirculation is discussed. Agreement between theory and practice is examined, and application of this work to a test furnace at IJmuiden noted.

CONSIDERABLE previous research on turbulent diffusion flames has shown how important it is from the practical point of view to determine the effect of the walls in a furnace upon the behaviour of the flame and its ambient medium[1]. In view of this therefore, we feel that the work described in this article may be of some use for later research on turbulent diffusion flames, despite the fact that it is concerned with the special case of a single constant density fluid. The approximate theory of the mixing characteristics of jets, which was established jointly some years ago by A. CRAYA and the author[2], has been the guiding line followed in this work.

It is shown how a theoretical approach makes it possible, whilst making only a very limited number of assumptions, to allow for the presence of the walls and the rate of flow of the ambient fluid, and to treat the free jet as a special case, whether the ambient fluid is in motion or not.

The calculation results are then compared with those obtained from systematic tests carried out with two-dimensional jets; a few characteristics of a jet with and without recirculation are given.

It will finally be shown that the theory of jets can be used to forecast the laws governing three-dimensional recirculating flow to a good degree of agreement with practical experience.

APPROXIMATE THEORY OF THE MIXING OF JETS

Notation

δ_*	Displacement thickness of boundary layer
u_1	Outer velocity (ambient fluid)
u	Component of this velocity in direction Ox
h	Half-height of chamber at x
y	Ordinate of point M
w	Excess velocity at M
w_0	Excess velocity along OX
Q	Total discharge
q	Excess discharge
q_1	Nozzle discharge
K	Momentum coefficient

q_r	Recirculation discharge
l	Effective width
$R=q/Q$	Discharge ratio
$\lambda=l/h$	Effective width ratio
p_0	Static pressure at duct wall
X	Relative abscissa
m	Similitude parameter
m_a	Ambient fluid flow
m_0	Nozzle mass flow
S	Cross sectional area of chamber
$U=Q/S$	Mean velocity
D	Characteristic chamber dimension where $2h/D=1+3{\cdot}30\,a/h$
T	Oscillation period of two-dimensional jet
θ_r	Thring and Newby parameter

(a) *Definitions*

We propose to study the mixing of two fluid streams, either two-dimensional or axisymmetric, of the same density, but having different initial velocities [*Figures 1*(a) and (b)]. If we consider the velocity distribution curve in

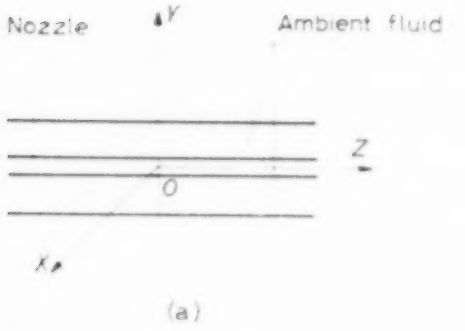

Figure 1 (a). *Two-dimensional jet*

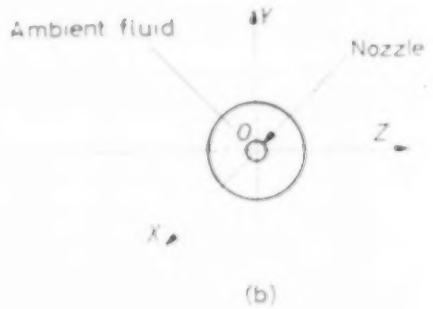

Figure 1 (b). *Axisymmetric jet*

the plane *XOY* (*Figure 2*) at a certain abscissa x, whose origin is at the point of entry of the two jets, it shows that the space in the chamber is divided up into two zones: one of these, the mixing zone or jet, has a steep velocity gradient, and the other, in which the velocity is practically constant, lies outside this jet. The transition of the velocity distribution curve to zero at the wall occurs in the boundary layer, the displacement thickness of which is δ_1. Now, let h be the half-height of the chamber at the abscissa x, let u_1 be the velocity in the ambient fluid and u the velocity component in the direction Ox at a point M, of ordinate y. Furthermore, let an excess velocity $w=u-u_1$ be defined at point M, and call the value of w along the axis w_0. The area bounded by the excess velocity curve then represents an excess discharge q; moreover, we can introduce an effective width l, which is defined by $q=2w_0l$ for the two-dimensional case, and by $q=\pi w_0l^2$ in the axisymmetric case. The variables w_0, u_1 and l are unknown functions of x for the time being, and we have to find three interconnecting relations for them.

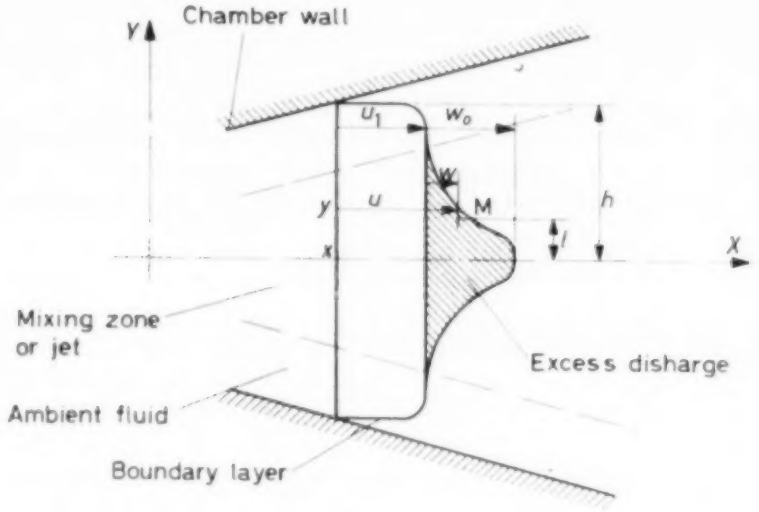

Figure 2

(b) *General equations and hypothesis used*

The mean values of the Navier–Stokes equations have been used as the basic equations (i.e. the well known Reynolds equations[3]). For the two-dimensional case, in the plane XOY:

$$\bar{u}\frac{\partial \bar{u}}{\partial x} + \bar{v}\frac{\partial \bar{u}}{\partial y} + \frac{\partial \overline{u'^2}}{\partial x} + \frac{\partial \overline{u'v'}}{\partial y} = -\frac{1}{\rho}\frac{\partial \bar{p}}{\partial x} + \nu\left(\frac{\partial^2 \bar{u}}{\partial x^2} + \frac{\partial^2 \bar{u}}{\partial y^2}\right) \quad \ldots\ldots[1]$$

$$\bar{u}\frac{\partial \bar{v}}{\partial x} + \bar{v}\frac{\partial \bar{v}}{\partial y} + \frac{\partial \overline{u'v'}}{\partial x} + \frac{\partial \overline{v'^2}}{\partial y} = -\frac{1}{\rho}\frac{\partial \bar{p}}{\partial y} + \nu\left(\frac{\partial^2 \bar{v}}{\partial x^2} + \frac{\partial^2 \bar{v}}{\partial y^2}\right) \quad \ldots\ldots[2]$$

This set of equations can be simplified, since the streamlines in a jet generally only form a small angle with the mean direction of flow and it can be assumed that the mean quantities vary more rapidly in the direction OY than along OX. Equation 2 can then be written

$$\bar{p} + \rho\overline{v'^2} = \bar{p}_o$$

where $\bar{p}_o$ is the static pressure at the duct wall and solely a function of x. Equation 1 becomes

$$\bar{u}\frac{\partial \bar{u}}{\partial x} + \bar{v}\frac{\partial \bar{u}}{\partial y} + \frac{\partial\left(\overline{u'^2} - \overline{v'^2}\right)}{\partial x} + \frac{\partial \overline{u'v'}}{\partial y} = -\frac{1}{\rho}\frac{\partial \bar{p}_o}{\partial x} + \nu\frac{\partial^2 \bar{u}}{\partial y^2}$$

Experience shows that, in a free jet, the difference $(\overline{u'^2} - \overline{v'^2})$ is small compared to $\bar{u}^2$, and we shall accordingly neglect the third term. If we introduce the shear stress

$\tau/\rho = -\overline{u'v'} + \nu\dfrac{\partial \bar{u}}{\partial y}$ we have

$$\bar{u}\frac{\partial \bar{u}}{\partial x} + \bar{v}\frac{\partial \bar{u}}{\partial y} + \frac{1}{\rho}\frac{\partial \bar{p}_o}{\partial x} = \frac{1}{\rho}\frac{\partial \bar{\tau}}{\partial y} \quad \ldots\ldots[3]$$

The basic equation for axisymmetric jet flow can be written down from similar considerations, and the two relations can be expressed by a single

equation, thus

$$u\frac{\partial u}{\partial x}+v\frac{\partial u}{\partial y}+\frac{1}{\rho}\frac{\partial p_0}{\partial x}=\frac{1}{\rho}\frac{1}{y^\delta}\frac{\partial (vy^\delta)}{\partial y} \qquad \ldots.[4]$$

where $\delta=0$ for the two-dimensional jet and $\delta=1$ for the axisymmetric jet. Note that the bar indicating a mean velocity is suppressed from this point.

We now have to complete equation 4 with the continuity condition

$$\frac{\partial u}{\partial x}+\frac{1}{y^\delta}\frac{\partial (vy^\delta)}{\partial y}=0 \qquad \ldots.[5]$$

It will be useful to introduce relative variables, in order to allow for a later essential assumption in the theory, concerning the approximate affinity of the reduced velocity profile: our tests with a two-dimensional jet showed that, for the portion of the jet lying downstream of the potential core and upstream of the point at which it reaches the walls, the curve $w/w_o=f(y/l)$ becomes practically independent of x. Let $\eta=y/l$, and let K be a parameter depending on x (which will be defined later on); we can write, in general,

$$w/w_o=f(\eta, K) \qquad \ldots.[6]$$

We shall also assume frictionless flow outside the jet proper, so that

$$\frac{1}{\rho}\frac{\partial p_o}{\partial x}+\frac{\partial}{\partial x}\left[\frac{u_1^2+v_1^2}{2}\right]=0$$

and, if the streamlines only form a small angle with the axis, v_1^2 is negligible compared with u_1^2.

Having made these assumptions, we can substitute the v deduced from equation 5 into equation 4, and, by integrating the latter with respect to y, we have, after manipulation,

$$\begin{aligned}-(\delta+1)\frac{v\eta^\delta}{\rho w_o^2}=&-\frac{(u_1^2w_ol^{\delta+1})_x}{u_1w_o^2l^\delta}F-\frac{(Kw_o^2l^{\delta+1})_x}{w_o^2l^\delta}M\\&+\frac{(w_ol^{\delta+1})_x}{w_o^2l^\delta}fF+\frac{(u_1l^{\delta+1})_x}{w_ol^\delta}f\eta^{\delta+1}\\&-\frac{u_1}{w_o}lK_x\frac{\partial F}{\partial K}-lK_x\left[K\frac{\partial M}{\partial K}-f\frac{\partial F}{\partial K}\right] \qquad \ldots.[7]\end{aligned}$$

in which the notations are defined as follows:

$$\left.\begin{aligned}l^{\delta+1}&=(\delta+1)\int_0^{+\infty}\frac{w}{w_o}y^\delta dy \qquad K=(\delta+1)\int_0^{+\infty}\frac{w^2}{w_o^2}\eta^\delta d\eta\\F&=(\delta+1)\int_0^{\eta}f\eta^\delta d\eta \qquad KM=(\delta+1)\int_0^{\eta}f^2\eta^\delta d\eta\end{aligned}\right| \qquad \ldots.[7a]$$

$(\ )_x$ = derivative with respect to x.

(c) *Mean equations for confined jets*

We obtain, from equation 7, a first mean equation of the jet by writing that

the shear stress is zero at the boundary of the mixing zone

$$\frac{(u_1^2 w_o l^{\delta+1})_x}{u_1 w_o^2 l^{\delta}} + \frac{(K w_o^2 l^{\delta+1})_x}{w_o^2 l^{\delta}} = 0 \qquad \ldots . [8]$$

It should be noted that this relation applies everywhere without any hypothesis on the evolution of the velocity profile.

A second mean relation is obtained by writing that the total fluid discharge Q is independent of the abscissa

$$Q/\pi^{\delta} = [u_1 (h - \delta_*)^{\delta+1} + w_o l^{\delta+1}] 2^{1-\delta} \qquad \ldots . [9]$$

In order to obtain the third and last relation, we shall first use the experimental fact already stated, that the reduced excess velocity profile defined by equation 6 becomes independent of x, so that $w/w_o = \mathrm{f}(\eta)$, and only the first four terms of the RHS of equation 7 remain. Allowing for equation 8, equation 7 then becomes

$$-(\delta+1)\frac{\tau \eta^{\delta}}{\rho w_o^2} = -K\frac{(w_o^2 l^{\delta+1})_x}{w_o^2 l^{\delta}}(M-F) + \frac{(w_o l^{\delta+1})_x}{w_o l^{\delta}} \mathrm{f}F + \frac{(u_1 l^{\delta+1})_x}{w_o^2 l^{\delta}} \mathrm{f}\eta^{\delta+1} \qquad \ldots . [10]$$

The terms $(M-F)$, $\mathrm{f}F$ and $\mathrm{f}\eta^{\delta+1}$ on the RHS of equation 10 are solely functions of η, so that the RHS of equation 10 becomes a sum of three terms of the form $\Phi(x)\Psi(\eta)$. If the three terms $(M-F)$, $\mathrm{f}F$ and $\mathrm{f}\eta^{\delta+1}$ were always similarly related equation 10 would reduce to

$$-(\delta+1)\frac{\tau \eta^{\delta}}{\rho w_o^2} = \Phi_o(x)\Psi(\eta)$$

i.e.

$$-(\delta+1)\frac{\tau}{\rho w_o^2 \Phi_o(x)} = \frac{\Psi(\eta)}{\eta^{\delta}} \qquad \ldots . [11]$$

Under these conditions, the shear stress could be represented by a reduced curve that would be independent of the abscissa. In fact, although the three terms $(M-F)$, $\mathrm{f}F$ and $\mathrm{f}\eta^{\delta+1}$ are not quite in fixed ratio, they nevertheless satisfy this condition fairly well, as can be seen from the curves in *Figures 3*(a) and (b). These were plotted by considering the Gaussian

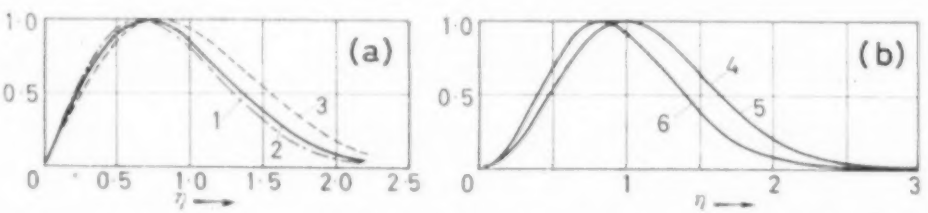

Figure 3. (a) *Two-dimensional, and* (b) *axisymmetric, jet.* 1: 6·02 $(M-F)$; 2: 2·37 $\mathrm{f}F$; 3: 2·07 $\mathrm{f}\eta$; 4: 4 $\mathrm{f}F$; 5: 8 K $(M-F)$; 6: 2·718 $\mathrm{f}\eta^2$

functions $\mathrm{f} = \exp(-\pi\eta^2/4)$ and $\mathrm{f} = \exp(-\eta^2)$ for the two-dimensional and axisymmetric jet cases respectively, which were found to lie close to the experimental curves.

We shall now consider equation 11 and try to find a mean value for each side within the mixing zone. First, let each side be multiplied by a given function $\chi(\eta)$ and, next, let the product obtained in this way be

integrated across the mixing zone. The two integrated sides of equation 11 are bound to be equal, whatever the value of $\chi(\eta)$. If we now repeat the operation, but this time on equation 10, integration will, on the other hand, produce results depending on $\chi(\eta)$. However, in view of our previous remarks regarding the approximate proportionality of the three functions of η and as we shall show with a numerical example later on, the mean equation obtained by integration is not usually very sensitive to changes in $\chi(\eta)$. The mean equation obtained in this way gives us the third relation we require

$$\sigma = -a\frac{(w_o^2 l^{\delta+1})_x}{w_o^2 l^\delta} + \frac{1}{2(\delta+1)}\frac{(w_o l^{\delta+1})_x}{w_o l^\delta} + b\frac{(u_i l^{\delta+1})_x}{w_o l^\delta} \quad \ldots [12]$$

where a and b are numerical coefficients, and σ is a function of x defined by

$$\sigma = -\int_0^{+\infty} \frac{1}{2}\frac{\tau\eta^\delta}{\rho w_o^2}\frac{\chi(\eta)}{fF}\,d\eta \quad \ldots [13]$$

The set of equations 8, 9 and 12 is the basic set of differential equations for the approximate theory of confined jets. It is resolved by making explicit the variables l, u_i and w_o as functions of x, when the quantities Q, $h-\delta_*$, $\sigma(x)$ and $f(\eta)$ are supposed given.

The numerical values of coefficients K, a and b depend on the choice of the functions $f(\eta)$ and $\chi(\eta)$. For f we have considered both the Gauss curve and the cosine curve introduced by H. B. SQUIRE and J. O. TROUNCER[4], and taken equation 7a into account. The function $\chi(\eta)$ was taken either as 1, or as $df/d\eta$, giving the equations for the moment of momentum and the energy for the mean motion respectively. The values found for K, a and b are given in *Table 1* and *Table 2* (page 390).

Table 1. Two-dimensional jet

Constant	K	$\chi(\eta)=1$		$\chi(\eta)=df/d\eta$	
		a	b	a	b
Gauss curve	0·707	0·132	0·636	0·134	0·612
Cosine curve	0·750	0·101	0·595	0·100	0·600

The results of our tests with a two-dimensional jet produced the following values:

$$K = 0{\cdot}720 \qquad a = 0{\cdot}120 \qquad b = 0{\cdot}620$$

FREE JET WITHOUT AMBIENT VELOCITY

A considerable amount of experimental research has been carried out on free jets with zero ambient velocity, providing a reliable working basis for the more complex study of a confined jet. Our basic equations can be simplified in this particular case, for the continuity equation 9 is not required, and the momentum equation 8 becomes

$$(Kw_o^2 l^{\delta+1})_x = 0 \qquad \text{i.e.} \qquad Kw_o^2 l^{\delta+1} = K_1 w_1^2 a^{\delta+1} \quad \ldots [14]$$

where K_e, w_e and a are the momentum coefficient, the velocity and the half-height of the nozzle respectively. Equation 12 can now be reduced to

$$\sigma = \frac{1}{2(\delta+1)} \frac{(w_a l^{\delta+1})_x}{w_a l^\delta} \quad \ldots [15]$$

or, because of equation 14,

$$(l)_x = 4\sigma x \quad \ldots [16]$$

For σ = constant we find the well known result of the linear expansion of a jet, so that

$$\frac{w_a}{w_e} = \left[\frac{K_e}{K} \frac{a^{\delta+1}}{(4\sigma x)^{\delta+1}}\right]^{\frac{1}{2}} \quad \ldots [17]$$

expresses the law for the evolution of the velocity on the axis. The value of σ can be deduced from the tests carried out by the following:

Two-dimensional jet

E. FÖRTHMANN[3]	$\sigma = 0{\cdot}031$
H. REICHARDT[6]	$\sigma = 0{\cdot}030$
H. ROUSE *et al.*[7]	$\sigma = 0{\cdot}034$

Axisymmetric jet

H. ROUSE *et al.*[7]	$\sigma = 0{\cdot}0285$
J. O. HINZE and V. D. H. ZIJNEN[8]	$\sigma = 0{\cdot}029$
S. CORRSIN[9]	$\sigma = 0{\cdot}0285$

Although the above results do not agree exactly with each other, there seems to be some agreement among the values for the two-dimensional and axisymmetric jet cases respectively. We shall discuss this coefficient in more detail after describing our tests.

FREE JET AT CONSTANT AMBIENT VELOCITY CONDITIONS

Although this particular case (u_1 = constant) is equally important for the physics of jets, we feel that only very few really conclusive tests have been carried out in this connection so far, because of the difficulty of obtaining an appreciable ambient velocity without the presence of walls interfering with the mixing process. Actually, the known tests provide examples of confined jets, which can only be compared with free jets at constant ambient velocity conditions, within the limits that we shall define below.

On the other hand, the equation is easy to integrate, since, when u_1 = constant, relation 8 is an exact differential which, when integrated for the axisymmetric jet case for instance, gives

$$u_1 w_a l^2 + K w_a^2 l^2 = u_1^2 H^2 \quad \ldots [18]$$

which defines a reference length H, so that l/H can be made explicit as follows

$$l/H = p/\{p+K\}^{\frac{1}{2}} \quad \text{where} \quad p = u_1/w_a$$

Once l/H has been replaced, a curve for $\int_0^x \sigma \mathrm{d}x/H = \phi(p) = \xi$ can be obtained from equation 12 by integration.

In order to show how sensitive the results of the calculations are to the values of cofficients K, a and b, we have plotted four examples of the curves for $u_1/w_o = f(\xi)$ in *Figure 4*, corresponding to the values given for

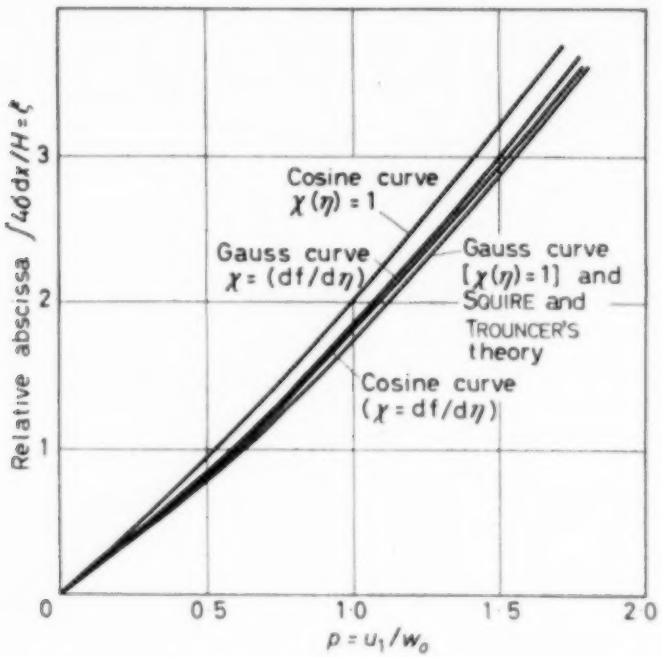

Figure 4. Axisymmetric free jet with ambient velocity

K, a and b respectively in *Table 2* (axisymmetric jet) and we have also shown the curve deduced from Squire and Trouncer's theory[4]. All the overall calculation results clearly lie within a comparatively narrow range and the Gaussian curve is seen to be less affected by the function $\chi(\eta)$ than the cosine curve.

Table 2. Axisymmetric jet

Constant	K	$\chi(\eta) = 1$		$\chi(\eta) = df/d\eta$	
		a	b	a	b
Gauss curve	0·500	0·125	0·425	0·125	0·378
Cosine curve	0·579	0·096	0·0283	0·083	0·363

CONFINED JET IN A DUCT OF CONSTANT HEIGHT

The interest of a jet confined in a duct of constant height is that it occurs very frequently in practice. Furthermore, if the displacement thickness δ_1 of the boundary layer is neglected with respect to the half-height h of the chamber, the set of jet equations can be integrated in close form. The variable u_1 obtained from equation 9 is substituted into equation 8, which gives us, after integration,

$$-\frac{3}{2}R^2 + R + K\frac{R^2}{\lambda^{\delta+1}} = 2^{1-\delta}\frac{Mh^{\delta+1}}{Q^2} = m \qquad \ldots\ldots [19]$$

where $q/Q=R$ and $l/h=\lambda$. Coefficient m is a similitude parameter expressing both the constancy of the discharge Q and of the thrust term ρM (sum of momentum flux and pressure force) and plays an essential part in the physics of confined jets. Since relation 19 applies both in an established regime (K = constant) and in the potential core (K varying with x), the value of m can be deduced by substituting the values of R, λ and K at the nozzle mouth section, equation 19.

If we substitute the value deduced in equation 19 for λ into equation 12, we can integrate this and, by calculation [Gaussian curve with $\chi(\eta)=1$], find the set of curves for the excess discharge as a function of a reduced abscissa shown in *Figures* 5(a) (two-dimensional jet) and 5(b) (axisymmetric

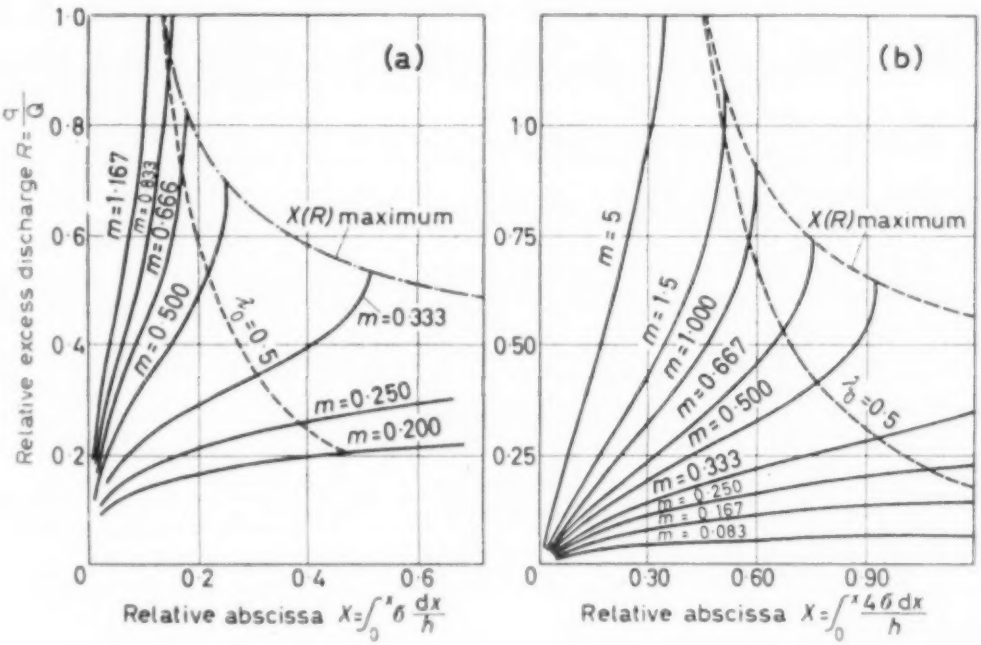

Figure 5. Relative excess discharge versus X for (a) *two-dimensional, and* (b) *axisymmetric, jet*

jet) respectively. These are used to find the sets of curves giving the relative effective width λ of the jet as a function of X for various values of the parameter m [*Figures* 6(a) and 6(b)]. It should be noted that these calculations do not require any special assumptions to be made regarding coefficient σ.

It may be useful to examine whether these curves can be reduced to a single one by affinity, and we should also like to show how the free jet with ambient velocity can be obtained as a limiting case of a confined jet. If h and Q become very large, the variables R and λ become very small; furthermore, m becomes equivalent to $KR^2/\lambda^{\delta+1}$ and also tends to disappear. We can avoid this difficulty by transforming the non-dimensional variables of the confined jets (h = constant) in such a way as to bring out the variables we have already used for u_1 = constant. We merely have to divide $\lambda^{\delta+1}$, R and $\chi^{\delta+1}$ by m to obtain the sets of curves in

Figure 7(a) (two-dimensional case) and *Figure 7*(b) (axisymmetrical jet case) giving the relative effective width in terms of the reduced abscissa; the case of a free jet with an ambient velocity occurs when $m=0$. The tangent to the common origin of the whole set of curves represents the case of a free jet with zero ambient velocity. It does not seem therefore as if a universal theoretical curve can be obtained for a confined jet.

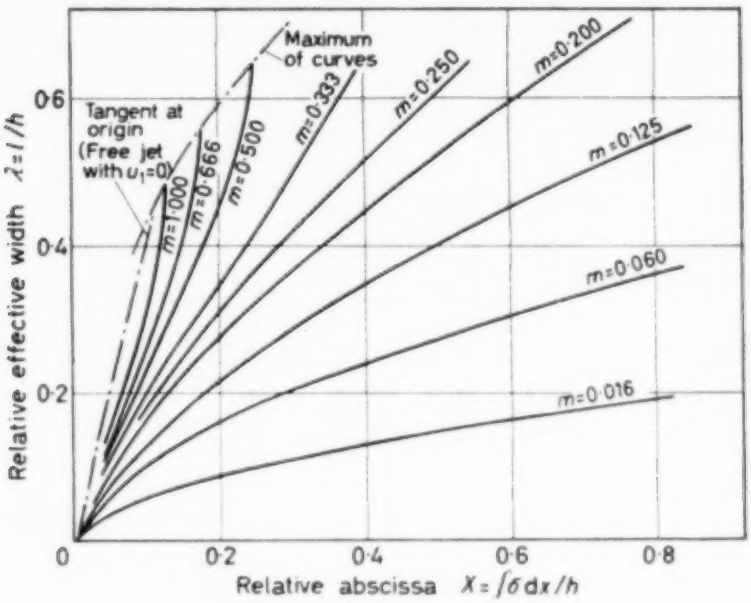

Figure 6 (a)

Figure 6. Relative effective width versus X for (a) *two-dimensional, and* (b) *axisymmetric, jet*

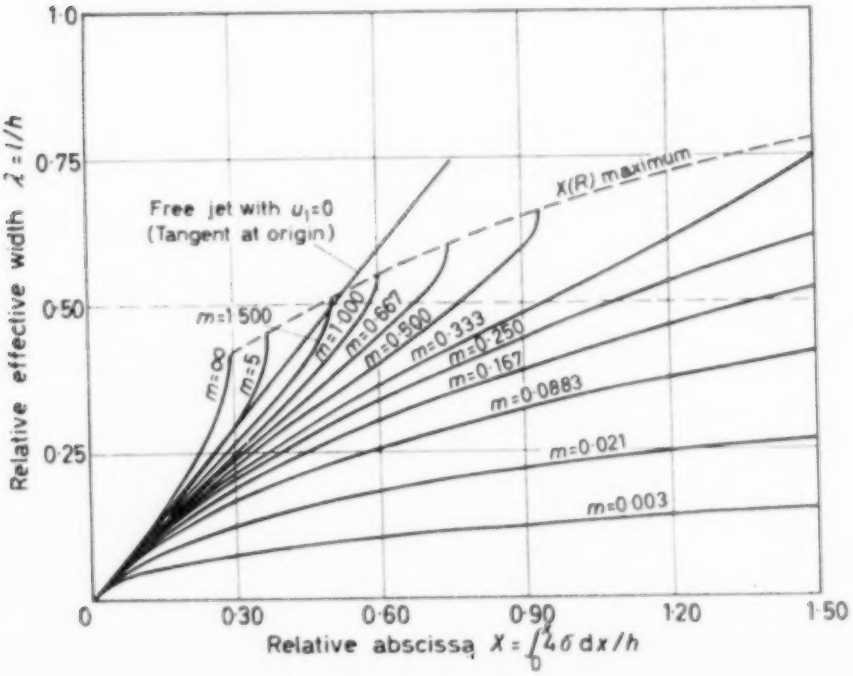

Figure 6 (b)

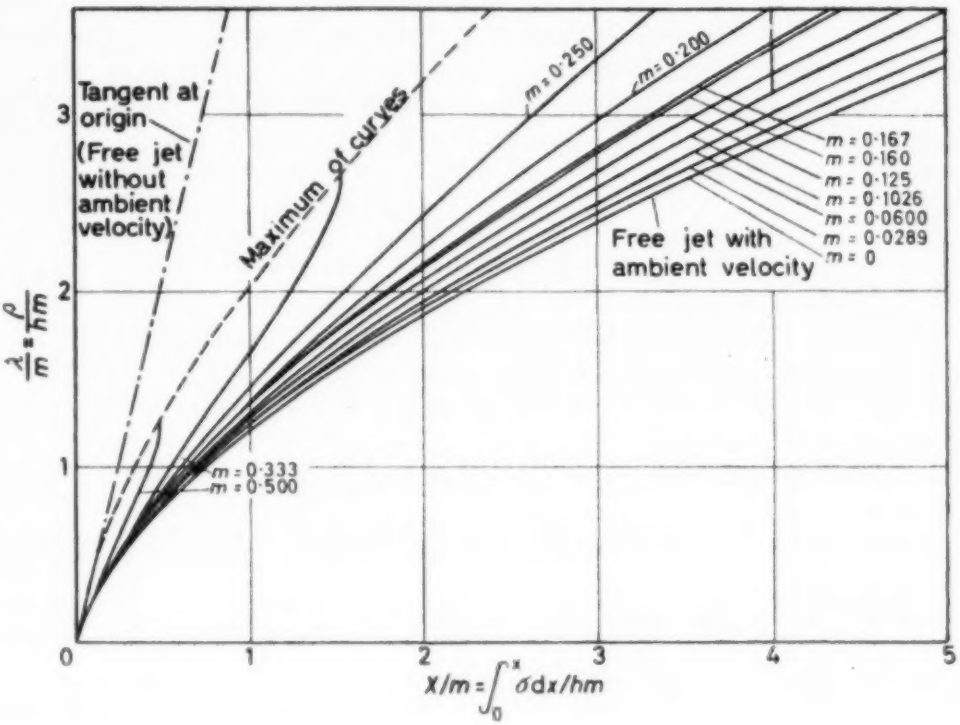

Figure 7 (a)

Figure 7. X/m versus λ/m for (a) *two-dimensional, and* (b) *axisymmetric, jet*

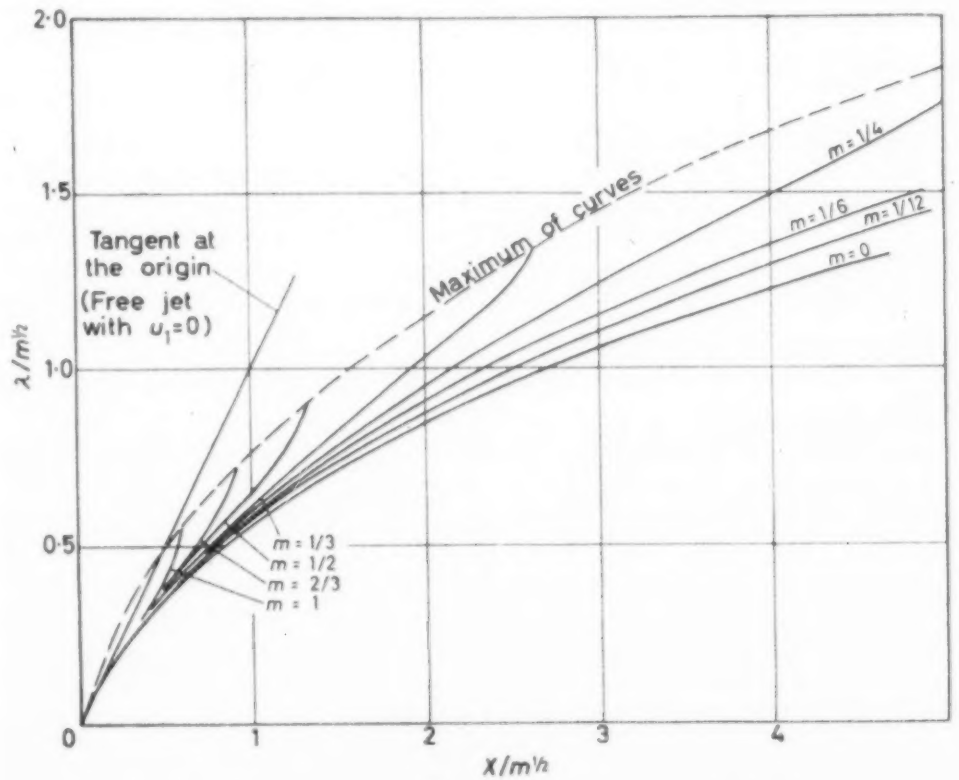

Figure 7 (b)

Figure 8 is a reduced coordinate graph featuring the set of curves (two-dimensional jet) showing how the reciprocal of the square of the excess velocity on the axis evolves along the abscissa. These show that, at conditions near those of a free jet with an ambient velocity ($m < 0{\cdot}2$), the curves can be considered as straight lines, thus providing theoretical confirmation of an experimental result obtained by A. A. WEINSTEIN, J. F. OSTERLÉ and W. FORSTALL[10]. At the same time, it is seen that this result

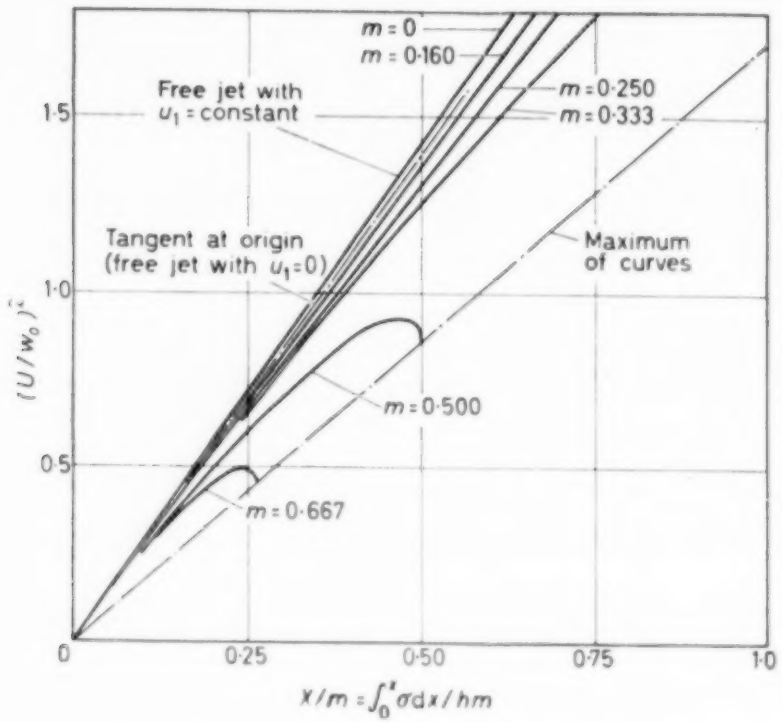

Figure 8. X/m versus $(U/w_0)^2$ for two-dimensional jet

only applies to a certain range of confined jets, which is also further confirmed by our own test results. In this connection, D. B. SPALDING'S recent success[10] in showing the predominant influence of the air supply on the rate of spread of pre-mixed flames is most interesting.

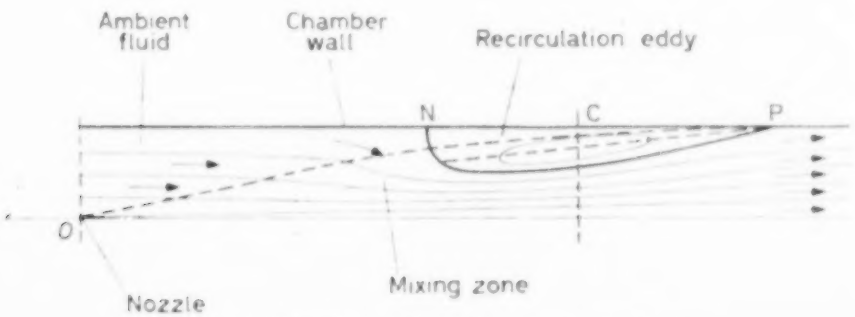

Figure 9. Two-dimensional jet with recirculation

RECIRCULATION

Owing to the existence of a positive pressure gradient, the secondary velocity u_1 tends to decrease along the chamber and to disappear if the excess discharge becomes equal to the total discharge, and we therefore have to find out what this disappearance of the velocity implies physically. If we draw the network of streamlines in the chamber (*Figure 9*), we find that, if at a certain section $u_1 = 0$, the streamlines inflect towards the jet axis, and that the total discharge is entrained at the abscissa N for which $u_1 = 0$. Beyond N, the jet tends to entrain further fluid, which it can only do at its own expense by creating a recirculation eddy. The concept of recirculation is therefore intimately related to the disappearance of the secondary velocity. The secondary velocity only occurs as long as the jet has not reached the walls, a condition that is expressed by setting a limit λ_0 of approximately 0·5 (according to the structure of the excess velocity curve) to the relative effective width λ. By drawing the limiting curve $\lambda_0 = 0{\cdot}5$ on to each set of $R(X)$ curves [*Figures 5*(a) and 5(b)], we define a range $\lambda < \lambda_0$ beyond which the theoretical curve ceases to have any physical meaning. Some of the curves within this range reach the ordinate $R = 1$ (recirculating jet), and others do not (non-recirculating jet), so that the limiting condition for the recirculation eddy is at $m = m_c = 0{\cdot}92$ in the two-dimensional case, and at $m_c = 1{\cdot}50$ in the axisymmetric jet case. This calculation also enables the point of zero velocity N to be located and its evolution for various parameters m to be investigated. It can even be used to analyse the characteristics of the recirculation eddy, as we shall see in detail later on, when we consider the axisymmetric jet case.

EXPERIMENTAL RESULTS ON TWO-DIMENSIONAL CONFINED JETS

(a) *Experimental rigs*

Two different test rigs were constructed. The first of these was used to bring the various régimes of the jet and the effect of the nozzle height on the general properties of the mixing process into evidence. The second rig was designed for a detailed analysis of the velocity and pressure distribution inside the chamber, in order to be able to compare the experimental results with the theory.

Both rigs included primary and secondary water supply systems, a mixing entrance, a diffuser with an included angle of 7°, and a collecting chamber for the overall flow. *Figures 10*(a) and *10*(b) show the respective entrance cross sections of the two chambers and their nozzles; the length of the mixing box was 400 mm in both cases. The profiles of both the nozzle and the converging section supplying the secondary flow to the rig were specially designed to ensure that both flows would be parallel when they came into contact with each other, and that the streamlines would converge smoothly upstream of this point [*Figure 10*(c)]. Provision was made for moving the induction nozzle about its major axis, to enable the jet to be aimed accurately along the centre line of the mixing chamber.

The velocities were derived from total and static pressure measurements. Static pressure tappings were provided at a large number of points on the chamber wall and hollow cold drawn nickel needles with a bore of 0·5 mm

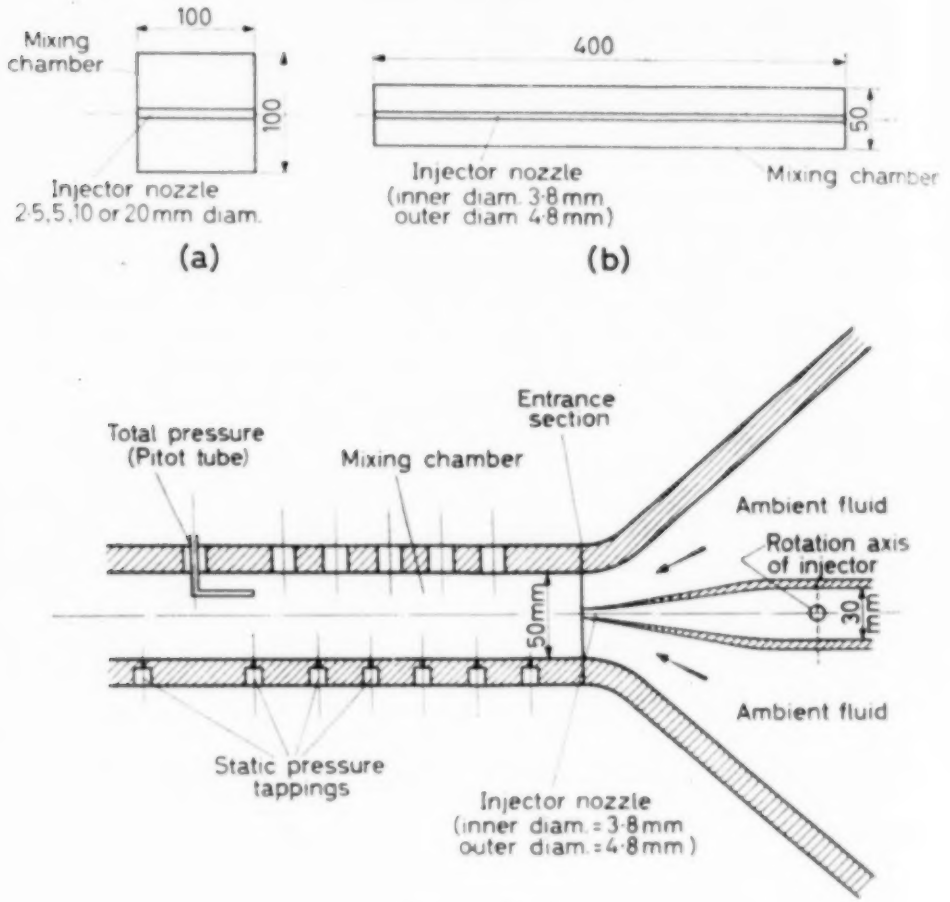

Figure 10 (c)

Figure 10. Entrance cross section of (a) *first rig, and* (b) *second rig;* (c) *arrangement of second rig. Dimensions given in mm*

and an outside diameter of 1 mm were used for the total pressure measurements. The pressures were indicated by a mercury U-tube manometer reading to within 1/50 mm. The Young and Mass correction was applied to the pressure readings. The mixing chambers on both rigs were made of Perspex, to render the mixing zone visible and to bring the various states of flow into evidence.

(b) *Qualitative study of principal flow régimes*

On a given installation, which was characterized by the ratio of the nozzle height $2a$ to the chamber height $2h$, we observed the changes in direction of the trajectories in the mixing chamber at decreasing ambient discharge and for a constant nozzle discharge.

Symmetrical trajectories about the plane of the major axis of the nozzle were observed at high ambient discharges [*Figure 11*(a)]. The trajectories outside the jet then inflected towards the axis and the slope of the pressure line steepened as the ambient discharge decreased. A further reduction in the discharge caused two eddies to form at a definite moment and at a definite abscissa of the chamber, subsequently becoming wider as the

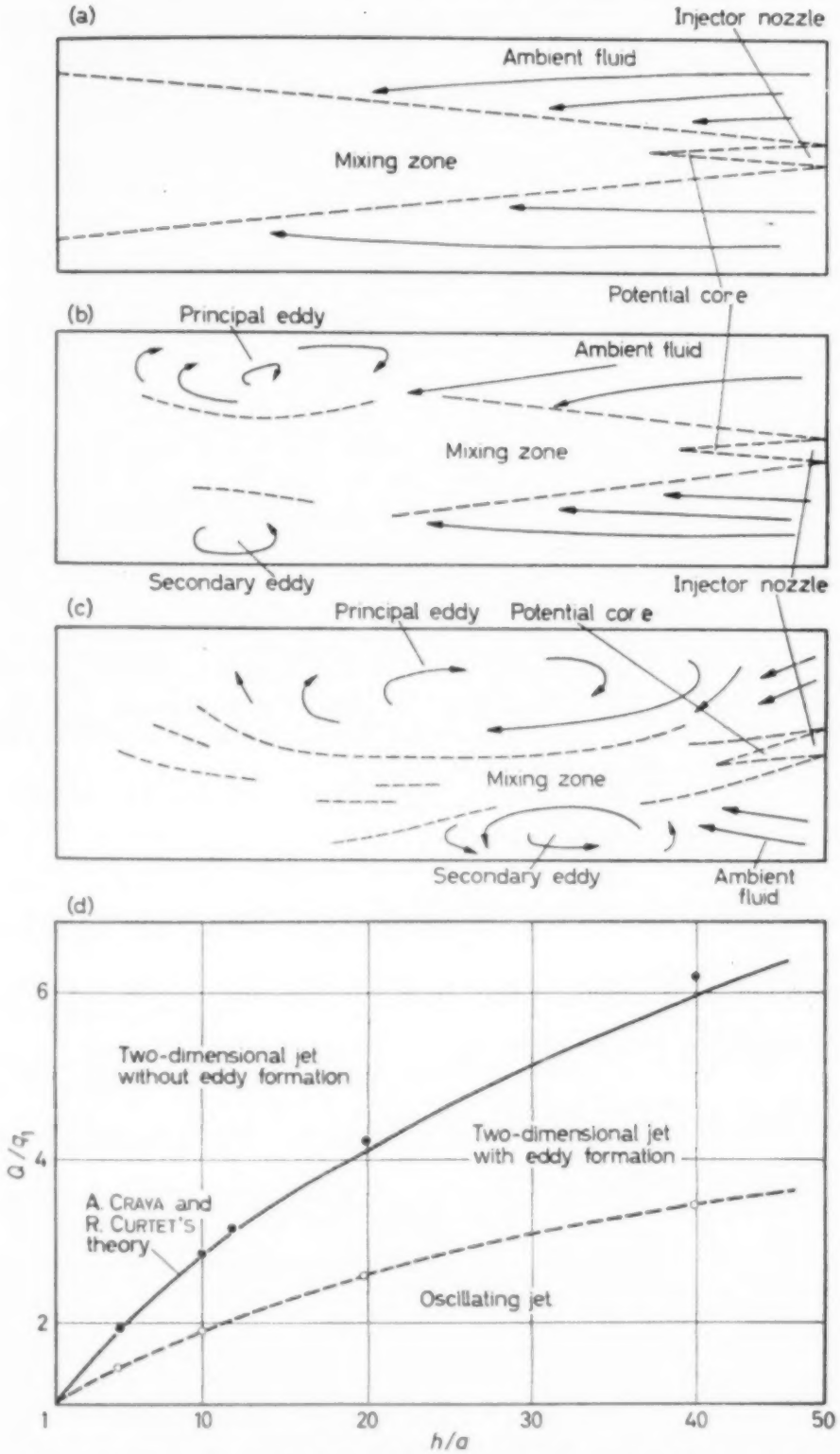

Figure 11. Two-dimensional jet (a) *without, and* (b) *with, eddy formation.* (c) *Oscillating two-dimensional jet—instantaneous view.* (d) *Performance characteristics of two-dimensional jets. Full line: theoretical;* ●, ○ *experimental*

discharge continued to fall off; the upper and lower eddies were also seen not to be of the same size [*Figure 11*(b)]. At still lower discharges, we found that these eddies, which had originally remained stationary, were now in a state of sustained oscillatory movement [*Figure 11*(c)]. The tests were carried on until the entire nozzle discharge flowed back into the ambient fluid supply duct, at which point the oscillation of the jet reached a maximum.

A similar development of these phenomena was observed when these operations were repeated at other h/a ratios. The essential results of these observations are shown in condensed form in *Figure 11*(d), which also gives the limits separating the three principal flow régimes (i.e. non-recirculating symmetrical jet, jet with stationary eddies, oscillating jet). A more detailed analysis of each of these states now follows.

(c) *Two-dimensional jet with eddy formation*

We have compared the experimental limiting curve [dashed, *Figure 11*(d)] for the formation of an eddy and the theoretical condition found earlier on. The theoretical limiting curve is plotted in *Figure 11*(d) and shows good agreement with the experimental points while noting that $k_c = 0{\cdot}93$ at the entrance to the chamber. We also compared some of the characteristics of the principal eddy with the theory, especially the abscissa of the upstream zero velocity point N, by visualizing the flow with powdered aluminium and (cotton) threads to indicate the local flow directions. The theoretical curve was calculated assuming $\sigma = 0{\cdot}024$, this coefficient having been obtained from the tests with a symmetrical jet described below. *Figure 12* contrasts the experimental and theoretical values for conditions at points N and P of *Figure 9*.

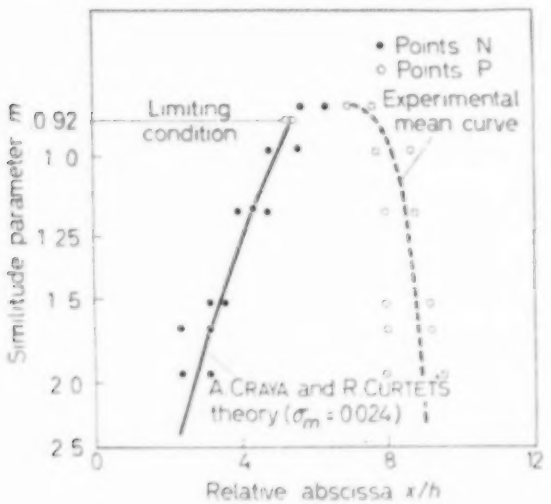

Figure 12. Two-dimensional jet with recirculation eddy as in Figure 9

In the case of the oscillating jet, we measured the oscillation period T occurring at various primary and secondary discharge ratios and for various nozzle sizes. The question arises as to whether the period is not in fact related to the similitude parameter m, which combines the essential parameters such as a, h, Q and the primary discharge q_1; in order to

investigate this we plotted the graph shown in *Figure 13*, with the values for m deduced from the test conditions on the abscissa, and the non-dimensional group D^2/QT on the ordinate, D being a characteristic dimension of the chamber defined by $2h/D = 1 + 3{\cdot}30\,a/h$. The experimental points all lie in a group around a single curve that is close to the straight line

$$m^{1/2} - 1{\cdot}45 = 50\,D^2/QT$$

except when m is small (<2). These results emphasize the predominating influence of the term m and also reveal that the ratio a/h has a certain effect which becomes negligible as a/h itself becomes very small.

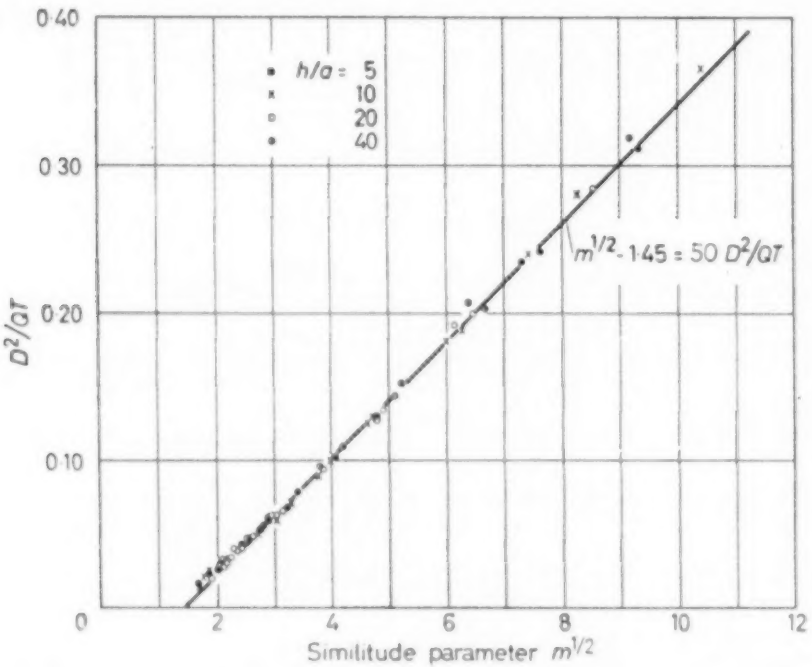

Figure 13. D^2/QT versus $m^{1/2}$ for the oscillating two-dimensional jet

(d) *Two-dimensional jet without eddy formation*

The symmetrical flow pattern of the two-dimensional jet without eddy formation allowed a more detailed analysis of the mixing process to be conducted than in the previous case. We began by examining the evolution of the excess velocity along the axis at various values of m, both positive and negative, depending on whether the velocity in the nozzle was greater or less than that of the ambient fluid at the mixing chamber entrance. *Figures 14* and *18* show the set of curves obtained, plotted on a non-dimensional basis; the highest value of m was obtained at a régime close to that at which an eddy appears, and the lowest value of m expresses the zero nozzle discharge case, or, in other words, provides an example of a wake between walls. *Figure 15* shows the variation of the effective width of the jet at positive values of m. As m approaches 0, the concept of an effective width becomes more difficult to define, for the velocity curves take on the trend shown in *Figure 16* and are affected by the wake due to

the thickness of the nozzle walls. The distribution of the excess velocities along the axis is also disturbed by this wake, so that the case in which the nozzle velocity and that of the ambient fluid are equal appears only as an ideal. Another interesting fact that came to light when we examined the negative values of m was that there can be two velocity curves on the axis for the same given value of the parameter m. This is explained by *Figure 17*, which shows the relation 19 at the entrance to the mixing chamber. It is seen that there is a minimum value of m for a given h/a ratio, and this value also corresponds to a limiting curve in *Figure 14*.

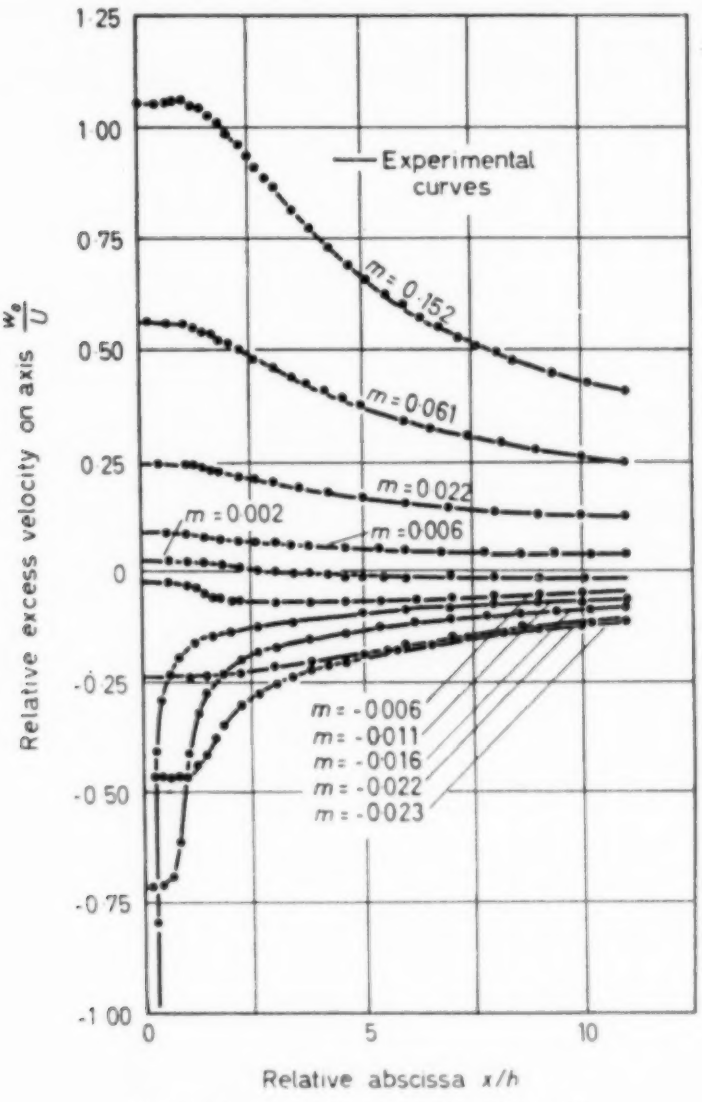

Figure 14. Two-dimensional confined jet

The excess velocity and effective width curves can be compared with the curves obtained from our theory. Before making this comparison, we verified the invariance of the total discharge and of the coefficient m. The first analysis provides a check of the two-dimensionality of the flow and the second measures the effect of the boundary layer growth, which

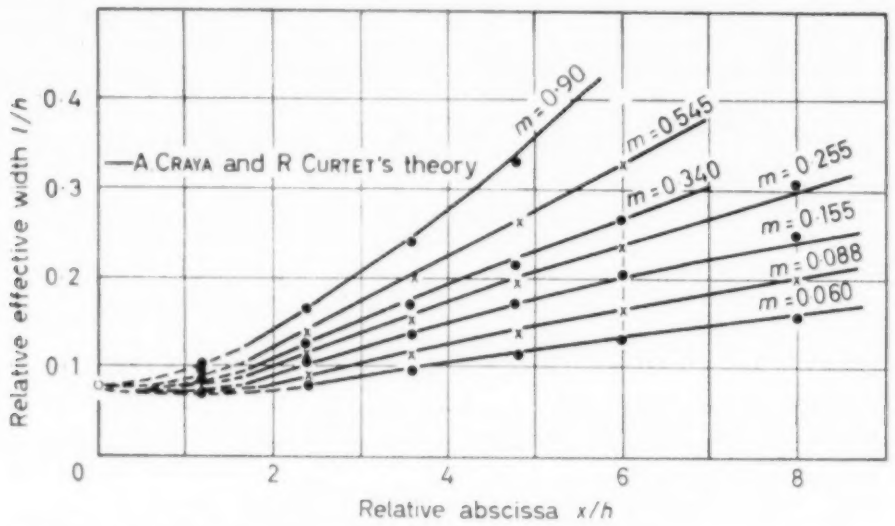

Figure 15. Variation of effective width at positive values of m for two-dimensional confined jet. $\sigma = \sigma_m$—see Figure 19

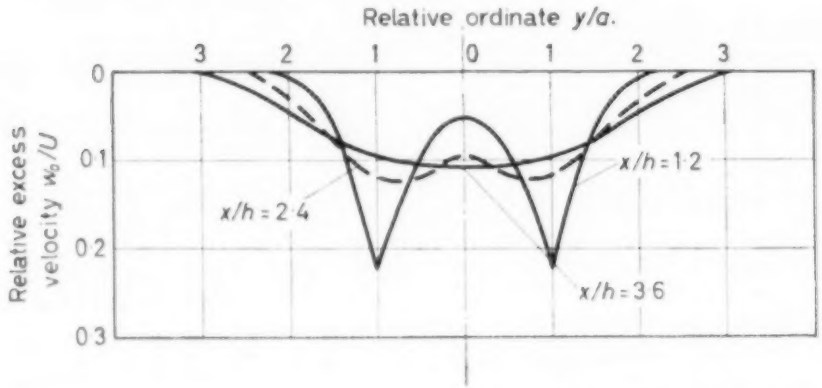

Figure 16. Velocity curves for negative values of m approaching zero

is neglected in the theory and tends to reduce m as calculated from equation 19. This probably explains the fact that the excess velocity curves plotted on a logarithmic scale in *Figure 18* diverge from the calculated curves. Examination of these curves then reveals four characteristic zones

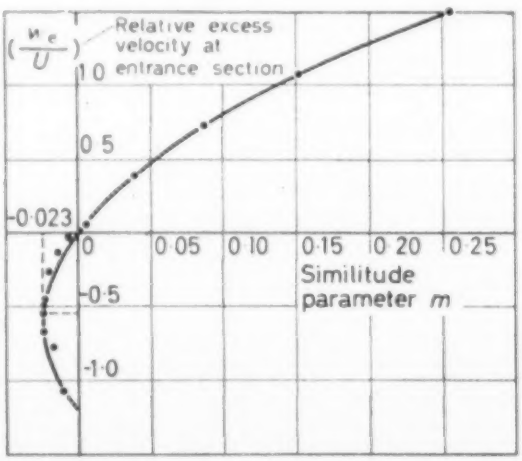

Figure 17. Curve of equation 19 at mixing chamber entrance when $K_e = 0{\cdot}93$

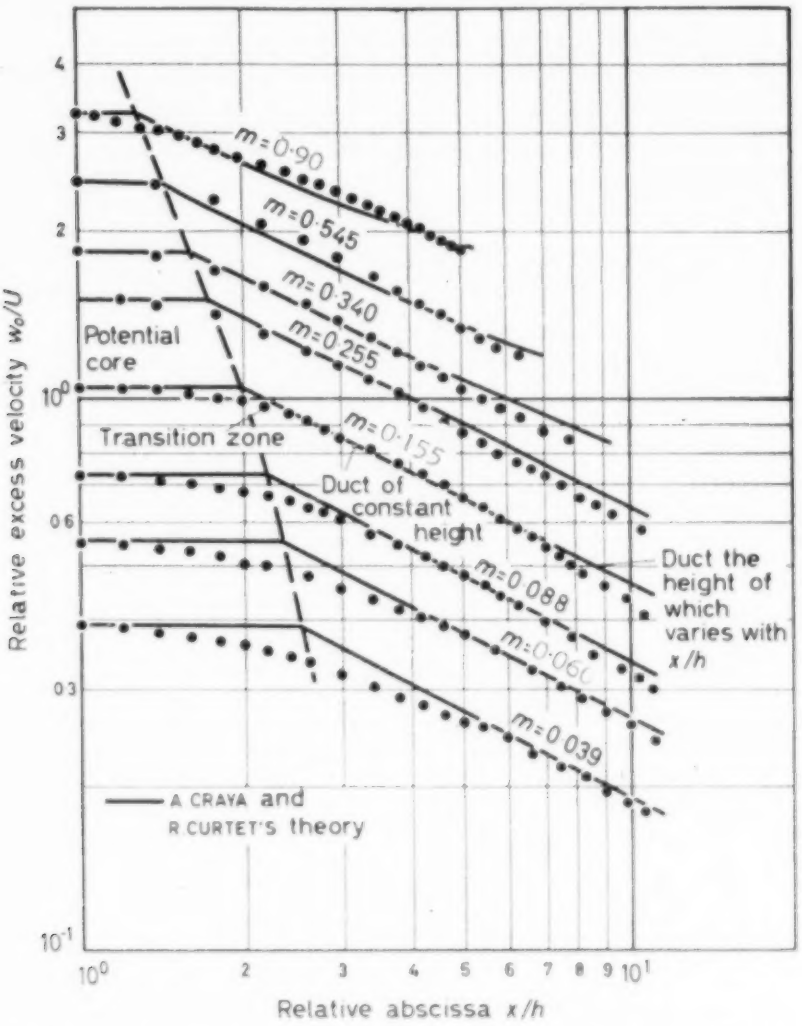

Figure 18. Excess velocity curves for two-dimensional confined jet on log/log *basis.* $\sigma = \sigma_m$ — see Figure 19

for the jet: the potential cone, a transition zone, an established régime in a duct of practically constant height and, subsequently, an established régime in a duct the height of which varies with the abscissa as a result of the boundary layer. Later on, of course, a new region appears when the jet reaches the walls.

Our theory of confined jets can be compared with the tests by first assuming that coefficient σ is independent of x and equal to an average value σ_m. Good agreement within the established régime zone has been obtained between the experimental results and the calculation made on this basis, as can be seen from *Figures 15* and *18*, provided the values of σ_m are those plotted against m in *Figure 19*.

The values thus obtained for σ_m are seen to vary between 0·024 and 0·034, whereas the free jet tests described previously produced values for σ_m lying between 0·028 and 0·034. The values therefore agree to within a good degree of approximation, although one is quite justified in speculating

about the reasons for the variation of σ_m displayed in *Figure 19*. During our experimental study, we had to vary the velocity at the nozzle within wide limits, for positive values of m, since the ambient fluid discharge was limited; the supply conditions to the nozzle may therefore have affected σ_m (e.g. nozzle convergence, degree of turbulence, eddy formation at the nozzle mouth, etc. . . .). We need hardly stress the importance of variations of σ_m; this fact has already been brought into evidence in previous work,

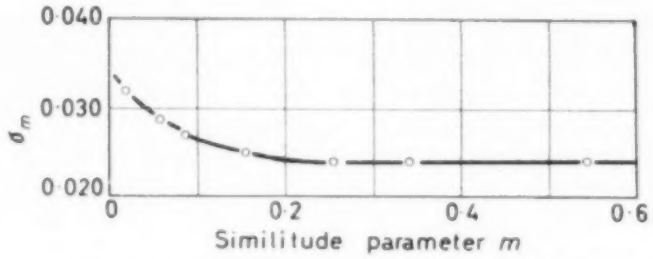

Figure 19. Average value of shear stress intensity versus similitude parameter

and W. D. BAINES[11] in particular has analysed all the known results obtained with free jets to date, from which it appears that the initial evolution of the jet seems to depend upon the conditions upstream and possibly upon the Reynolds number.

We have so far been assuming a mean value σ_m for σ, but σ also seems to vary in terms of the abscissa (see *Figure 20*), and this in a range in which the coefficient K has reached a constant value at which the reduced velocity curve is in equilibrium. This variation of σ was computed in inserting into the RHS of equation 12 the experimental values of w_m, l and

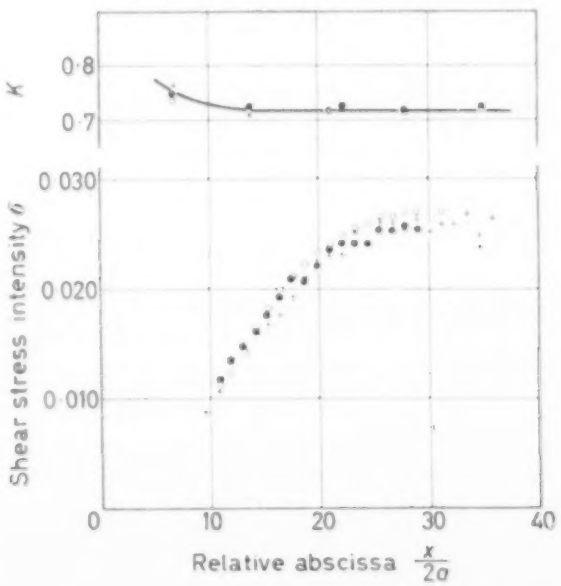

Figure 20. Variations of shape coefficient K of excess velocity curve and of σ with relative abscissa $x/2a = 6{\cdot}6\, x/h$

$\pm m = 0{\cdot}255$

$\bullet m = 0{\cdot}340$

$\circ m = 0{\cdot}545$

u_1; the derivation of σ from direct measurements of the stress are contemplated.

EXPERIMENTS ON A CONFINED AXISYMMETRIC JET WITH RECIRCULATION

For an experimental study of an axisymmetric jet along the same lines as our two-dimensional jet investigation, we have been using a similar rig to the one described above, but our results are incomplete as yet. As in the two-dimensional case, there are two possible essential régimes, depending on whether or not the mixing process occurs with a recirculation eddy in the chamber. The existence of this eddy causes the jet to recirculate its own fluid, an idea that appears to be highly important for diffusion flame furnace research (e.g. open-hearth furnaces). Tests have recently been carried out along this line at the S.O.G.R.E.A.H. laboratories in Grenoble on behalf of the International Flame Research Foundation. At the suggestion of Professor A. CRAYA, Chairman of its Aerodynamics Panel, we compared the results of these tests with those obtainable from our theory of confined jets. The following is a brief description of these results.

(a) *Experimental model (Figure 21) and tests carried out by the S.O.G.R.E.A.H.*

Two schematic furnaces were built by S.O.G.R.E.A.H. to a scale roughly of 1/10 of the experimental furnace at IJmuiden. One of these models was square in cross section, measuring 200 × 200 mm, and the other had a 225 mm diameter circular cross section; both were 630 mm long. The nozzle in each model was fitted at the mixing chamber entrance, its centre-

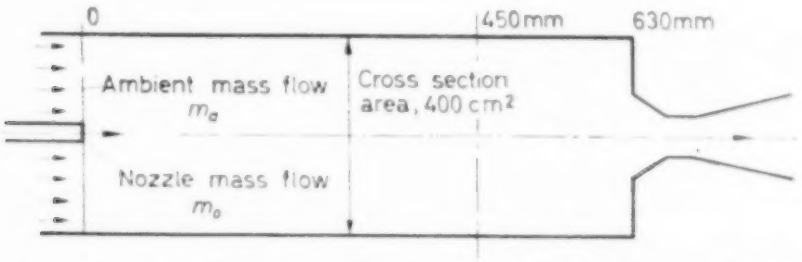

Figure 21. Experimental model furnace used by the S.O.G.R.E.A.H.

line coinciding with that of the mixing chamber, and was supplied with air at ambient temperature. Air at the same conditions was used for the secondary fluid, which entered the mixing chamber in an evenly distributed stream around the nozzle. The ambient velocity was low enough in all cases for the jet to be accompanied by a recirculation eddy. In their first set of tests G. COHEN DE LARA and R. PERRIN (S.O.G.R.E.A.H.) investigated the symmetry of the flow pattern within the chamber and were able to obtain a stable ring vortex with its axis of symmetry coincident with that of the furnace[12]. This symmetry was observed in all the tests during which the nozzle radius a and the ratio of the ambient fluid and nozzle

mass flows m_a/m_o were varied. The range of the M. W. THRING and M. P. NEWBY[13, 14] parameter θ_r considered in this way

$$[\theta_r = (m_o + m_a)\, a/m_o h]$$

ly between 0·08 and 0·32, the a/h ratios ranging from 0·027 to 0·09.

The velocity distribution within the recirculation zone obtained from the test measurements was of the form shown in *Figure 22*. It contains two

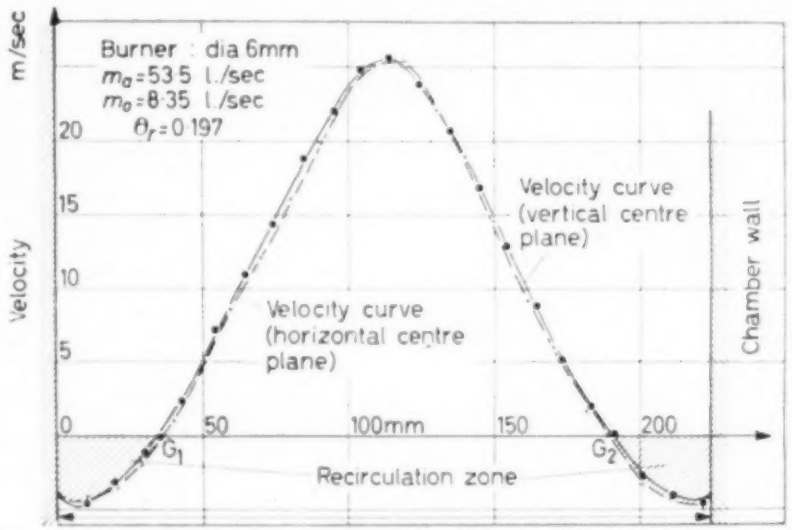

Figure 22. Velocity distribution found in circular cross section chamber during the S.O.G.R.E.A.H. tests

points G_1 and G_2 at which the longitudinal velocity is zero: their locus in a meridian plane of the furnace forms the boundary of the recirculation zone. The S.O.G.R.E.A.H. tests showed that the recirculation zone increases as θ_r decreases, although it undergoes practically no change if the nozzle (or burner) momentum is varied for a constant θ_r. The two examples in *Figure 22* show that the recirculation area is quite considerable compared with the chamber area [*Figures 23*(a) and *23*(b)].

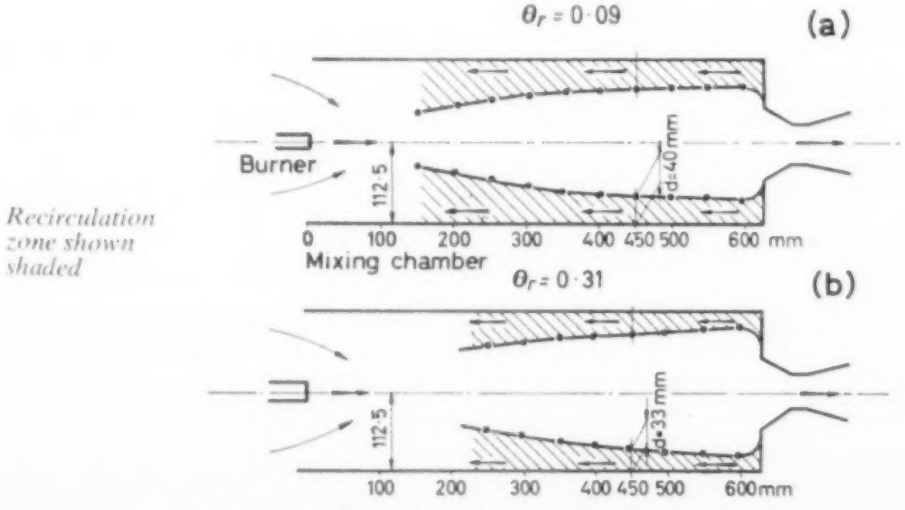

Figure 23. Recirculation boundaries (S.O.G.R.E.A.H. tests)

The recirculation discharge along the furnace was investigated for $\theta_r = 0{\cdot}264$ on the circular model. This recirculation discharge is defined by the integral of the negative velocities across the cross section shown by shaded areas in *Figure 23*. *Figure 24*(a) shows the variation of the ratio of the recirculation discharge to the total discharge q_r/Q, which is zero between the burner and a point some distance away from it, then increasing

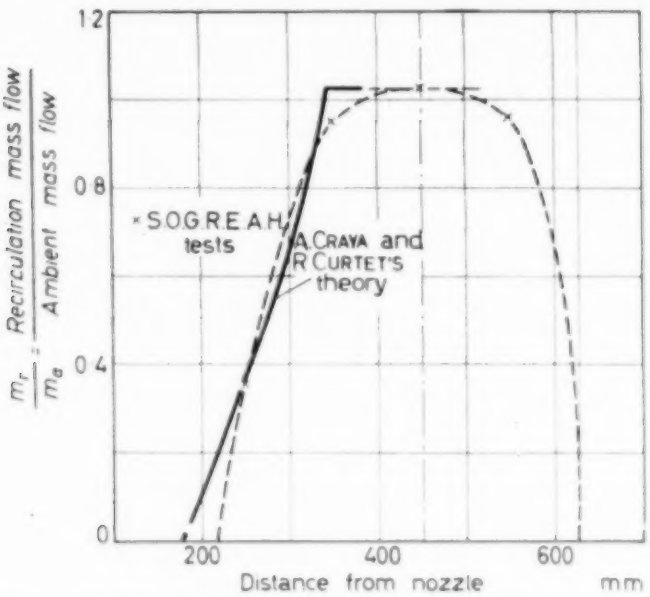

Figure 24 (a). *Variation of ratio of recirculation discharge to total discharge with distance from nozzle (or burner)*

and tending towards a maximum before finally falling off. The diagram shown in *Figure 24*(b), which was plotted by taking both the test results and the continuity equation into account, shows the mean streamlines in the furnace. This distinguishes clearly between the recirculation boundary, the mixing zone boundary and the effective width of the jet. It also brings

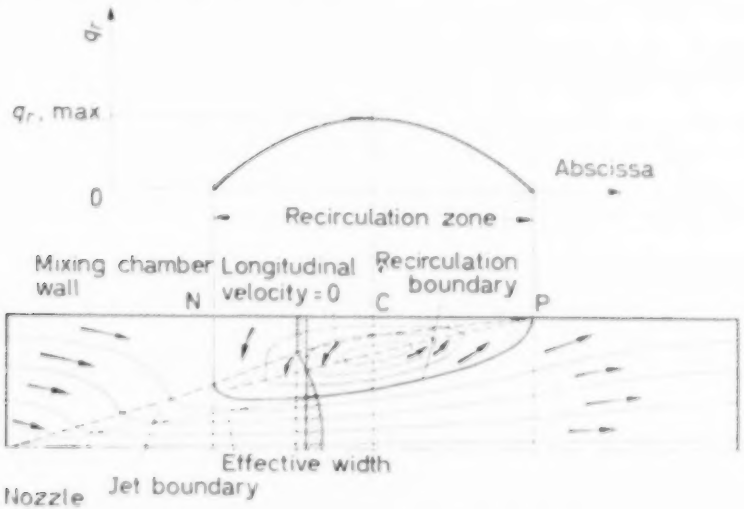

Figure 24 (b). *Axisymmetric jet streamlines with recirculation eddy*

out the fact that, beyond the centre C of the eddy corresponding to the maximum recirculation discharge, the jet feeds fluid back to its own eddy before reaching the wall at P.

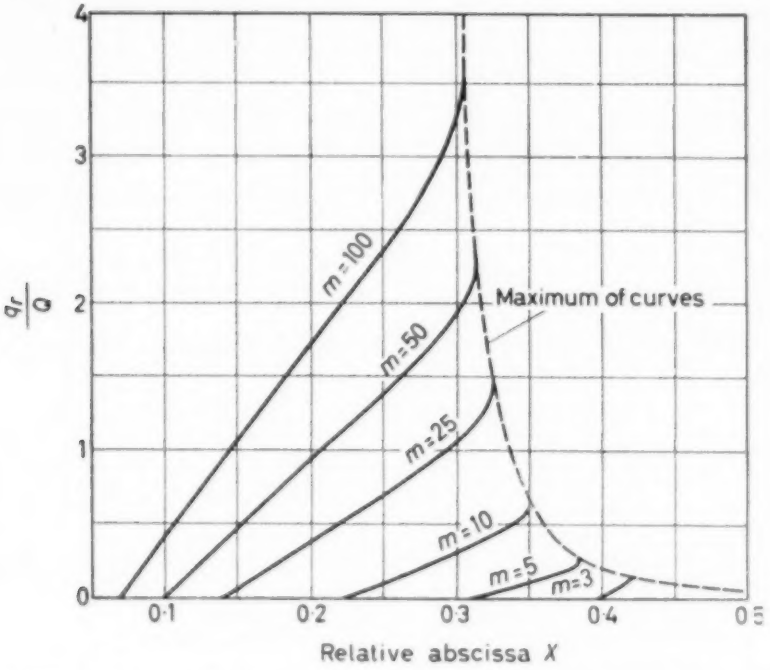

Figure 25. Variation of relative recirculation discharge $[q_r/Q = m_r/(m_a + m_g)]$ *against relative abscissa* $[X = \int_0^x (4r/h)\,dx]$

The S.O.G.R.E.A.H. team followed up this preliminary investigation with several systematic tests in order to find the maximum recirculation discharge for various values of θ_a, as well as hot air test points investigating the temperature distribution along the centreline. The test points for the maximum recirculation discharge are plotted in *Figure 27*.

(b) *Recirculation theory*

The recirculation discharge can be deduced easily from the three main variables previously considered in our approximate theory of jets: if we know the total discharge Q, the excess discharge q, and the effective width l in a cross section of radius h, we can show, by means of *Figure 22*, and assuming the velocity curve to be Gaussian, that

$$\frac{q_r}{Q} = (R-1)\left\{\lambda^2\left(1 - \log\left[\frac{\lambda^2(R-1)}{R}\right]\right) - 1\right\}$$

We shall assume that the basic hypotheses of the theory still hold good in the zone of the eddy lying between N and C [*Figure 24*(b)]. The affinity of the velocity profile was actually observed by the S.O.G.R.E.A.H. team, and our two-dimensional tests showed us that the energy of the ambient fluid only varies slightly in the zone NC.

Under these conditions, calculation leads to the set of curves shown in *Figure 25*, which expresses the variation of the recirculation discharge in

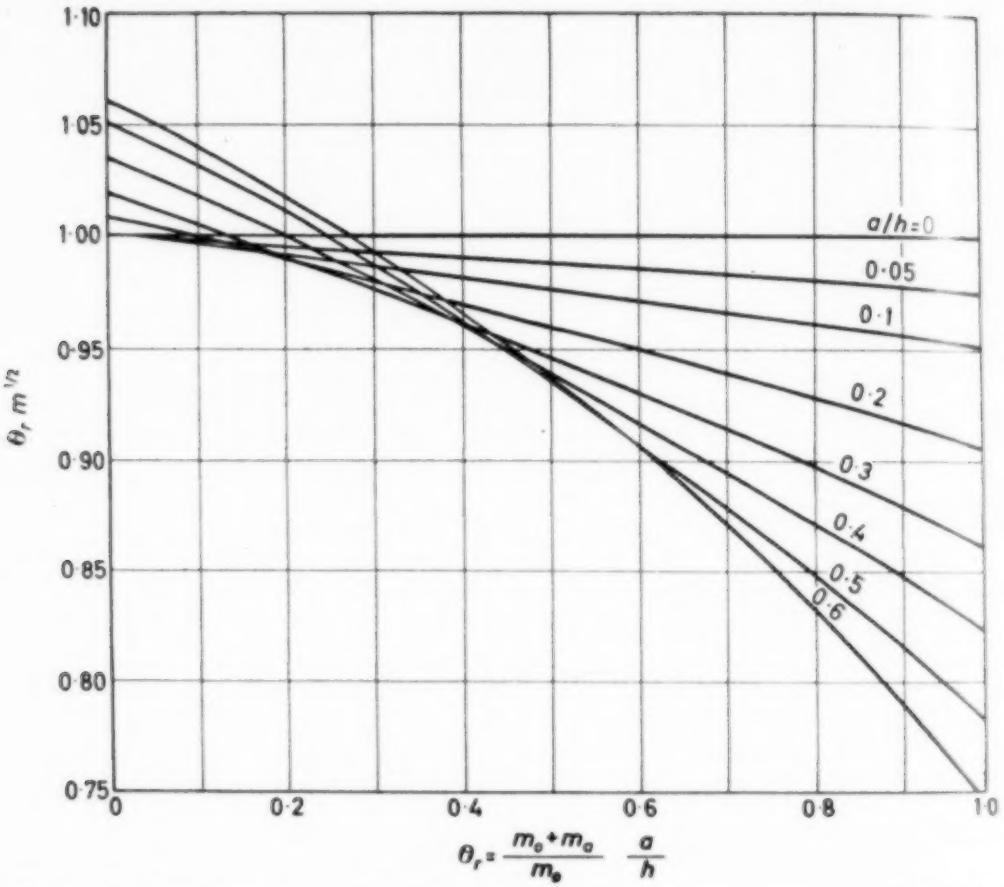

Figure 26. Comparison of similitude parameters m (this work) and θ_r developed by Thring and Newby

terms of the abscissa and the conditions at the chamber entrance included in parameter m. The theory shows that the recirculation discharge increases from a certain abscissa onwards, tending towards a critical value that is related to a maximum abscissa. We shall assume that this critical discharge value corresponds to the maximum recirculation discharge observed experimentally.

Before comparing the calculations with the tests, it is important to verify whether a link exists between our similitude parameter m and Thring and Newby's parameter θ_r. By eliminating the discharge ratio between relation 19 defining m and that defining θ_r

$$\theta_r = (m_o + m_a)\, a / m_o h$$

we obtained an equation of the form

$$\theta_r m^{1/2} = \mathrm{f}(\theta_r, a/h)$$

which is expressed by the set of curves plotted in *Figure 26*. When

$$a/h = 0,\ \theta_r m^{1/2} = 1,$$

and we can see that it remains equal to 1 within 1 per cent over the range investigated by the S.O.G.R.E.A.H. team, which is also the range which includes conventional diffusion flame furnaces.

(c) *Comparison between the calculations and the tests*

For $\theta_r = 0{\cdot}265$, the theoretical curve showing the change in the recirculation discharge in terms of the abscissa agrees fairly well with the results [see *Figure 24*(a)]. For this comparison, we have assumed a constant shear stress coefficient $4\sigma = 0{\cdot}114$, this being the mean value found for a free jet.

The maximum recirculation discharge as a function of m was deduced from the set of curves in *Figure 25* and plotted in *Figure 27*. It evidently agrees well with the S.O.G.R.E.A.H. test points over the whole zone considered and also shows good agreement with the experimental results

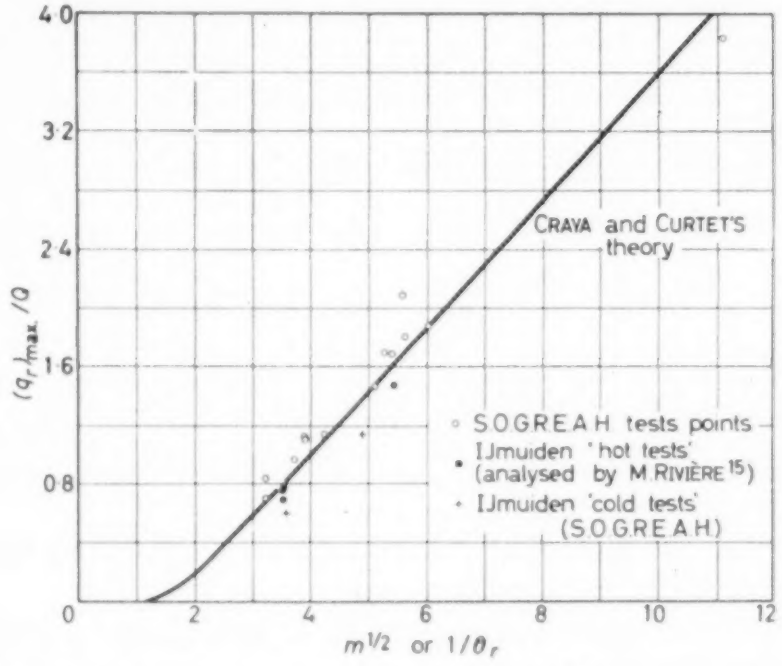

Figure 27. Recirculation maximum relative discharge versus $m^{1/2}$ *or* $1/\theta_r$

obtained on the IJmuiden test furnace, at 'cold' conditions by S.O.G.R.E.A.H. and from the 'hot' tests carried out by the International Foundation and analysed by M. RIVIÈRE[15].

Finally, we would point out that the recirculation boundaries obtained by calculation are similar to those resulting from the S.O.G.R.E.A.H. tests (from N to C) [*Figures 23*(a) and *23*(b)].

(d) *Comparison between our theory and that of Thring and Newby*

With a view to finding a theory relating the flame length to a 'cold' model, M. W. THRING and M. P. NEWBY[13] analysed a confined jet under 'cold' conditions in terms of a free jet; as a result, they were able to determine the zero velocity points N and P as well as an approximate value for the maximum recirculation discharge. We should now like to compare this approximate study with our own second approximation.

We have assumed for this that points N, P and C (*Figure 28*) are such such that C lies half way along NP. The curves obtained from Thring and

Newby's calculations and our theoretical curves are plotted together in *Figure 28*, showing good agreement between the various results.

Thring and Newby[13] also give an approximate formula for the maximum recirculation discharge, with an unknown coefficient lying between 1 and 0·5; the value 0·5 brings this formula close to our own results.

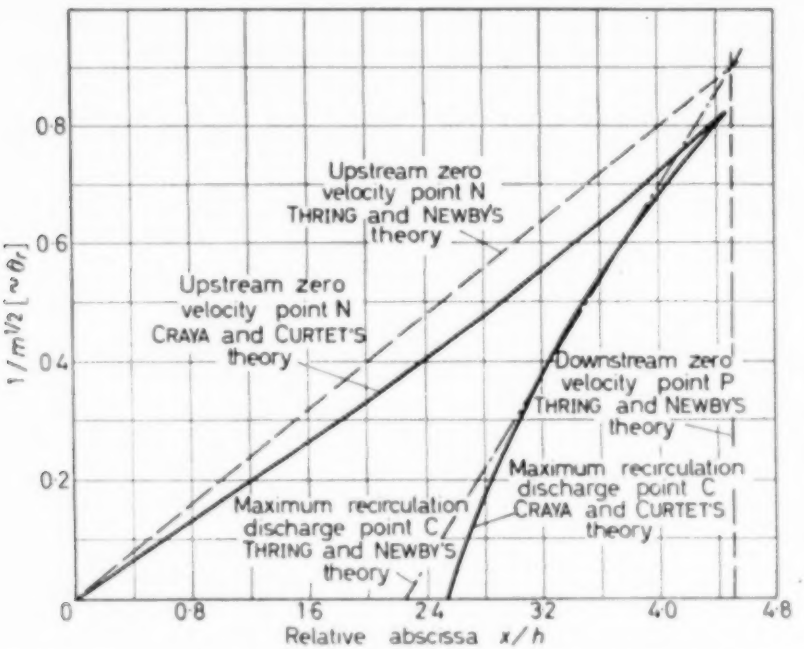

Figure 28. $1/m^{1/2}$ [$\sim \theta_r$] versus relative abscissa x/h from Thring and Newby's work compared with results of present work

It should be noted in this connection that, according to our theory, a confined jet spreads more rapidly than a free jet accompanied by an eddy, and more slowly if there is no such eddy [*Figure 6*(b)]. The curve for the reciprocal of the velocity on the centreline under axisymmetric flow conditions shows a similar trend; this fact seems to link up with the experimental results obtained under the direction of Professor M. W. THRING[14] for the distribution of the reciprocal of the concentration along the centreline, which must be connected with the velocity distribution.

CONCLUSIONS

In this paper we have shown that it is both possible and interesting to take the wall effect into account when studying the mixing of a jet with a surrounding stream enclosed in a duct.

We started by developing an approximate theory of confined jets established jointly by Professor A. Craya and the author, for two-dimensional and axisymmetric flow conditions, using the smallest possible number of hypotheses. Although the characteristics of a free jet (with or without ambient velocity) can be reduced in the form of a single curve by calculation, this cannot be done for a confined jet flowing between parallel walls, and the evolution of the mixing process is linked to the similitude parameter h/b in this case.

We then described our experiments which showed that two distinct régimes can be identified, depending on the value of parameter m, one in which the jet is accompanied by a recirculation eddy, and the other in which no eddy is formed. From the comparison with the theory in the second case, the variation along the axis of a suitable shear stress parameter and its dependence upon the supply conditions to the nozzle were investigated. In addition to this, we found it possible to bring some of the properties of a two-dimensional jet with eddy formation into evidence, particularly the localization of the eddy and the oscillation frequency of the jet.

We finally examined the recirculation of an axisymmetric jet during tests carried out at the S.O.G.R.E.A.H. laboratories in Grenoble on behalf of the International Flame Research Foundation. We calculated the recirculation discharge along the centreline and its maximum value in terms of the velocities at the entrance to the schematic furnace and we were able to obtain good agreement with the experimental results.

The data obtained so far clear the way to further research and, in particular, we are considering a direct measurement of the shear stress and an examination of the mixing zone beyond the abscissa at which the maximum recirculation discharge occurs. Furthermore, temperature or concentration variations could also be taken into account in the calculations.

Our research on the mixing of jets in a confined space was carried out in the Fluid Mechanics Laboratory of the University of Grenoble under the direction of Professor A. Craya.

University of Grenoble,
France

(Received September 1958)

REFERENCES

[1] See, e.g.: KUNUGI, MASANAGA and JINNO, HIROSHI: *Sixth Symposium (International) on Combustion*, p 311. Reinhold: New York, 1957
[2] CRAYA, A. and CURTET, R. *C.R. Acad. Sci., Paris* 241 (1955) 621
[3] TOWNSEND, A. A. *The Structure of Turbulent Shear Flow*. Cambridge University Press: London, 1956
[4] SQUIRE, H. B. and TROUNCER, J. O. *Aeronaut. Res. Coun. tech. Rep. R. and M. No. 1974* (1944)
[5] FÖRTHMANN, E. *Ingen.-Arch.* 5 (1934) 42
[6] REICHARDT, H. *Forschungsh. Ver. dtsch. Ing. No. 414* (1942)
[7] ALBERTSON, M. L., DAI, Y. B., JENSEN, R. A. and ROUSE, H. *Proc. Amer. Soc. civ. Engrs* 74 (1948) 1571
[8] HINZE, J. O. and VAN DER HEGGE ZIJNEN, B. G. *Appl. sci. Res., Hague* A1 (1949) 435
[9] CORRSIN, S. *Nat. Adv. Comm. Aero., Wash., Wartime Rep. A.C.R. No. 3L23 W 94* (1943)
[10] WEINSTEIN, A. A., OSTERLE, J. F. and FORSTALL, W. *Amer. Soc. mech. Engrs Paper No. 55-A 60* (1955)
[11] BAINES, W. D. *Proc. Amer. Soc. civ. Engrs* 75 (1949) 1018
[12] COHEN DE LARA, G. and CURTET, R. *Troisième Journée d'Etudes sur les Flammes*, Paris, February 1958
[13] THRING, M. W. and NEWBY, M. P. *Fourth Symposium (International) on Combustion*, p 789. Williams and Wilkins: Baltimore, 1953
[14] THRING, M. W., HULSE, C., SUNAVALA, P. and HORN, G. 'Mixing and combustion in free and enclosed turbulent jet diffusion flames'. International Flame Research Foundation, *Doc. No. G02/C/2* (1953)
[15] RIVIÈRE, M. *Deuxième Journée d'Etudes sur les Flammes*, Paris, December 1955
[16] SPALDING, D. B. *Seventh Symposium (International) on Combustion*. Paper No. 82. Butterworths: London, 1959

On the Calculation of Properties of Gases at Elevated Temperatures

I. AMDUR and J. ROSS

The role of the potential of intermolecular force in determining properties of gases at elevated temperatures is discussed, and the following points are emphasized. (a) *The calculation of accurate values of such properties requires potential parameters which are valid at interaction distances which are important at the temperatures in question.* (b) *Extrapolation of potentials obtained from low temperature properties for calculation of high temperature properties is, in general, not justified, and leads to values of transport coefficients and second virial coefficients which differ considerably from those calculated from potentials based on the elastic scattering of high energy molecular beams.* (c) *The high temperature range, in which such beam potentials are useful, is not determined by the kinetic energy of the beam particles, but by the small fraction of this energy which is converted into potential energy in the scattering process. For purposes of illustration, coefficients of viscosity and self-diffusion, isotopic reduced thermal diffusion ratios, and second virial coefficients for helium, argon and nitrogen at 1 000°, 5 000° and 15 000° K have been calculated from extrapolated potentials, Lennard Jones (12–6) and modified Buckingham (exp – 6), and from beam potentials.*

THE prediction of equilibrium and non-equilibrium macroscopic properties of matter from appropriate statistical mechanical theories and sufficient information of the molecular constituents (intermolecular forces, spectroscopic constants, etc.) has attracted much attention in the past decade[1]. In particular, attempts have been made to obtain thermodynamic and transport properties at temperatures and densities which, for the most part, are not readily accessible to experiment, for instance, properties of gases at extremely high temperatures.

It is the purpose of this article to comment on the choice of intermolecular forces for such computations, and the influence of this choice on the numerical results. The illustrations given, limited to several transport coefficients and the second virial coefficients for non-polar gases, may serve as indications of the reliability of past and future calculations in this field. Although available statistical mechanical theories which relate the molecular properties of a system to measurable quantities have distinct regions of applicability which may be, and indeed have been, exceeded, the effects of such misapplications are not discussed here.

Potentials of intermolecular force between atoms or molecules may be determined by three methods: (*1*) *a priori* calculations based upon solutions of the Schrödinger equation[1–4]; (*2*) interpretation of molecular scattering experiments[5–8]; and (*3*) deduction from macroscopic measurements with the aid of a statistical mechanical theory[1]. The determination of the intermolecular potential by the first two methods requires only the laws of

quantum mechanics or classical mechanics*. This theoretical simplicity, unfortunately, is difficult to exploit in practice. Except for a few very simple atomic systems exact *a priori* calculations of intermolecular potentials are beyond the capacity of the most advanced electronic computers, and molecular scattering experiments, although done, are extremely complex.

The third method has been used extensively despite the fact that many macroscopic properties are not particularly sensitive to the choice of intermolecular potentials. The determination of intermolecular potentials follows this procedure: (*1*) a transport or equilibrium property is determined as a function of temperature in a *given, finite* temperature range; (*2*) an analytical form is assumed for the intermolecular potential and the property under consideration is evaluated *a priori* with the parameters in the potential function as required by a statistical mechanical theory; (*3*) the best parameters are chosen on comparison with the experimental results. In Appendix I expressions are given for some properties to which this procedure may be applied: the coefficients of viscosity and self-diffusion, the isotopic reduced thermal diffusion ratio, and the second virial coefficient.

The conditions to be met by a generally valid intermolecular potential for a given system are clear. In principle, all thermodynamic and transport quantities should be determined by such a potential (together with other molecular properties, if necessary) at all temperatures and densities, with a single set of parameters in the potential function. To realize this it is essential to have extensive knowledge of the proper analytical form of the potential. Although the quantum theory provides a reasonably adequate answer to this problem for the interaction leading to attraction between molecules (London dispersion forces) equivalent information has not been obtained for repulsive forces. The inadequacy of simple forms of the intermolecular potential such as the Lennard-Jones potential may be illustrated as follows. Suppose an estimate of the parameters of the Lennard-Jones potential (Appendix II) is obtained for a given system from data on the second virial coefficient in a temperature range $T_2 - T_1$. If this range is not too large† a single set of parameters will suffice to reproduce the measured values to within experimental error (generally of the order of 1 per cent). If, however, the temperature range is extended it becomes necessary to ascribe an apparent temperature dependence to the potential parameters, namely, more than one set is necessary to reproduce properly the original measurements. Furthermore, the prediction of other macroscopic properties, for instance, self-diffusion coefficients, is not as satisfactory as with potential parameters which were originally determined from self-diffusion measurements.

The conclusions are evident. *Information on molecular properties gleaned from measurements of transport or second virial coefficients should be*

*Under some circumstances scattering experiments may be interpreted according to classical mechanics.

†The temperature range must, of course, not be too small. It is not possible to derive information concerning the form and magnitude of the intermolecular potential from measurements at a single temperature. This can be verified from the equations given in Appendix I.

viewed as intermolecular potentials of a very restricted kind which may be used with some confidence as interpolation devices for predicting the property from which they were derived. They may be used as an interpolation device for predicting other properties with varying degrees of success depending on the analytical form of the potential, the number of parameters, and the specific properties involved.

The equations listed in Appendix I appear to show that all portions of the potential function contribute to the calculation of the transport and thermodynamic coefficients at all temperatures. This is literally true, but it is apparent on closer inspection that a coefficient at a given temperature is determined essentially by a limited region of the potential. Although there is no direct correspondence between a temperature and an intermolecular distance, at low temperatures the potential of forces of attraction contributes to the macroscopic behaviour, whereas at sufficiently high temperatures this region of the potential is completely unimportant. Conversely, measurements of macroscopic properties at low temperatures yield information about potentials of forces of attraction, whereas measurements at high temperatures can be interpreted by a well defined potential of

Table 1. High temperature properties of helium

Temp. °K	$10^4[\eta]_1$ g cm^{-1} sec^{-1}			$10^4\rho[D_{11}]_1$ g cm^{-1} sec^{-1}		
	12-6	exp-6	beam	12-6	exp-6	beam
1 000	4·3	4·4	4·4	5·9	6·6	6·4
5 000	12·3	—*	16·3	16·9	—*	24·4
15 000	25·6	—*	41·0	35·2	—*	61·5

Temp. °K	$[k_T^*]_1$			$B(T)$ cm^3 mole^{-1}		
	12-6	exp-6	beam	12-6	exp-6	beam
1 000	0·57	0·42	0·33	10·0	9·1	17·0
5 000	0·54	—*	0·33	8·0	—*	7·6
15 000	0·54	—*	0·33	6·0	—	4·3

*Values of collision integrals and reduced second virial coefficients have not been tabulated for values of T^* as large as those required for these entries.

Table 2. High temperature properties of argon

Temp. °K	$10^4[\eta]_1$ g cm^{-1} sec^{-1}			$10^4\rho[D_{11}]_1$ g cm^{-1} sec^{-1}		
	12-6	exp-6	beam	12-6	exp-6	beam
1 000	5·4	5·4	5·6	7·1	7·3	8·1
5 000	15·2	15·6	18·6	20·6	21·7	26·6
15 000	30·7	33·2	42·0	42·0	47·4	60·1

Temp. °K	$[k_T^*]_1$			$B(T)$ cm^3 mole^{-1}		
	12-6	exp-6	beam	12-6	exp-6	beam
1 000	0·56	0·51	0·41	20·9	21·2	48·6
5 000	0·57	0·50	0·41	26·1	24·6	27·2
15 000	0·57	0·50	0·41	22·8	20·3	18·3

repulsive forces combined, in some cases, with a variety of potentials of attractive forces. This shows that if potential functions have been determined from measurements in one temperature interval, their use for predicting properties outside this temperature interval will lead to errors, except for rare, fortuitous coincidences. Stated in other terms, *the use of the intermolecular potential as an extrapolation device will lead to unreliable results.*

Table 3. High temperature properties of nitrogen

Temp. °K	$10^4[\eta]_1$ g cm^{-1} sec^{-1}			$10^4 p[D_{11}]_1$ g cm^{-1} sec^{-1}		
	12-6	exp−6	beam	12-6	exp−6	beam
1 000	4·0	4·0	3·8	5·4	5·3	5·5
5 000	11·5	11·2	13·2	15·6	15·1	19·1
15 000	23·1	—*	30·9	31·7	—*	44·8
Temp. °K	$[k_T^*]_1$			$B\ (T)$ cm^3 mole^{-1}		
	12-6	exp−6	beam	12-6	exp−6	beam
1 000	0·57	0·58	0·35	29·4	31·3	70·1
5 000	0·57	0·60	0·35	31·7	32·1	36·1
15 000	0·57	—*	0·35	27·1	—*	22·9

*Values of collision integrals and reduced second virial coefficients have not been tabulated for values of T^* as large as those required for these entries.

To support the above contentions, the coefficients of viscosity and self-diffusion, isotopic reduced thermal diffusion ratios, and second virial coefficients for helium, argon and nitrogen (*Tables 1 to 3*) have been calculated as functions of temperature. Three potential energy functions have been used: (*1*) a Lennard–Jones (12–6) potential evaluated from measured transport properties in a temperature interval near room temperature; (*2*) a modified Buckingham (exp − 6) potential evaluated from various bulk properties below 1 000 °K; and (*3*) a potential derived from the interpretation of experiments on the scattering of molecular beams. The analytical forms and the parameters of the potentials are given in Appendix II; the three potentials for the argon system are shown graphically in *Figure 1*, and numerical values at selected separation distances are given in *Table 4*.

Table 4. Magnitudes of various potentials for argon system

Lennard-Jones (12-6)		*Modified Buckingham* (exp-6)		*Beam* K/r^s	
r, Å	$\phi(r)\times10^{15}$, ergs	r, Å	$\phi(r)\times10^{15}$, ergs	r, Å	$\phi(r)\times10^{15}$, ergs
(2·18)	(14 110)	(2·18)	(4 819)	2·18	2 058
(2·60)	(1 473)	(2·60)	(935)	2·30	1 317
(3·10)	(98·2)	3·10	93·6	2·43	833
3·60	−13·4	3·60	−12·0	2·55	558
3·837	−17·1	3·866	−17·0	2·69	357
4·30	−12·9	4 30	−13·1		
4·80	−7·76	4·80	−7·69		
		5·30	−4·41		

NOTE. Values in parentheses have been extrapolated beyond the estimated range of validity of the parameters listed in *Table 5*, Appendix II.

Of the three potentials, that derived from scattering experiments requires further comment. The description of a molecular beam apparatus for the study of scattering of neutral atoms and molecules, the measurements of total collision cross sections as a function of velocity, and the intermolecular potentials deduced from these experiments have been reported in a series of articles[3–8]. A potential function representing repulsion invariably accounts adequately for the observed scattering cross sections. The range of applicability of the potential as an interpolation device can be inferred approximately from a simple rule, as shown in Appendix III. The accuracy of these potentials is of the order of 20 per cent as estimated from internal consistency and comparison with quantum mechanical calculations[4], as well as with potentials derived from measurements of thermodynamic functions at high temperatures.

Some pertinent conclusions may be deduced from the calculations presented here. *Figure 1* and the entries in *Table 4* show that appropriate

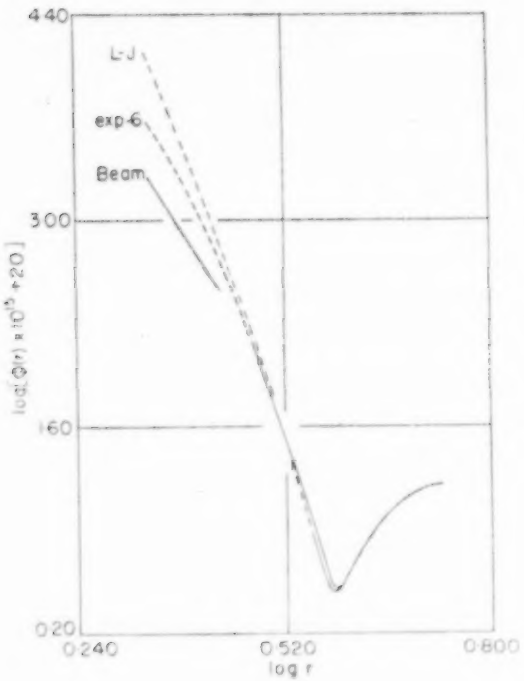

Figure 1. Various intermolecular potentials for the argon system. Dashed portions of the curves represent extrapolations corresponding to parenthetical values in Table 4

potential functions may differ significantly from 'extrapolated' potential functions. (An 'extrapolated' potential function is one determined from properties in one temperature interval corresponding approximately to a given range of intermolecular distance, which has been extrapolated to another range of distance corresponding to a widely different temperature interval.) For example, the Lennard-Jones potential for argon determined from the temperature dependence of the viscosity as a function of temperature from 80° to 300° K, differs from the potential derived from molecular beam experiments in its appropriate range (2·18 Å $\leq r \leq$ 2·69Å) by as much as a *factor of seven*.

Errors of this order of magnitude in intermolecular potentials are not reflected directly as errors of equal order in the same macroscopic properties. For instance, comparison of viscosities of argon evaluated from the two potentials cited, *Table 2*, shows a maximum deviation of only 27 per cent. The calculation of quantities such as vibrational relaxation times[9, 10], reaction rate constants, and barriers to intramolecular rotation[11, 12], may be more sensitive to the choice of intermolecular potential.

As suggested in the introductory paragraphs, the present discussion has been in the nature of a guide for those interested in calculating properties of gases at high temperatures, or in assessing the usefulness of such calculations made by others. No attempt has been made to present a complete review of the very extensive literature associated with topics mentioned in the discussion, or to repeat derivations of fundamental relations which can be readily found elsewhere.

APPENDIX I

(A) The expressions, to the first approximation, for the coefficient of viscosity, $[\eta]_1$, the coefficient of self-diffusion, $[D_{11}]_1$, and the isotopic reduced thermal diffusion ratio, $[k_T^*]_1$, as obtained from solutions of the Maxwell–Boltzmann equation of transport for dilute gases, are as follows:

$$[\eta]_1 = \frac{5}{16N}\left(\frac{MRT}{\pi}\right)^{1/2}\frac{1}{r_m^2\Omega^{(2,2)^*}(T^*)}$$

$$[D_{11}]_1 = \frac{3}{8N}\left(\frac{MRT}{\pi}\right)^{1/2}\frac{1}{\rho r_m^2\Omega^{(1,1)^*}(T^*)}$$

$$[k_T^*]_1 = \frac{15}{16}\frac{(6C^*-5)}{A^*}$$

where

$$\Omega^{(l,s)^*}(T^*) = \frac{2}{(n+1)!(T^*)^{n+2}}\int_0^\infty e^{-g^{*2}/T^*} g^{*2n+3} Q^{(l)^*}(g^*)\,dg^*$$

$$Q^{(l)^*}(g^*) = \left[1 - \frac{1+(-1)^l}{2(1+l)}\right]\int_0^\infty (1-\cos^l\chi)\, b^*\, db^*$$

$$\chi(g^*, b^*) = \pi - 2b^*\int_{r_0^*}^\infty [1 - b^{*2}/r^{*2} - \phi^*(r^*)/g^{*2}]^{-1/2}\, dr^*/r^{*2}$$

χ = relative angle through which initial relative velocity is turned by collision.

$A^* = \Omega^{(2,2)^*}(T^*)/\Omega^{(1,1)^*}(T^*)$

$C^* = \Omega^{(1,2)^*}(T^*)/\Omega^{(1,1)^*}(T^*)$

$T^* = kT/\varepsilon$ = reduced temperature

$-\varepsilon$ = minimum value of intermolecular potential

$$g^{*2} = \tfrac{1}{2}\mu g^2/\varepsilon$$

where g = initial relative speed and μ = reduced mass of colliding particles

$b^* = b/r_m$ = reduced impact parameter

r_m = separation distance at which intermolecular potential is a minimum

$\phi^*(r^*) = \phi(r)/\varepsilon$ = reduced intermolecular potential

r_0^* = reduced distance of closest approach

= smallest positive root of $[1 - \phi^*(r_0^*)/g^{*2}]\, r_0^{*2} = b^{*2}$

N = Avogadro's number

M = molecular weight

T = absolute temperature

R = gas constant per mole

k = gas constant per molecule

ρ = mass density of molecules

(B) The second virial coefficient is related to the potential of intermolecular force by the equation

$$B^*(T^*) = -\frac{1}{T^*}\int_0^\infty r^{*2}\frac{\mathrm{d}\phi^*(r^*)}{\mathrm{d}r^*}\,\mathrm{e}^{-\phi^*(r^*)/T^*}\,\mathrm{d}r^*$$

$$= -3\int_0^\infty r^{*2}\left[\mathrm{e}^{-\phi^*(r^*)/T^*} - 1\right]\mathrm{d}r^*$$

where

$$B^*(T^*) = \frac{B(T)}{\frac{2}{3}\pi N r_m^3} = \text{reduced second virial coefficient}$$

APPENDIX II

The Lennard–Jones (12–6) potential has the analytical form

$$\phi(r) = \varepsilon\left[(r_m/r)^{12} - 2(r_m/r)^6\right]$$

and the modified Buckingham (exp – 6) potential has the form

$$\phi(r) = \frac{\varepsilon}{1 - 6/\alpha}\left\{6/\alpha \exp\left[(1 - r/r_m)\right] - (r_m/r)^6\right\} \qquad r \geqslant r_{\max.}$$

$$\phi(r) = \infty \qquad r \leqslant r_{\max.}$$

where ε and r_m are parameters which specify the magnitude and position of the minimum potential energy, α is a parameter which permits variation of the steepness of the repulsive portion of the potential, and $r_{\max.}$ is the value of r where $\phi(r)$ has a (spurious) maximum. The potentials derived from scattering experiments are represented by

$$\phi(r) = K/r^s$$

where K and s are parameters. The values of the parameters used in the calculation of $[\eta]_1$, $[D_{11}]_1$, $[k_f^*]_1$, and $B(T)$ are given in *Table 5*.

Table 5. Numerical values of potential parameters

System	ε/k °K	r_m Å	s	K/k °K-Å^s	s	Reference
Helium	10·22	2·891				1
	9·16	3·135	12·4			13
				$5{\cdot}471\times10^4$	5·94	
Argon	124	3·837				1
	123·2	3·866	14·0			14
				$9{\cdot}855\times10^6$	8·33	7
Nitrogen	91·5	4·132				1
	101·2	4·011	17·0			14
				$6{\cdot}911\times10^6$	7·27	8

APPENDIX III

The very limited region of the intermolecular potential which influences properties of gases at given temperatures can readily be inferred from the following analysis based on material previously published by E. J. Le Fevre[15].

It will be assumed that at very high temperatures the potential of intermolecular force may be represented by $\phi(r)=K/r^s=\varepsilon(r_m/r)^s$ where ε and r_m are now to be regarded merely as energy and distance parameters which, together with s, characterize the potential. For a potential of this form the reduced collision integral $\Omega^{(2,2)^*}(T^*)$ may be written

$$\Omega^{(2,2)^*}(T^*)=W_0(s)/(T^*)^{2/s} \quad \ldots\ldots [1]$$

so that

$$W_0(s)=1/T^{*1-2/s}\int_0^\infty e^{-g^{*2}/T^*}\,g^{*3}\left[\int_0^\infty \sin^2\chi\, b^*\mathrm{d}b^*\right]\mathrm{d}g^* \quad \ldots\ldots [2]$$

Le Fevre and others[16] have evaluated $W_0(s)$ for selected values of s from 2 where $W_0(2)=1{\cdot}0557$ to ∞ where $W_0(\infty)=1$, so that for the present purpose $W_0(s)$ may be set equal to unity for all values of s. In addition, for *hard spheres* for which $s=\infty$, $T^{*2/s}=1$ so that $\Omega^{(2,2)^*}(T^*)=1$. If, therefore, for *any* value of T^* we set

$$R^2=\Omega^{(2,2)^*}(T^*) \quad \ldots\ldots [3]$$

by definition it follows that Rr_m is the equivalent hard sphere diameter, σ_0, which, at a given temperature, gives the same value of the viscosity as the actual inverse power potential. From equations 2 and 3 it follows directly that

$$T^*=kT/\varepsilon=[\{W_0(s)\}^{\frac{1}{2}}/R]^s=(1/R)^s=(r_m/\sigma_0)^s \quad \ldots\ldots [4]$$

or, since $\phi(r)=\varepsilon(r_m/r)^s$,

$$kT=\phi(\sigma_0) \quad \ldots\ldots [5]$$

Equation 5 states that, to the extent that $W_0(s)$ may be set equal to unity, for $\phi(r) = K/r^s$, at sufficiently high temperatures, it is effectively the single value of the potential energy corresponding to $\phi(r)$ at $r = \sigma_0$ that determines the magnitude of the coefficient of viscosity at the temperature T. Thus, at 1 000°K, a potential energy of about 0·1 eV determines the magnitude of the viscosity, and at 10 000°K, a potential energy of about 1 eV. In experiments on the scattering of high velocity neutral particles, it is the range of the derived potential energy, *not* the kinetic energy of the beam particles, which fixes the range of temperature for which gas properties may be calculated justifiably. For example, if beam particles with kinetic energies in the range 100 eV to 1 000 eV are elastically scattered through a relative angle of the order of 10^{-3} radians, the deduced interaction potentials for the distance of closest approach will be in the range 0·1 eV to 1 eV. The appropriate temperature range corresponding to this range of potential energy will be 1 000° to 10 000°K, and not temperatures (which would be about 1 000 times larger) incorrectly associated with the beam energies.

The relations based on an inverse power potential and applied to the coefficient of viscosity, are very nearly the same for other potential forms applied to viscosity and other gas properties at elevated temperatures.

This work was supported in part by the U.S. Office of Naval Research under Contract Nonr 1841 (23) and in part by the Office of Research of the Atomic Energy Commission.

Department of Chemistry, Massachusetts Institute of Technology.

Department of Chemistry, Brown University, Providence, R.I.

(Received July 1958)

REFERENCES

[1] HIRSCHFELDER, J. O., CURTISS, C. F. and BIRD, R. B. *Molecular Theory of Gases and Liquids*. Wiley: New York, 1954
[2] JAMES, H. L. and COOLIDGE, A. S. *J. chem. Phys.* 1 (1933) 825
[3] ROSEN, P. *J. chem. Phys.* 18 (1950) 1182
[4] MASON, E. A., ROSS, J. and SCHATZ, P. N. *J. chem. Phys.* 25 (1956) 626
[5] AMDUR, I., GLICK, C. F. and PEARLMAN, H. *Proc. Amer. Acad. Arts Sci.* 76 (1948) 101
[6] AMDUR, I. and HARKNESS, A. L. *J. chem. Phys.* 22 (1954) 664
[7] AMDUR, I. and MASON, E. A. *J. chem. Phys.* 22 (1954) 670
[8] AMDUR, I., MASON, E. A. and JORDAN, J. E. *J. chem. Phys.* 27 (1957) 527
NOTE. Various other papers have appeared in *J. chem. Phys.* which deal with derivation of potential energy information from scattering of molecular beams.
[9] SCHWARTZ, R. N., SLAWSKY, Z. I. and HERZFELD, K. F. *J. chem. Phys.* 20 (1952) 1591
[10] SCHWARTZ, R. N. and HERZFELD, K. F. *J. chem. Phys.* 22 1954) 767
[11] MASON, E. A. and KREEVOY, M. M. *J. Amer. chem. Soc.* 77 (1955) 5808
[12] KREEVOY, M. M. and MASON, E. A. *J. Amer. chem. Soc.* 79 (1957) 4851
[13] MASON, E. A. and RICE, W. E. *J. chem. Phys.* 22 (1954) 522
[14] MASON, E. A. and RICE, W. E. *J. chem. Phys.* 22 (1954) 843
[15] LE FEVRE, E. J. 'The classical viscosity of gases at extreme temperatures.' Paper 3, Section 3 in *Conference on Thermodynamics and the Transport Properties of Fluids*. Institution of Mechanical Engineers: London, 1957
[16] See ref. 15 for bibliography on this topic

Recent Developments and Notes

COMBUSTION INSTITUTE MEDALLISTS

At the opening meeting of the Seventh International Symposium on Combustion at the Royal Institution, London, on 28 August, the gold medal of the Combustion Institute was presented to Dr BERNARD LEWIS by Dr THEODORE VON KÁRMÁN. Dr Lewis has served as president of the Combustion Institute since its incorporation in 1954.

Another gold medal was awarded to Sir ALFRED EGERTON, chairman of the British Section of the Combustion Institute, 'for his distinguished, continuing and encouraging contributions to the field of combustion'.

VORTEX FURNACE

T. R. CAVE-BROWNE-CAVE has described some experiments carried out in 1954–55 by John Thompson Water Tube Boiler Ltd, in a vortex furnace devised by himself. The work was initially encouraged by the Ministry of Fuel and Power and by the National Coal Board [*Engineer, Lond.* 206 (1958) 292].

In order to obtain high rates of heat release from the burning of solid fuel, the air for combustion should have high velocity relative to the solid fuel. This is to maintain a rapid supply of oxygen and also to sweep away the products of combustion which would otherwise separate the fuel from the oxygen. Such conditions are not present in a pulverized fuel furnace but should be provided by a furnace operating on the vortex principle.

In the vortex furnace described in this paper comparatively large particles of fuel were stuck to the molten surface of a bowl of slag and burnt with air passing over them at high relative speed. The primary object of the development was to use coal of high ash content in such a way that the ash did not seriously interfere with combustion. The ash content of the fuel remained as molten slag, building up on the surface of the bowl until it drained away through a central hole. It was carbon-free slag, which is a valuable product. Air was introduced through a gallery with high circumferential speed and formed a free vortex sweeping over the fuel held stationary on the intensely hot surface of the bowl. The very high relative speed made possible rates of heat release, perhaps about 2·0 to $2{\cdot}2 \times 10^6$ B.Th.U./ft^3 per hour, which is far in excess of normal practice.

BROWN COAL AS TURBINE FUEL

The Commonwealth Government's Aeronautical Research Laboratories in Melbourne have been engaged for some years on the problem of using indigenous fuels for the gas turbine. It is now believed that a successful method has been found of using brown coal, of which there are very large deposits in the State of Victoria. An account of this work has recently been published by J. C. WISDOM [*Engineer, Lond.* 206 (1958) 328].

A Ruston and Hornsby type 'TA' 1 200 h.p. gas turbine is at present being installed with a view to undergoing experimental operation towards the end of 1958. A straight-through all-metal combustor, based on aircraft gas turbine principles, has been designed to deal with the critical problem associated with the use of pulverized coal as turbine fuel, that of the damaging effects on the turbine blades of erosion, corrosion and deposition arising from impurities in the coal.

It is planned to operate the engine initially with a maximum turbine inlet temperature of 650°C, and it is expected that ash fouling problems will be confined to the first stator and rotor stage. The combination of high temperature and relatively low gas velocity approaching the stator blades will lead to the deposition of ash. Different possible methods of controlling ash deposition have been examined, including effect of gas temperature, addition of fine sand to increase erosion and so reduce deposition, addition of kaolin for the absorption of the bonding agent, and the injection of water to quench the sticky ash constituents. It is hoped that the main instrument of control will be intermittent injection of large quantities of water to remove deposits by heat shock.

THE CARBON MONOXIDE BOILER

The problem of the disposal of the waste gases from the regeneration of catalysts in circulating catalytic systems in use in petroleum refineries is now satisfactorily solved by the use of the carbon monoxide boiler. A review of how this boiler fits into the refinery cycle has recently been published by T. J. HARVEY and P. C. TROUNCE of Canadian Oil Companies Ltd [*Combustion (int. Combust. Engng. Corpn)* 30 (No. 2) (1958) 34].

In the fluid catalytic, Thermofor and Houdriflow processes, the catalyst moves through the oil zone to bring about the reactions and then into a regeneration zone where air continuously burns the coke deposits from the catalyst. There are, however, restrictions on the rate at which the coke can be burnt off. The regeneration bed temperature is limited to about 595°C for a synthetic catalyst and to about 575°C for a natural catalyst, otherwise deactivation of the catalyst occurs due to sintering. Moreover, the air for regeneration is used at about 20 lb/in² gauge, and since the cost of compression is high, the excess air admitted to the process is kept as low as possible. Consequently considerable quantities of gas with a low heating value, about 15 B.Th.U./ft³, are evolved from the regenerator at about 540°C, and contain carbon monoxide.

The carbon monoxide boiler combines the features of waste heat recovery equipment and a conventional boiler. Steam is generated by burning the carbon monoxide in the regenerator flue gas and recovering this heat as well as the sensible heat of the gas.

MOTOR EXHAUST GASES

The photochemical formation of air contaminants from motor exhaust gases has already been shown to be a major factor in the development of the type of smog that accumulates periodically over the Los Angeles basin. In this connection there has been interest in the possibility of reducing these

contaminants by modification of the type of fuel used and the effects of different motor fuels has recently been studied by P. P. MADER, J. GLIKSMAN, M. EYE and L. A. CHAMBERS, of the Air Pollution Control District, Los Angeles, California [*Industr. Engng Chem.* 50 (1958) 1173].

Under controlled experimental conditions during the comparison of two fuel blends, the composition of exhaust gases and their ability to take part in photochemical reactions resulting in smog were shown to depend on the amounts and type of olefins present in the fuel blend. The exhaust products of the two fuels differed significantly in their effect on the formation of eye irritants, aldehydes, organic peroxides and ozone.

THE CARBON–STEAM REACTION

J. D. BLACKWOOD and F. MCGRORY, of the Division of Industrial Chemistry, C.S.I.R.O., Melbourne, have published a paper describing an investigation on the carbon–steam reaction at high pressure [*Austral. J. Chem.* 11 (1958) 16]. The work was planned to elucidate the kinetics of this system at pressures between 1 and 50 atm and in the temperature range of 750° to 830° C. Purified carbon was used in a differential silica tube reactor, the reactant gases flowing up through the heated carbon bed at a predetermined velocity. The effect of hydrogen was examined by adding hydrogen in varying proportions to steam supplied to the reactor bed.

The product gases consist essentially of an equimolecular mixture of carbon monoxide and hydrogen, together with carbon dioxide and methane. At high steam and hydrogen partial pressures and low temperatures a considerable proportion of the carbon is gasified as methane and this is a feature of particular interest for the kinetics of the carbon–steam system. A mechanism is proposed whereby methane is formed by the direct attack of steam on a carbon atom already having at least two hydrogen atoms attached. The formation of methane is considered to be accompanied by the production of adsorbed oxygen which is liberated as carbon monoxide

$$(CH_2) + H_2O \longrightarrow CH_4 + (O)$$

Taking this reaction in conjunction with that producing carbon monoxide from sites having no attached hydrogen, the following rate equation has been derived

$$\text{Rate} = \frac{k_1 p_{H_2O} + k_4 p_{H_2} p_{H_2O} + k_5 p^2_{H_2O}}{1 + k_2 p_{H_2} + k_3 p_{H_2O}}$$

The terms in $p^2_{H_2O}$ and $p_{H_2} p_{H_2O}$ are small at low steam and hydrogen partial pressures and can be neglected.

It is suggested that the active sites for oxidation are positions on the edge of the carbon lattice where oxygen is already present. Production of carbon monoxide is accompanied by the formation of another oxygen group for each one destroyed.

COAL DUST EXPLOSIONS

A critical review of a theoretical nature has recently been made of the characteristic phenomena of coal dust explosions by G. SCHNEIDER,

Ingénieur général des Mines, Paris [*Ann. Min., Paris* (1958) 77–92]. Its particular objective is to present some basic problems which still remain to be resolved in order to make progress in safety measures in mines.

In considering the close relationship between the physicochemical and mechanical phenomena of dust explosions, the author points out that these phenomena are complicated by reflected compression waves which become superimposed on the direct waves resulting from an explosion. In actual mine conditions these wave reflections would depend on the geometry of an unpredictable zone in which the dust explosion occurred. In this connection experimental gallery conditions fall considerably short of leading to results which are directly applicable to underground conditions.

The character of the zone of dispersed dust in which preheating occurs is important. Heating of this zone by radiation is discussed and, just as the flame front is not a straight section of the gallery, it is likely that preheating may commence farther from the flame at the top of the gallery than it does at the bottom. An experimental investigation of the opacity of dust clouds might be of practical interest for remote control of barriers activated by flame radiation. The nature and amount of gases released by distillation in the preheating zone should be studied since the flame proceeds in combustible gases.

The author examines the ignition process, the distillation of the coal dusts, and the chemical reactions that may occur. He suggests that the distillation of the dust in the reaction zone is probably only partial and that the central nuclei of the particles remain practically intact under a crust of coke. The part played by some of the reactions will depend considerably on the speed of renewal of the air in contact with the combustible gases and it may not be correct to assume, as in many previous considerations of the subject, that the air is renewed very quickly. Probably the overriding characteristic of the transformations that take place is their extreme rapidity, so that chemical equilibria and homogeneity in the gaseous phase do not obtain. Although the combustible is generally in excess, there may be some oxygen remaining behind the reaction zone.

A section of the paper is devoted to deriving an expression to characterize the tendency of a coal dust to propagate an explosion. In earlier work this had often been attempted on the basis of the yield of volatile matter from coal and of the fineness, but the results have been misleading. In the present work the dust studied is the fine dust present in any mine, without having recourse to a standard degree of fineness. The basic expression includes the heat, determined in a conventional manner, necessary for pre-distillation of the dust, and the heat of reaction at the temperature of the reaction zone of the dispersed dust. This is then equated to a practical formula containing the temperatures of incipient distillation and of the reaction zone, the coefficient of pre-distillation, the masses of air and dust, and the heat of reaction. It may be preferable to replace the temperature of incipient distillation by the temperature of ignition of the gases at the beginning of distillation. (Indebted to translation by E. Godwin, Safety in Mines Research Establishment, Ministry of Power.)

CATALYTIC COMBUSTION OF GASES

F. DEVORE, C. EYRAUD and M. PRETTRE have published an interesting note on the combustion of methane and hydrogen on an incandescent platinum wire [*C.R. Acad. Sci., Paris* 246 (1958) 1200]. A heterogeneous–homogeneous process has previously been postulated for this type of combustion, notably by M. V. POLYAKOV [*Usp. Khim., Mosk.* (*Adv. Chem., Moscow*) 17 (1948) 351], based on spectrophotometry, volatilization of the platinum, and the examination of used samples of catalyst by means of the microscope and electron microscope. But it does not appear possible by these techniques to evaluate the relative importance of the heterogeneous and homogeneous reactions. The present authors have used a calorimetric technique, different, however, from that used by C. O. GABRIELSON [*Svensk kem. Tidskr* 63 (1951) 145; 65 (1953) 241; 67 (1955) 59; 68 (1956) 200]. The method consists of comparison of the transfer of energy to the catalyst surface in the presence and absence of reaction.

It was found that below 1 200°C as the temperature of the wire, the thermal effects of the combustion of a 3 per cent methane–air mixture were produced very close to the wire, and fairly near to the wire for the same mixture diluted with nitrogen. The combustion of a 3 per cent hydrogen–air mixture on the filament or very close to it appears to occur at much lower temperatures. The results indicate that the combustion reactions take place in two or more stages, one a heterogeneous phase, followed by a chain reaction in the gas phase. There is a participation in the reaction phenomena of zones more and more remote from the filament.

COMBUSTION OF PENTANE ISOMERS

A recent paper by M. LUCQUIN, of Laboratoire de Chimie Générale, Faculté des Sciences de Paris, describes the results of further investigations on the combustion of pentane [*Bull. Soc. chim. Fr. Docum.* (1958) 1003]. In previous papers he has reported studies on the cool flames of pentane and shown the role played by aldehydes in this stage of combustion which is essentially of a peroxide character. Later he examined the second stage of combustion of different linear saturated hydrocarbons, with their two minimum and two maximum critical pressure limits of ignition. These can be placed in two groups depending on whether the first maximum has a higher or lower value of pressure than the second.

In the present paper an account is given of an investigation of the second stage combustion of *iso*pentane and *neo*pentane, and in addition *cyclo*pentane, as well as mixtures of these hydrocarbons. The method used consisted essentially of admitting hydrocarbon–oxygen mixtures of known composition at known pressures into a small Pyrex vessel, 100 mm in length and 22 mm in diameter, heated to a known temperature. The reaction was followed visually.

A comparison of the critical pressure limits of these hydrocarbons of different structures, particularly *neo*pentane, has indicated the possibility of establishing a connection between the form of the limits and their structures, in particular, the role of the primary and secondary carbon atoms, as well as that of the aldehydes produced as intermediate

products. Whereas the author had previously suggested a connection between the formation of formaldehyde and the second maximum, it now appears more likely that there is a connection between it and the second minimum and the second maximum. The second minimum may be due entirely to the combustion of formaldehyde and in a less degree of higher aldehydes, whilst the second maximum may be essentially due to the reduced accumulation of formaldehyde. This would explain the extreme sensitivity of the second maximum to addition of formaldehyde.

NEW TECHNIQUE FOR STUDY OF AUTOIGNITION PROCESSES

K. G. WILLIAMS, J. E. JOHNSON and H. W. CARHART presented a paper to the 'Seventh Symposium (International) on Combustion, London and Oxford, 1958' describing a new method of studying the various stages which lead to normal flames in the autoignition of gases. The first clearly marked phase in this process is the development of a low intensity combustion wave known as a cool flame. The maximum temperature attained in this phase is not more than about 500°C and is insufficient to initiate directly a normal combustion process. The additional temperature required for this is derived from a second chain-branching process, separated in time from the cool flame. The induction period of this second stage is concerned with the generation of an appropriate concentration of chain initiators, and the culmination of this stage is a blue flame in which the temperature rise depends primarily on the availability and proportions of reactants. With suitable conditions, normal combustion is initiated. The discrete stages of such an autoignition process may be studied by separation in either time or space. The present paper describes an experimental technique based on a vertical tube reactor for separating the stages leading to normal combustion so that each stage can be examined in either the presence or absence of the next succeeding stage.

Since there is a very rapid transition from second stage to normal combustion in static systems, it was thought that a flow system in which the oxygen concentration could be raised gradually to the critical level might give the best chance of success, wider separation of the stages being likely to be obtained if the tube were heated. Vertical mounting of the tube appeared desirable so that a flame could be obtained having axial symmetry.

The actual apparatus described consisted of a vertically mounted Pyrex tube 20 in. long and tubes of 16, 25, 42 and 62 mm i.d. have been used successfully. The tube was heated electrically by means of a transparent conductive coating of tin oxide fused on to the outer surface. Streams of oxygen and nitrogen could be admitted to the bottom of the tube via flowmeters, the nitrogen being saturated with fuel vapour by passing through a temperature-controlled fuel bubbler.

Most of the work reported was carried out with *n*-hexane but other fuels were used and initial tube temperatures of between 300° and 500°C all permitted successful flame development. The following flame stages were noted: (*i*) diffuse pre-cool flame luminosity, (*ii*) coalesced cool flame, (*iii*) cool flame plus wall luminescence and diffuse luminosity, (*iv*) cool

flame and blue second-stage flame, (*v*) developing orange flame, (*vi*) cylindrical, cusped flame, (*vii*) thermally self-sustaining flame stabilized at the bottom of the tube. The stability of the cool flame was such that colour photographs taken with a ten-minute exposure showed no appreciable movement, and the stability of the various phases was sufficiently good to allow temperature measurements, sampling studies and spectrographic observations to be made.

SPARK IGNITION OF GASES

Two papers were presented to the 'Seventh Symposium (International) on Combustion, London and Oxford, 1958', by H. E. ROSE and T. PRIEDE, one describing an investigation of the characteristics of spark discharges as employed in ignition experiments, and the other dealing with a study of spark ignition phenomena in hydrogen–air mixtures. Spark discharges have often been used for research on the initiation phenomena of the ignition process of fuels and for the determination of minimum ignition energies. Variations in the shape of the electrodes in these investigations and other differences in experimental conditions have had profound effects on the results and many earlier data have little significance as regards, for example, providing an answer to the question as to whether this type of ignition is of a thermal or electrical nature.

In the work described in both of these papers the important feature of instrumentation was a high-speed oscillograph with a resolution capable of distinguishing time intervals of the order of 10^{-9} sec. This instrument was built by the authors and was used for recording the current through the spark gap and the gap voltage. The first of the papers, describes an investigation of the factors controlling the spark discharge characteristics in air and in hydrogen–air mixtures.

From the results obtained in the first investigation there was derived the design of the bomb used for the ignition of the hydrogen–air mixtures, the study of which is dealt with in the second paper. Various parameters were studied, such as electrode configuration, electrode material and the rate of energy release, which affect the ignition energy. The experiments were carried out to cover electrode separation greater and less than the quenching distance of the mixture.

In discussing the results and drawing conclusions therefrom, it has been assumed that with the particular three-electrode configuration used all the electrical energy released at the spark gap is imparted to the gas mixture. Additional circuit resistance was not incorporated, consequently all the discharges were of an oscillatory nature and the electrical energy released at the gap was practically equal to that charged in the capacitor.

It was found that for capacitive discharges, with a gap distance greater than that at which quenching of the flame by the electrodes takes place, changes in the gap geometry and in the circuit conditions can produce two- to five-fold changes in the experimentally derived values of the minimum energy to be liberated in the gap in order to produce ignition. Consequently the prevailing opinion that minimum ignition energy is

independent of the experimental details cannot be supported. The minimum ignition energy, expressed as electrical energy released at the spark gap, decreases with the following factors: (*i*) reduction in electrode size, (*ii*) electrode material in the order platinum, aluminium, silver, cadmium, (*iii*) increase in value of the series resistance in the discharge circuit.

Most of the factors that influence the electrical energy required for ignition are in conformity qualitatively with a thermal theory of ignition. For example, only a proportion of the electrical energy released at the spark gap takes part in the ignition process, since some of the energy is lost to the electrodes. The energy imparted to the electrodes decreases with the reduction of energy required to bring a critical area of the electrode material to boiling temperature and with the electrode size. The ignition energy decreases with a reduction of the spark channel diameter and discharge time, both of which depend on the characteristics of the test circuit.

There are, however, indications that electrical phenomena can produce effects which may lower the minimum ignition energy. Amongst such indications are the time intervals during which the spark channel remains in a conducting state, after the energy release, and the voltage level at which the energy is being released. Both these factors are dependent upon the parameters of the circuit.

WORLD PETROLEUM CONGRESS

The Fifth World Petroleum Congress is to be held in New York from 30 May to 5 June 1959. The previous congresses have been held in London 1933, Paris 1937, The Hague 1951, Rome 1955. E. V. MURPHREE, president of Esso Research and Engineering Co. is president of the Congress and chairman of the Board of Directors of the Fifth World Petroleum Congress, Inc.

The papers to be presented will be divided into nine sections: (*i*) geology and geophysics, (*ii*) drilling and production, (*iii*) oil processes and refining, (*iv*) chemicals from petroleum and natural gas, (*v*) composition, analysis and testing, (*vi*) utilization of petroleum products, (*vii*) engineering, equipment and materials, (*viii*) transportation and distribution, (*ix*) operations research, statistics and education. There is to be also a symposium on the applications of atomic energy to the petroleum industry, to be conducted by Dr R. L. DOAN, of the Atomic Energy Division, Phillips Petroleum Co. Information about the congress may be obtained from The General Secretary, Fifth World Petroleum Congress, Inc., 527 Madison Avenue, New York 22.

LIQUID FUELS CONFERENCE

The second liquid fuels conference now being arranged by the Institute of Fuel, will be held in Torquay from 11 to 14 May 1959 and will be concerned with 'Major Developments in Liquid Fuel Firing 1948–1959'. Eighteen papers have been set down for presentation and the subjects include: liquid fuel specifications and their significance; atomization and combustion of liquid fuel; design and performance of high momentum

oil burners; physical properties of open-hearth furnace flames; pressure jet burners for boiler use; flow patterns as affecting furnace design; emissivity and radiation of steam and air atomized liquid fuel flames; operating conditions in shell boilers; packaged boilers; liquid fuel in the steel, metal, glass and ceramics industries, for domestic heating and for the manufacture of town gas; works and power station boilers and gas turbines.

Information about the conference may be obtained from the Institute of Fuel, 18 Devonshire Street, Portland Place, London W.1.

ERNST TERRES

Professor Dr Ing. Dr techn. h.c. ERNST TERRES died in Munich on 1 July 1958 at the age of seventy one after a severe illness. He was one of the most distinguished fuel chemists in Germany and from 1949 to 1955 was director of Deutschen Vereins von Gas- und Wasserfachmännern. After holding several academic and industrial appointments Terres became in 1948 professor of gas technology and fuel utilization in the Technische Hochschule, Karlsruhe. He was Direktor des Gasinstituts, Karlsruhe, and from 1950 Direktor of the newly established Engler-Bunte-Institutes für Mineralöl- und Kohleforschung. He was associated for many years with the journal *Das Gas- und Wasserfach* and was its editor for some time. From 1949 he was also editor of *Brennstoff-Chemie*.

FLAT FLAMES

Further work on the structure of flames, making use of certain of their optical properties, was presented to the 'Seventh Symposium (International) on Combustion, London and Oxford, 1958' by A. LEVY and F. J. WEINBERG, and the results have been used to draw some conclusions concerning the propagation of flat flames and the mechanism of flame propagation in general. The flames investigated, of ethylene–air mixtures, were burned on a modified version of the Powling–Egerton flat flame burner. The flow of the flame was examined by a particle track method, using sudden injections into the flow system of bentonite particles of mean diameter 4 microns. The particles were illuminated by a stroboscopically interrupted Tyndall beam passing horizontally above the stream-lining 'matrix' of the burner. The distribution of temperature through the flame was determined by a modified ray reflection method described previously [J. H. BURGOYNE and F. J. WEINBERG, *Proc. Roy. Soc.* A 224 (1954) 286; F. J. WEINBERG, *Sixth Symposium (International) on Combustion*, p 765, Reinhold: New York, 1956] in which the distorted image of a parallel-light illuminated inclined slit is photographed beyond the flame. Its shape is, in effect, an instantaneous graph of a calculable function of the refractive index distribution.

Records obtained by this method of the flat flame flow field suggest solutions to hitherto unexplained aspects of such a flame. For example, it is found that the reactant stream emerging within 3 mm of the burner periphery is diverted through a system of vortices before entering the flame to burn at a level rather higher than that of the central part of the flame, thus producing the familiar rim. Again, the normal temperature

distribution over the matrix, due to a self-preheating effect, shows a maximum at the edge of the matrix and this has been difficult to explain on the sole basis of conduction and radiation from the hotter parts of the burner and flame gases. The flow patterns now recorded show that there is also convection in that the hot product gases are partly recirculated due to the vortex ring around the port periphery. Combination of this effect with that of radiation appears to explain satisfactorily the observed temperature distributions.

Another observation, by Sir Alfred Egerton and his co-workers, which now receives explanation is that of a reduction in stability of the flame when a stream of inert gas is used as an outer sheath. This would be expected if, as seems probable, the toroidal vortices now recorded in the flow patterns, play some part in anchoring the flame.

LIMITS OF INFLAMMABILITY

Considerable attention has been paid recently to the problem of the existence of limits of inflammability. For many years these have been regarded as fundamental properties of inflammable mixtures, perhaps due to the internal structure of the flames, but recently the view has been put forward that the observed limits are essentially quenching phenomena, arising from some interaction of the flames with their environment. At the same time it may be that a fundamental limit is required by some internal condition in the flame. A contribution to the subject was made by G. DIXON-LEWIS and G. L. ISLES, of the staff of the Joint Research Committee of the Gas Council and the University of Leeds, in a paper presented to the 'Seventh Symposium (International) on Combustion, London and Oxford, 1958'. These investigators examined the properties of ethylene–air flames near the lower limit on a modified flat flame burner in which the top of the chimney was closed by an electrically heated, perforated stainless steel plate, and has been described previously [G. DIXON-LEWIS and G. L. ISLES, *Trans. Faraday Soc.* 53 (1957) 193]. Burning velocity and temperature profile measurements were made.

The results confirm those of a previous investigation by the same authors, on methane–air mixtures, that in this type of system convection plays an important part in determining the flame behaviour near the inflammability limits. It was found that much weaker mixtures than had previously been thought are able to support self-propagating flames, and it is concluded that the limits of inflammability in the burner are essentially functions of the apparatus and environment. Either convection limits or quenching limits may be obtained depending on the conditions. There is as yet no evidence from the results of this work for the occurrence of any fundamental limit depending only on the internal properties of the flame.

TURBULENT FLAME PROPAGATION

D. B. SPALDING, in a paper contributed to the 'Seventh Symposium (International) on Combustion, London and Oxford, 1958', discussed the theory of the rate of spread of confined turbulent pre-mixed flames. The type of flame considered is one which spreads from the wake of a flame

stabilizer mounted in a steady stream of pre-mixed combustible gas, flowing at high speed through a duct of constant area. The problem set for solution is to discover what governs the axial distance between the flameholder and the section of the duct where the flame reaches the wall. No new experimental data are put forward, but old data are reviewed. It is shown that these have features which contradict current theories of turbulent flame propagation. The work and views in particular of A. C. SCURLOCK and J. H. GROVER; G. DAMKÖHLER; B. KARLOVITZ, D. W. DENNISTON, and F. E. WELLS; H. S. TSIEN; J. FABRI, R. SIESTRUNCK and C. FOURÉ; and H. IIDA, are examined.

There are two essential steps in the new approach of the present author. First, from existing knowledge of jet mixing, there is reason to suppose that the changes in jet properties from one plane to the next downstream depend only on the local velocity and density distribution and not on how the jet originated. Secondly, in turbulent jet conditions it is known that entrainment is accompanied by a mixing process in which composition and energy interchanges occur. It is these interchanges between hot products and unburnt combustible which are necessary if the latter is to burn at an appreciable rate. Now if the reaction rate of the mixture is sufficiently high for the fresh gas entrained by the central jet to be almost instantly burned, but not so high that the laminar flame speed is comparable with the stream velocity, then the entrainment rate will control the rate of burning. The new theory advanced by the present author is, therefore, based on *jet-forgetfulness* and *entrainment-control*. The author derives an entrainment law and this is followed by calculation of the rate of flame spread. Quantitative agreement with this theory, that the rate of flame spread is governed by the rate of entrainment of cold gas by hot, is fairly good, the most likely cause of the discrepancies being that only jet-mixing data for streams of uniform density are available.

A practical implication of this theory, according to the author, is that little can be done to increase the rate of flame spread from baffles. Preheating the gas stream decreases the rate, whereas even adding oxygen only increases it as a secondary result of the decrease in density of the burnt gases. The outcome of the new theory is that an axial length of three to five duct widths should be provided if the flame anchored to a central baffle is to hit the wall.

MODEL STUDY OF OPEN HEARTH FURNACE

A paper by A. HOGG, C. HOLDEN and R. G. SIDDALL was presented to the 'Seventh Symposium (International) on Combustion, London and Oxford, 1958', dealing with the use of aerodynamic models in the study of industrial furnaces, particularly open hearth furnaces. The work described extends in a particular direction an earlier investigation on combustion and heat transfer in an oil-fired open hearth furnace by S. W. PEARSON, M. W. THRING and J. H. CHESTERS [*Spec. Rep. Iron St. Inst., Lond., No. 59* (1956)]. Some gas analyses were made in the latter investigation for comparison with the mixing in a 1/24th scale model, but not sufficient results were available to

substantiate the similarity theory. Hence further work described in the present paper was undertaken to obtain a more comprehensive survey of the rate of mixing in and around the flame for comparison with the mixing results in a 1/24th scale geometrically similar model. The fuel was represented in the model by compressed air and the flow rates for combustion air and nozzle fluid were determined on the basis of similarity of Reynolds number.

It was found that the model results do not, in general, agree with the results obtained from the furnace. In the furnace the air/fuel ratios are lower inside and higher outside the flame than at corresponding positions in the model, which indicates that the rate of mixing in the furnace is slower than would be predicted from the model. An explanation put forward is that the effective eddy diffusivity in the flame is less than in the air jet used in the model. This implies a smaller jet angle for the furnace than for the model and corrections of the model results made on this assumption lead to a good correlation. Consequently a further similarity criterion, that of jet angle, should be added in future work with models. It is suggested that the use of different flow media could achieve this, for example, a cold air jet entraining hot air.

Air infiltration above the stage level for this furnace was of the order of 25 per cent of the total air for combustion and when allowance was made for this in the model a good correlation was obtained for the gas analysis immediately below the roof.

GAS ANALYSIS FOR COMBUSTION CHAMBER DEVELOPMENT

B. Toone and F. Arkless, of Rolls-Royce Ltd, described the application of gas analysis techniques to the development of aero gas turbine combustion chambers in a paper presented to the 'Seventh Symposium (International) on Combustion, London and Oxford, 1958'. Rapid physical methods have been adopted in their work and the chief determinations required are for kerosine, carbon monoxide, carbon dioxide, hydrogen, oxygen and carbon. The concentration of water can be calculated from the other primary gaseous constituents. They describe the application of the techniques with reference to the combustion process in a combustion chamber of the swirler type with high pressure fuel spray injection, in which there are four main zones: (*i*) fuel cone consisting of high velocity fuel droplets, (*ii*) primary reaction zone, in which combustion takes place at fairly high temperatures, (*iii*) reversal zone, in which combustion products are re-circulated to mix with incoming combustibles in order to ensure combustion stability, (*iv*) dilution zone, in which products from zones *ii* and *iii* are diluted to give a gas temperature sufficiently low to ensure a long turbine working life. In the zones *ii* and *iii*, information is required on fuel distribution, gas temperatures, fuel efficiency and oxygen availability. The fuel combustion efficiency at the turbine must be known with an accuracy of $\pm 0{\cdot}5$ per cent at some engine conditions in order that by development testing the efficiency may be raised to better than 99 per cent over a wide range of conditions.

Infra-red analysers are used to determine the two oxides of carbon, hydrogen is measured by changes in heat conductivity, unburnt kerosine is determined by oxidizing the combustion gas to give the total carbon dioxide by means of a catalytic furnace, and oxygen is determined by a paramagnetic meter. Smoke estimation in the exhaust gases is carried out by means of an absorption cell using the near i.r. band of the spectrum. The radiation is measured by an i.r. photocell.

With regard to the way the unburnt constituents vary with the level of efficiency, between 98·5 and 100 per cent efficiency, carbon monoxide is the cause of inefficiency, while below 98·5 per cent the unburnt fuel inefficiency increases rapidly. Appreciable quantities of hydrogen are rarely found even at low efficiencies.

Since the reversal zone is normally over-rich, little free oxygen is available and the amount of fuel oxidation is considered to be small. It is suggested the composition in this zone may be controlled by an attempt by the gases to attain the water gas equilibrium, $CO_2 + H_2 \rightleftharpoons CO + H_2O$. The other reaction of importance in this zone is the pyrolysis of the fuel. In the presence of hot reaction products and little oxygen, the fuel cracks to carbon and hydrogen.

The results of gas analysis from a traverse plane of the reaction zone adjacent to the dilution zone show that in this plane inefficient products are usually found in one of three possible patterns: (*i*) unburnt kerosine existing mainly near the wall of the combustion chamber, being typical of fairly low pressure conditions, where fuel reaction rates are low, (*ii*) the centre being very rich in unburnt kerosine, typical of a sluggish over-rich reversal zone, (*iii*) the centre being very rich in carbon monoxide while kerosine is absent, typical of high pressure conditions with high fuel reaction rates.

It is found that in the dilution zone reactions not already complete are not necessarily chilled out in this zone, and since approximately 20 per cent of the final combustion efficiency is gained in this zone, it has evident value as a reaction zone.

BURNING LIQUID DROPS

Rates of burning of single drops of liquid fuels have been obtained in several investigations by measurement of the change in drop dimensions, as well as by the use of theoretical expressions which indicate that the rate is a function of heat transferred to the drop per unit mass vaporized. Calculations of the distribution of temperature with time within burning drops have led to the conclusion that the temperature at the centre of hydrocarbon drops burning under natural convection becomes comparable to the surface temperature, at least in the later stages of burning. Recently A. R. HALL has determined experimentally the temperature gradients in burning drops ['Seventh Symposium (International) on Combustion, London and Oxford, 1958'].

Temperatures were measured at two points within drops of tetralin and decane, suspended on a silica filament, during their ignition and initial

burning in air at atmospheric pressure. A fine thermocouple, 0·025 mm diameter, was used and simultaneous measurements were made of the change in drop dimensions.

The general order and rate of change of the temperature gradients found for burning drops of the liquids examined, apart from those in the earliest stage of combustion, appear to be confirmed by heat conduction requirements. There would thus seem to be no significant internal motion within the drops in the periods in question.

The order of the temperature gradients is such that initially over half the heat transferred to the drop is conducted into the interior of the drop, and this component remains a significant proportion of the total heat transferred until appreciably more than half the mass of the drop has been burnt. It is further concluded that by the time the evaporation 'constant' has reached a relatively constant value, the temperature level within the drop has been raised appreciably and the density is much less than it was originally. This must be taken into account when deducing mass rates of burning, especially at elevated pressure, for then the boiling point, and thus the mean temperature of the drop, may be raised considerably.

W. A. KIRKBY

FUEL

The following *Notes* appeared in the October issue of *Fuel* and may be of interest to readers of *Combustion and Flame*:

French award to Dr D. T. A. Townend
Oxidation of diesel oil
Research for industry
Methods of control of coke oven heating

Publications

DANGEROUS PROPERTIES OF INDUSTRIAL MATERIALS

N. I. Sax. New York: Reinhold; London: Chapman and Hall, 1957.

v + 1467 *pp.* 180*s*

THE purpose of this weighty book, as of its predecessor, the *Handbook of Dangerous Materials*, is a worthy one. It is to provide, in one volume, a comprehensive yet convenient source of information upon the hazardous properties of some 8 500 chemical compounds and other industrial materials and upon appropriate precautionary measures.

The core of the book is in the thousand-page General Chemicals section, in which the materials are listed alphabetically and the relevant information on each is summarized. This is preceded by a number of explanatory sections, in which the nature of various hazards is discussed and, in some cases, a basis is given for the 'rating', in the General Chemicals section, of individual materials with respect to particular hazards. The subjects covered in these introductory chapters include: toxicology (followed by ventilation, personal protection, atmospheric pollution and allergic disease); radiation hazards and nuclear reactor safeguards; fire and explosion protection; and the storage and handling of hazardous materials. None of these sections is either long or deep, but several of them serve as a useful introduction to the subject concerned. They are documented, but only in a rather haphazard manner. Two final sections of the book contain respectively: a full reproduction of the Shipping Regulations of the Interstate Commerce Commission (Bureau of Explosives) effective on 18 June 1957; and an extensive index to synonymous names of chemical materials.

It is when one sets out to examine the General Chemicals section in some detail that serious doubts begin to arise. The hazard 'ratings' are too glib. It is not reasonable to attempt to categorize the fire or explosion hazards of materials as 'slight', 'moderate' or 'dangerous', for so many factors contribute to the hazard in practice. The classification with respect to toxicity is more detailed, but is still, it would seem, liable to mislead. Factual data, such as flash-points, ignition temperatures, maximum permissible concentrations and so on (which are, of course, often included with the 'ratings') seem to be healthier fare, for if the reader cannot interpret them he has no business to be making decisions with regard to safe practice.

Unfortunately, however, the author has permitted a considerable number of inaccuracies and inconsistencies to find their way into the General Chemicals section. The case of the three xylenes provides an example. One is immediately struck by the statement that the fire hazard of the *meta* compound is 'dangerous,' but only 'moderate' for the *ortho* and *para* isomers. This anomalous situation apparently finds its explanation in that 'dangerous' and 'moderate' ratings are related to flash-points of below and above 80°F respectively. The flash-point of *m*-xylene is given as 77°F (closed cup), but that of *o*-xylene as 115°F (open cup) and of *p*-xylene 103°F (open cup). These are consistent, and probably correct, but, in 'rating' the fire hazard from them, the author has ignored the difference between closed and open cup values. Why the explosion hazards are rated as 'moderate', 'slight' and 'moderate' for the *ortho*, *meta* and *para* compounds respectively is beyond the reviewer's understanding.

Another interesting comparison may be made between the separate entries for 'butanone' and 'ethylmethylketone', which most chemists regard as synonymous. Apart from some differences in numerical data, quite distinct toxicity ratings are given for these 'two' substances!

Confidence in the 'ratings' is further shaken when it is found that the fire hazard of celluloid, the explosion hazards of acetylene and acetone peroxide, and the dust explosion hazard of powdered aluminium and magnesium are no more than 'moderate';

whilst anhydrous ammonia, with its high ignition temperature and its high lower explosive limit, is given a similar rating as to both fire and explosion hazards.

It may be further noted that little distinction is made between the hazards of the organic peroxy compounds, that the tendency of diethyl ether to form a dangerous peroxide and the explosive reaction between carbon tetrachloride and the light metals receive no notice; and that the 'explosive range' of carbon disulphide is given as '50 per cent' (which is in fact its upper explosive limit) whilst that of zirconium (i.e. the dust, whose lower limit is about 0·04 g/l.) is '0·16 g/l.'!

Let it not be thought that the book does not contain a tremendous amount of accurate and useful information. But the dust cover proclaims that this is 'A Bible of Safety Information' and if this amounts to a claim to be comprehensive and infallible, it is simply not justified.

J. H. BURGOYNE

HEAT EXCHANGERS

W. HRYNISZAK. London: Butterworths Scientific Publications; New York: Academic Press 1958. *xii* + 343 *pp.* 63*s or* $10

MOST books on heat transfer are written by academic persons; they therefore tend to be scientifically sound and professionally written, but inadequately balanced by design and operating detail. The present book, being written by a designer, shows the opposite faults and virtues. Thus, although a number of errors of fact or interpretation can be pointed out in the more fundamental sections, Dr. HRYNISZAK has performed a very valuable service in bringing home to the reader the fact that heat exchanger design is governed at least as much by the geometrical requirements of ducting the fluids as by the magnitude of the attainable heat transfer coefficients. The many drawings and photographs of actual and projected heat exchangers, particularly those of the regenerative type, will surely have a stimulating, though sometimes also sobering, effect on engineers starting a design.

The non-mechanical sections must unfortunately be read with caution. To give three examples:—Figure 4 gives an erroneous picture of the relation between the laminar and turbulent boundary layers on a plate; the numbers in Tables IV and V (p 35) are all one thousand times too large because the comma has been used instead of the decimal point; and the viscosity/temperature law of equation 28 (p 46) is not really that of SUTHERLAND. Readers already well trained in heat transfer will not, however, be misled by such errors, and can learn much from the book.

D. B. SPALDING

Letters to the Editors

Letters to the Editors on points of scientific interest related to combustion and flames are invited. The Editors do not hold themselves responsible for opinions expressed in correspondence. Anonymous contributions cannot be accepted.

A Note on Polycyclic Hydrocarbons in Association with the Carbonaceous Residues from Diffusion Flames

In a previous study[1] of the carbonaceous residues from diffusion flames of aromatic, napthenic and paraffinic fuels, fractions were obtained which had similar i.r. spectra. In some cases the presence of oxygen in the molecule was inferred. Polycyclic aromatic compounds were not detected but coloured substances, probably fulvenes, and colourless liquids, probably long chain olefins, were present. It was suggested that some of these represent precursors of carbon formation.

More recently carbonaceous deposits from Butagas and acetylene diffusion flames have been examined by the method of P. Wedgwood and R. L. Cooper[2]. They were first extracted with chloroform in a Soxhlet apparatus and the extract was then evaporated to dryness (at a temperature below 50°C).

The residue was treated with *cyclo*hexane and the solution passed through a chromatographic column of alumina (100 to 200 mesh. Spence, type H) and the chromatogram developed with further amounts of solvent. The column was next well drained and extruded, then separated into five sections which were eluted with *cyclo*hexane. The u.v. absorption spectra were obtained using a Unicam S.P. 500 spectrophotometer and the second zone from the bottom of the column (which was yellow to pale orange in colour) proved to be of most interest.

Wedgwood and Cooper[2] have determined the absorption maxima characteristic of various polycyclic aromatic hydrocarbons in *cyclo*hexane within the region 200 to 500 millimicrons. Some of these are listed in *Table 1* together with some of those observed in the spectra of the above mentioned fraction from the deposits from the two fuels.

These results indicate the presence of the various polycyclic aromatic hydrocarbons although the individual members have not been separated. J. R. Arthur, B. T. Commins, J. A. S. Gilbert, A. J. Lindsay and D. H. Napier[3] in their recent more comprehensive examination of the deposits from *reversed* diffusion flames have given quantitative results for the various polycyclic hydrocarbons found in the *cyclo*hexane-soluble portion. It is interesting, however, to note that polycylic aromatic hydrocarbons are present in the deposits from both normal and reversed flames.

The above authors' suggestion that they represent either a stage in carbon formation or one route by which carbon is formed seems to be quite plausible but more information is required concerning the other products associated with carbonaceous residues. To account for some of these,

A. G. GAYDON[1] has suggested that carbon formation might occur through aromatic compounds whereas five-membered rings (fulvenes) cannot readily form graphite and remain to be detected. It is also worth noting that in the pyrolysis of benzene, naphthalene, anthracene, chrysene and pyrene,

Table 1.

Compound	*'Best' absorption maxima* (P. WEDGWOOD *and* R. L. COOPER[2]) *max.* mμ	*Absorption maxima in present work* mμ
Naphthalene	266, 276, 311	265† 275† 266*
Anthracene	357, 376	355† 375† 356* 376*
Phenanthrene	252, 293	250† 293* 250*
Fluorene	301	300*
Pyrene	319, 335	318† 335* 319* 336†
1.2-Benzanthracene	278, 288	277† 288† 278* 288*
Chrysene	268	268†
3.4 Benzpyrene	365, 384, 403	364* 383* 401† 366† 385† 403*
Perylene	409, 436	409† 435† 410*

*Represents peak in spectrum of fraction from carbonaceous deposit of acetylene.
†Represents peak in spectrum of fraction from carbonaceous deposit of Butagas diffusion flame.

C. R. KINNEY and E. DELBEL[5] detected small amounts of highly coloured products which might have been fulvenes.

Chemical Engineering Department,
The University, Birmingham 15

A. BADAKHSHAN
F. H. GARNER
R. LONG

(Received October 1958)

REFERENCES

[1] THORP, N., LONG, R. and GARNER, F. H. *Fuel, Lond.* 34 (1955) S 1
[2] WEDGWOOD, P. and COOPER, R. L. *Analyst* 78 (1953) 170
[3] ARTHUR, J. R., COMMINS, B. T., GILBERT, J. A. S., LINDSAY, A. J. and NAPIER, D. H. *Combustion & Flame* 2 (1958) 267
[4] GAYDON, A. G. *The Spectroscopy of Flames*, p 186. Chapman & Hall: London, 1957
[5] KINNEY, C. R. and DELBEL, E. *Industr. Engng Chem. (Industr.)* 46 (1954) 548

The Relation between Fuel Injection and Combustion in Diesel Engines

A PROGRAMME of research has been in progress at the C.A.V. Research Laboratory for the past three years aimed at establishing a quantitative relationship between the injection characteristic and the rate of heat release in a diesel engine. The success of such an investigation would put the

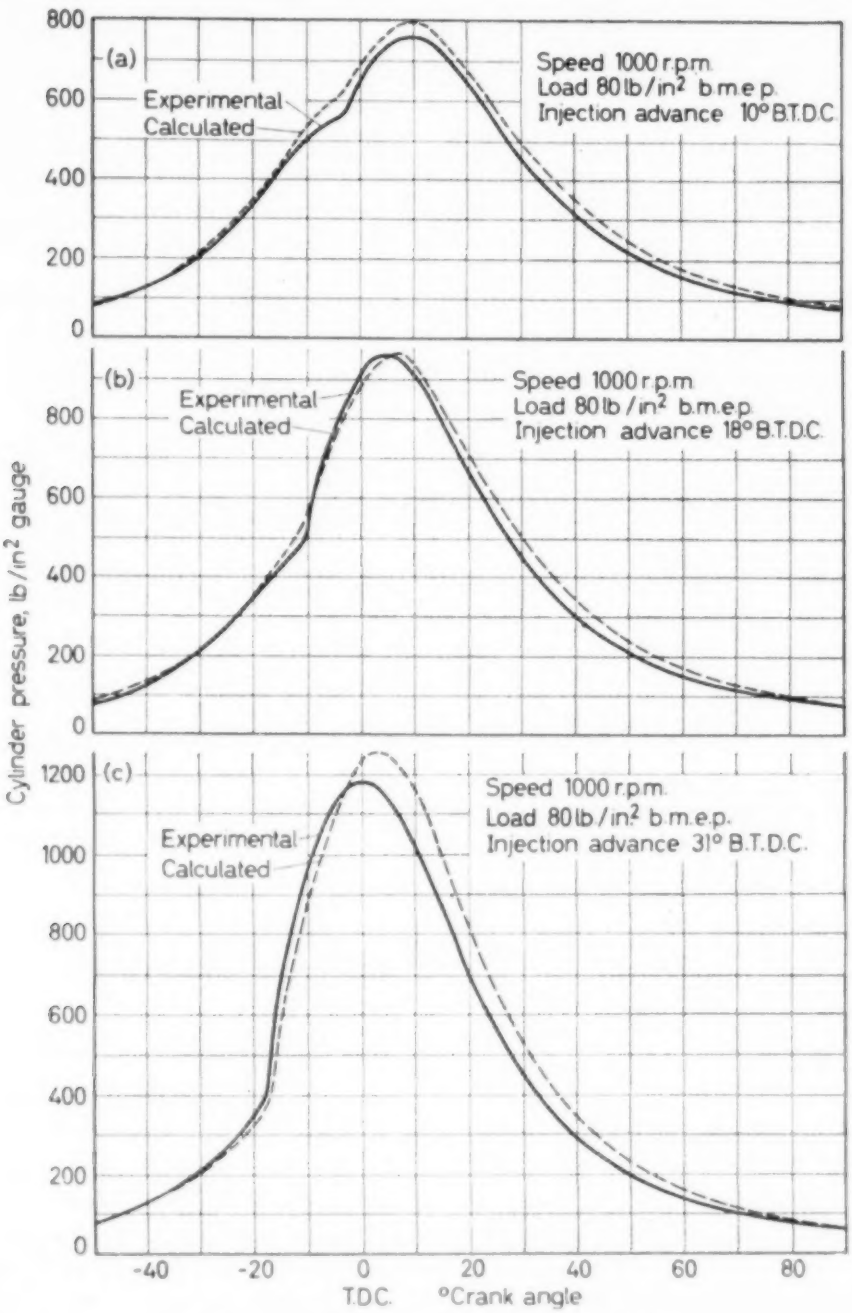

Figure 1. Effect of varying injection timing

prescription of fuel injection equipment on a more logical basis as well as enable many aspects of engine performance to be predicted from fuel injection characteristics. The method used is to calculate the rate of heat release from the cylinder pressure diagram and air-flow measurement, with the rate of heat loss taken into consideration. The injection characteristic is calculated from fuel-nozzle pressure and needle-lift diagram.

Many of these calculations, which are programmed for a digital computer, have been carried out for engine measurements over a wide range of operating conditions, and the relationship between injection characteristic and rate of heat release examined empirically.

The best means of expressing this relationship is still under investigation but satisfactory agreement has been obtained between 'measured' heat release (i.e. calculated from the cylinder pressure diagram), and the heat release calculated from the injection characteristic and measured delay period. It has been found that for a given engine and injector the same function relating heat release to fuel injection may be used over a wide range of load, injection rate and timing; and, provided rates are expressed in terms of degrees of crank angle, the relationship is also substantially independent of speed. *Figure 1* (a), (b) and (c) indicates the order of accuracy of the agreement (the comparison here being made in terms of cylinder pressure) under the range of conditions—variation of injection timing—for which the agreement is the poorest; with variation of either speed or load the agreement is better.

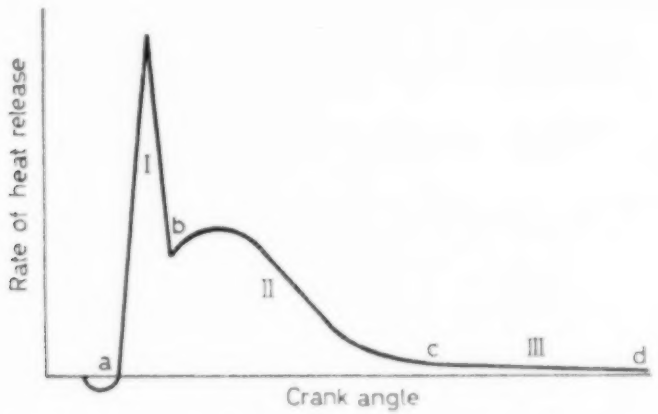

Figure 2. Rate-of-heat-release diagram typical of direct injection engine

This investigation also throws some light on the main combustion processes and has led to the simplified model described below. *Figure 2* shows schematically a typical rate-of-heat-release diagram for a direct injection engine. During the compression stroke the rate of heat release is practically negligible until the injection of fuel, when it shows a small negative value throughout the delay period due to fuel evaporation. During the combustion period (i.e. the period during which the rate of heat release is positive) three stages of burning may be distinguished. The first stage lasts for only a few degrees of crank angle (about 5 to 7°) and the rate of burning is generally very high. This corresponds to the period of rapid cylinder pressure rise. The second stage corresponds to the period of gradually decreasing rate of heat release and lasts for about 40° of crank angle. This is the main heat release period in which normally about 80 per cent of the total heat is released. In the third period which corresponds to the 'tail' of the diagram, a small but observable rate of heat release

persists throughout almost the whole exhaust stroke. The heat released during this period, however, is only about 10 per cent of the total.

The present interpretation of these three phases, which is supported by evidence from high-speed photography, is as follows. During the delay period, part of the fuel injected evaporates and mixes with air to form regions of ignitable mixture, which burns very rapidly once ignition occurs. The process occurring here lies in the border region of simultaneous auto-ignition and flame propagation because the prevailing temperature is well above the spontaneous ignition temperature. From high-speed photography, while ignition is observed to start from more than one centre, there is also evidence of flame propagation around the jets. This very short period but high rate of heat release characterizes the first phase of the combustion. That the combustion in this period is essentially that of a premixed flame is again supported by high-speed photography, since premixed flames are nearly non-luminous and in spite of the high rate of heat release, both the region of inflammation and the intensity of luminosity are much smaller than during the second period when the rate of heat release is comparatively low.

In a direct injection engine, the premixed flame during the first phase of burning generally starts around and downstream from the jets of the fuel spray. During this period, however, the flame spreads to enclose the jets which burn subsequently as a turbulent diffusion flame. Infra-red emission spectra taken during this period [LYN, W. T. 'Diesel combustion study by infra-red emission spectroscopy'. *J. Inst. Petrol.* 43 (1957) 25] also show predominantly continuous radiation from carbon particles characteristic of a diffusion flame.

The nature of the third phase, which corresponds to the tail of the heat release diagram, is not yet clear. It is significant, however, that this part is missing from the heat release diagram of a petrol engine.

It is possible that it is due to the relatively slow combustion of carbon formed during the second stage of the combustion. On the other hand it may be that, in this stage, as is thought to be the case in the second stage, mixing processes determine the rate of combustion.

The programme of research will continue for a considerable time but it is hoped to publish a full account of this part of the investigation shortly.

Research Department,
C.A.V. Ltd.

A. E. W. AUSTEN
W. T. LYN

(*Received September 1958*)

REFERENCE

A Note on the Influence of Hydrocarbon Structure on Aldehyde Formation during Low Temperature Oxidation

THE proportions of the lower aldehydes in the products of oxidation of a number of hydrocarbons have recently been determined. They are expressed in *Table 1* as a percentage of the total aldehyde. The vapour phase oxidation was carried out using the flow method in a Pyrex reaction

vessel. Also included is an earlier result obtained by R. G. TEMPLE[1] using a stainless steel reaction vessel.

Although the oxidation temperature varied between 360° and 383°C, the results indicate that hydrocarbon structure is of importance. The proportions of acetaldehyde and formaldehyde are very similar for *n*-heptane and *cyclo*hexane. With methyl*cyclo*pentane and methyl*cyclo*hexane there is relatively less formaldehyde and more acetaldehyde in the products of oxidation.

It is known that[2, 3] aldehydes are more readily oxidized than the corresponding hydrocarbons and consequently the nature of the oxidation products of hydrocarbons might be expected to be affected by the further oxidation of the aldehydes.

N. J. H. SMALL and A. R. UBBELOHDE[4] have also shown that the oxidation of acetaldehyde is inhibited by hydrocarbons, the inhibiting power being greater the more readily a hydrogen atom can be removed from the hydrocarbon molecule, i.e. the lower the energy of rupture of a C–H bond.

Table 1

Hydrocarbon oxidized	*Product*	*Aldehyde mol/mol. of hydrocarbon introduced*	*% of total aldehyde*
n-*Heptane (360°C)*	*Formaldehyde*	0·095	35·0
	Acetaldehyde	0·159	55·7
	Propionaldehyde	0·026	9·3
cyclo*Hexane (383°C)*	*Formaldehyde*	0·080	36·7
	Acetaldehyde	0·121	55·5
	Propionaldehyde	0·017	7·8
Methylcyclopentane (363°C)	*Formaldehyde*	0·009	10·1
	Acetaldehyde	0·073	82·2
	Propionaldehyde	0·007	7·7
Methylcyclohexane (380°C) R.G. TEMPLE[1]	*Formaldehyde*	0·052	16·7
	Acetaldehyde	0·221	70·6
	Propionaldehyde	0·033	10·6
	Butyraldehyde	0·007	1·8

It appears that the data in *Table 1* reflect this phenomenon; the proportion of acetaldehyde (expressed as a percentage of the total aldehyde), found in the products of methyl*cyclo*pentane and methyl*cyclo*hexane being considerably greater than in the products of oxidation of *n*-heptane and *cyclo*hexane. The proportion of formaldehyde is correspondingly lower, indicating that this is mainly formed by the further oxidation of acetaldehyde. (The amount of propionaldehyde found is small and the results for this aldehyde are only considered to give a rough indication of the proportion present.)

According to A. D. WALSH[5], the removal of a hydrogen atom occurs more readily at a tertiary C—H than at a secondary. Therefore, the further oxidation of acetaldehyde formed during the oxidation of methyl*cyclo*pentane might be expected to be inhibited to a greater extent than that

formed during the oxidation of *n*-heptane or *cyclo*hexane. Initial attack is believed to occur at secondary C—H bonds in *n*-heptane and *cyclo*hexane but principally at the tertiary C—H bond in the alkyl *cyclo*paraffins.

Chemical Engineering Department,
The University, Birmingham 15

D. H. ALLEN
R. LONG

(*Received October 1958*)

REFERENCES

[1] TEMPLE, R. G. *Ph.D. Thesis*. University of Birmingham, 1952
[2] KANE, G. P., CHAMBERLAIN, E. A. C. and TOWNEND, D. T. A. *J. chem. Soc.* (1937) 436
[3] CULLIS, C. F. *Bull. Soc. Chim. Fr. Docum.* 17 (1950) 863
[4] SMALL, N. J. H. and UBBELOHDE, A. R. *J. chem. Soc.* (1953) 637
[5] WALSH, A. D. *Trans. Faraday Soc.* 42 (1946) 269

Burning Times of Liquid Fuel Drops in a Convection–Radiation Field

CAPTIVE fuel drops burned in a variable convection–radiation field gave the following results which are reported here in outline since they seem to be of general interest:

(*1*) Ignition seems to depend on the ambient gas temperature rather than on the radiation intensity.

(*2*) In the square law relation between burning time (t_c) and initial drop diameter (d_0) (which relation was obeyed as expected) the burning constant K, as defined by the equation

$$t_c = K \cdot d_0^2$$

was found to vary with the intensity of the heat field.

Apparatus

The heat field was provided by two coils of resistance wire wound in flat spirals and set up with their planes either vertical or horizontal, a method of experiment originally developed as reported elsewhere[1] for studying the combustion of single particles of coal. The coils were 2·25 cm in diameter and were set 1·25 cm apart on a common axis with their planes parallel. The coil array was mounted on a pivot system so that when the coils had reached their steady operating temperature they could be shot into position, with a coil either side of the drop to be burnt; the drops were suspended from a fine silica filament bearing a tiny loop at the end. As reported previously[1] this method of operation could not be used with coal particles since the shock heating caused them to decrepitate; with coal particles the coils were allowed to heat up with the particles already in position between the coils.

When the coils were set up with their planes horizontal, a fuel drop was in the radiation field generated by both coils, and in the convection field produced by the lower coil; but with the coil planes vertical, the intensity of the convection field was reduced while leaving the radiation field unchanged. The intensity of the total field was varied by altering the voltage across the coils, and the coil temperature was measured with a disappearing filament pyrometer. Three fuels were used and their characteristics are given in *Table 1*.

Table 1. Fuel characteristics

Fuel	*Sp. gr.*	*Composition*
Kerosine	0·80	20% *Aromatics* 80% *Naphthenes and paraffins*
Gas oil	0·83	19% *Aromatics* 72% *Naphthenes and paraffins*
Pitch creosote	1·15	*Carbon* 88·6%; *Hydrogen* 6·16% C : H *ratio* 14·4

Ignition

With the coils respectively horizontal and vertical, the coil temperatures at which kerosine would just ignite were respectively 825 ± 25 °C and 1 050 ± 25 °C. For comparative purposes, the relative gas temperature of the centre of the zone between the coils was measured with a bare thermocouple and, for the two coil temperatures in the two positions mentioned above, the relative gas temperatures were 390° ± 20 °C and 400° ± 25 °C. These values suggest that ambient gas temperature was more important in ignition than was radiation intensity. With coil temperatures below the minimum required for ignition the droplets merely evaporated.

Both the kerosine and the gas oil ignited between vertical coils; like coal, the pitch creosote did not. Between horizontal coils the pitch creosote burned, also like coal, in two stages: first, a 'volatile' combustion with a carbon cenosphere formation; and secondly, combustion of the carbon cenosphere. There seems little doubt but that the pitch creosote would burn between vertical coils in a radiation field of sufficient intensity, but this necessary intensity was not achieved in these experiments.

Burning constant

Data on the variation of burning times with drop diameter, used to check the validity of the square law relation, were obtained from cine-records and used to calculate the value of the burning constant, K. The cine-records were obtained by projecting the image of the burning droplets on to a gridded, pre-calibrated screen, and photographing the projected image. Over the lower range of temperatures at which ignition occurred, the kerosine behaved as expected, and graphs similar to those given by previous investigators[2–6] were obtained; but in the higher temperature range it behaved unexpectedly by burning in two stages though without any solid or cenosphere formation. Over the first stage the cine-records indicated that there might be some swelling that partially counteracted the diameter

decrease due to fuel loss by combustion, i.e. the density was decreasing, so that for the second stage there was much less fuel to dispose of, and, once the swelling effect had ceased, the rate of vaporization accelerated. A. R. HALL[7] has quoted evidence to show that in large drops convection currents can be set up fairly readily, and D. J. RASBASH, Z. E. ROGOWSKI and G. W. V. STARK[8] have shown that under such conditions radiation penetrating to some depth below a liquid surface can raise an appreciable volume of the fluid to boiling point so that the fluid then bubbles steadily accompanied by appreciable expansion. This seems to be what happened with our drops. Both stages obeyed the square law so that a burning constant for each stage could be calculated. For comparison, the value of the burning constant was also determined with no background heat source after ignition with a small gas flame and the collected results are given in *Table 2*. The relatively small increase in the burning rate of kerosine and gas oil with increased temperature is of the same order as that predicted by the diffusion theory[9].

Table 2. Values of burning constant

Fuel	*Coil temperature °C*	*Values of K, c.g.s. units*	
		Horizontal coils	*Vertical coils*
Kerosine	—	117	(117)
	800	346 (*evaporated*)	—
	850	111	—
	900	108	—
	1000	106	314 (*evaporated*)
	1050	171/66	—
	1100	185/48	16
	1150	156/36	—
Gas oil	—	140	(140)
	850	125	—
	900	124	—
	1000	120	324 (*evaporated*)
	1050	114	—
	1100	111	73
Pitch creosote	—	*Did not burn without supporting heat source*	
	1050	350	*Did not burn*

Cenosphere formation

The pitch creosote would not burn without any supporting heat source and, as mentioned above, with the radiation intensities used, this had to include convected hot air. With the coils vertical, the pitch creosote would not burn but it did evaporate down to a cenosphere. The cenosphere formed when the drop merely evaporated was roughly twice the size of that formed when combustion occurs; this may have some bearing on the combustion properties of coal particles since qualitative observations on these, that have yet to be confirmed by measurement, have indicated that the same is true of these. This differential swelling would have some bearing on the assessment of particle size when attempting to predict emissivity and heat transfer from a p.f. flame. Similarly, the size and distribution of the cenospheres in an oil flame will affect the emissivity and combustion efficiency.

We should like to thank Professor M. W. Thring for advice in the preparation of this note and for permission to publish it.

E. G. MASDIN
R. H. ESSENHIGH

Department of Fuel Technology and Chemical Engineering, University of Sheffield

(Received October 1958)

REFERENCES

[1] ESSENHIGH, R. H. and THRING, M. W. Conference on 'Science in the Use of Coal,' Sheffield, April 1958. Paper 29, p D21
[2] BURGOYNE, J. H. and COHEN, L. *Proc. Roy. Soc. A* 225 (1954) 375
[3] HALL, A. R. and DIEDERICHSEN, J. *Fourth Symposium (International) on Combustion*, p 837. Williams and Wilkins: Baltimore, 1953
[4] SPALDING, D. B. *Fuel, Lond.* 29 (1950) 2, 25; 30 (1951) 121; 32 (1953) 169
[5] GODSAVE, G. A. E. *Fourth Symposium (International) on Combustion*, p 818. Williams and Wilkins: Baltimore, 1953
[6] SIMPSON, H. C. *Sc.D. Thesis*. Massachusetts Institute of Technology, 1954
[7] HALL, A. R. *Seventh Symposium (International) on Combustion*. Paper No. 59. Butterworths: London, 1959
[8] RASBASH, D. J., ROGOWSKI, Z. W. and STARK, G. W. V. *Fuel, Lond.* 35 (1956) 94
[9] GOLDSMITH, M. *Jet Propulsion* 26 (1956) 172

The Hydrogen Diffusion Flame as an Inflammable Gas Detector

MANY instruments have been devised for the detection of inflammable gases and most of these have been reviewed recently by E. H. COLEMAN[1]. Heated filament instruments require regular inspection, maintenance and adjustment and may with certain vapours give anomalous results because of de-activation of the filament; where catalysts are used, their activity may be reduced by poisoning.

The earliest inflammable gas detector was the flame safety lamp and one development of this employed a hydrogen flame[2, 3], the size of the flame cap formed being taken as a measurement of the concentration of gas in the air.

The hydrogen flame detector for gas–liquid chromatography devised by R. P. W. SCOTT[4, 5] is now well known and widely used. In the present work a rather similar flame detector has been used (*Figure 1*) but here a minute hydrogen diffusion flame burns in a surrounding atmosphere containing the inflammable gas. An iron–constantan thermocouple junction located above the flame develops an e.m.f. which is measured by a potentiometer.

Figure 2 illustrates the results obtained with a number of hydrocarbon vapours in air. The abscissa represents the concentration of hydrocarbon in the air expressed as a fraction of the lower limit mixture.

The results lie within a narrow band for those hydrocarbons (*n*-heptane, *iso*octane, *cyclo*hexane and methyl*cyclo*hexane) for which the net calorific values of the lower limit mixtures are of the same order. The results for

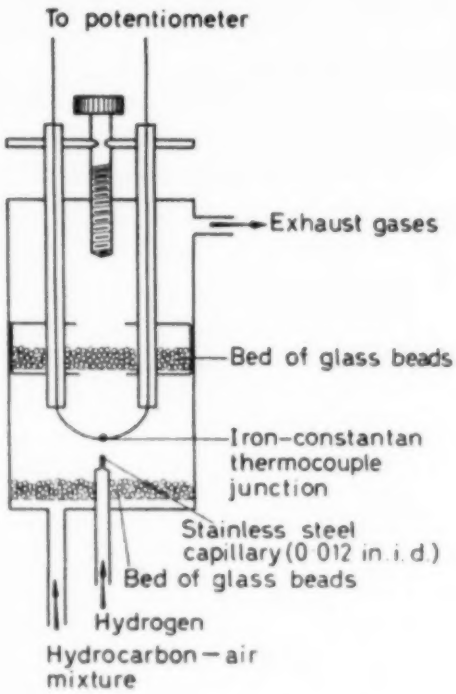

Figure 1

ethane and propane, for which the net calorific values of the lower limit mixtures are less but approximately equal, lie roughly on a single curve (cf. *Table 1*).

N. LE CHATELIER and O. BOUDOUARD[8] and later M. J. BURGESS and R. V. WHEELER[9] showed that the heat liberated per mol. of lower limit mixture is nearly constant for many combustible–air mixtures. If this generalization were obeyed accurately a single calibration curve would serve for many inflammable gases but in fact separate calibration for each

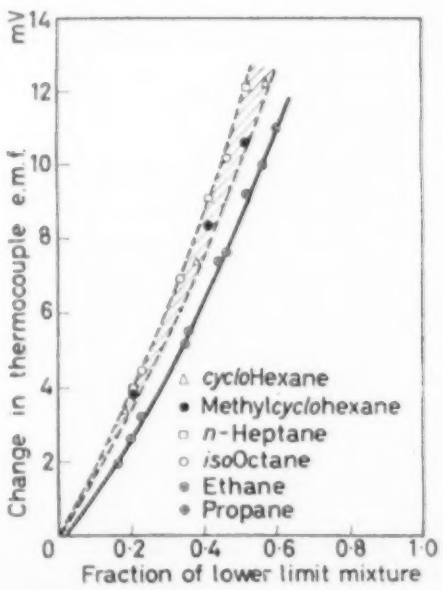

Figure 2

gas is necessary when the gas–air compositions are expressed as fractions of the lower limit mixtures.

It has been found, however, that if the net calorific values of the gas–air mixtures admitted to the detector are plotted on the abscissa then all the results fall roughly on a single curve (*Figure 3*).

It is quite easy to work out the approximate percentage by volume of one particular hydrocarbon in air (knowing its heat of combustion) from a given detector response (increase in thermocouple e.m.f.).

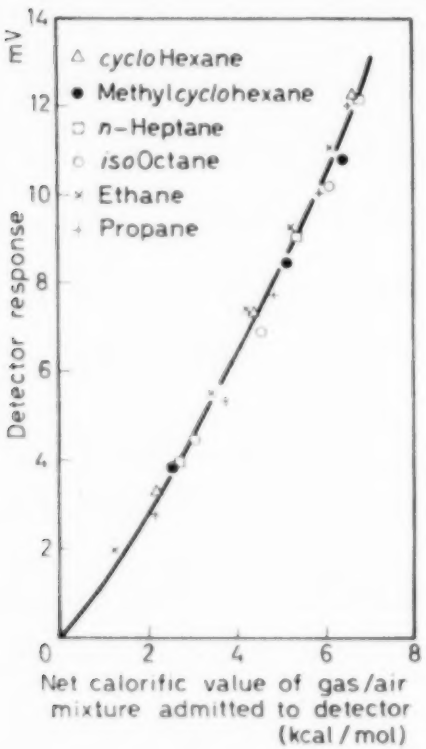

Figure 3

The advantages of this detector are its high sensitivity, lack of elements which may become de-activated, and rapid response. In the latter respect it is superior to the combustion instrument developed by H. M. BREWSTER[10].

The instrument would, of course, require to be modified by the incorporation of efficient flame traps if it were to be operated in an

Table 1

Hydrocarbon	*Heat of combustion*[6] *kcal/mol.* $H_2O_{(g)}$ $CO_{2(g)}$	*Lower limit of inflammability*[7] *in air, per cent*	*Net calorific value kcal/mol. of lower limit mixture*
n-*Heptane*	1075·8	1·2	12·91
iso*Octane*	1219·0	1·1	13·41
cyclo*Hexane*	881·7	1·3	11·47
Methylcyclohexane	1026·0	1·2	12·31
Ethane	341·3	3·0	10·24
Propane	488·5	2·2	10·75

inflammable atmosphere, and a portable form could probably be developed without great difficulty.

P. D. EDWARDS
R. LONG

Department of Chemical Engineering,
The University, Birmingham 15

(*Received October 1958*)

Since submitting this Note for publication the authors' attention has been directed to a methane detector developed at the Mining Research Establishment of the National Coal Board. This device employs an automatically controlled butane flame and thermocouples and it is covered by *Brit. Pat. No. 778 774.*

REFERENCES

[1] COLEMAN, E. H. *Brit. chem. Engng* 2 (1957) 143 and 202
[2] CLOWES, F. *Proc. Roy. Soc.* 50 (1891–92) 122; 51 (1892) 87; 52 (1892–93) 484
ASHWORTH, J. and CLOWES, F. *Brit. Pat. No. 6051/1892.* (19 December 1892)
[3] REDWOOD, B., CLOWES, F. and WATERS, S. *Brit. Pat. No. 187/1893.* (18 February 1893)
[4] SCOTT, R. P. W. *Nature, Lond.* 176 (1955) 793
[5] SCOTT, R. P. W. *Vapour Phase Chromatography*, p 131. Edited by DESTY, D. H. Butterworths: London, 1957
[6] PERRY, J. H. (Editor) *Chemical Engineers' Handbook*, 3rd ed., p 244. McGraw-Hill: New York, 1950
[7] COWARD, H. F. and JONES, G. W. *Bull. U.S. Bur. Min. No. 503* (1952)
[8] LE CHATELIER, N. and BOUDOUARD, O. *C.R. Acad. Sci., Paris* 126 (1898) Part I, 1510–13
[9] BURGESS, M. J. and WHEELER, R. V. *J. chem. Soc.* 99 (1911) 2013
[10] BREWSTER, H. M. *Sixth Symposium (International) on Combustion*, p 774. Reinhold: New York, 1957

A Note on the Influence of the Lewis Number on Flame Stability

THE description of a physical system can never be considered complete unless it is known whether the configuration is stable or not. The analysis of a plane deflagration wave (MENKES, J. *Stability of a Plane Deflagration Wave, Progr. Rep. No. 20–360.* Jet Propulsion Laboratory: Pasadena, Calif. Submitted for publication in *Proc. Roy. Soc*). revealed that disturbances of a sinusoidal nature which are characterized by large wave numbers (i.e. short wavelengths) are attenuated very rapidly. As the wave number decreases, the decay time becomes progressively longer till for zero wave number (corresponding to a step function) the system is unstable. In the analysis cited above, the crucial assumption made was that the Lewis number of the *unperturbed* flow was unity. The purpose of this note is to extend the applicability of the conclusions reached to small deviations from unity in the Lewis number, say, $N = 1 \pm \nu$ where $\nu \ll 1$.

The governing equations are:

$$\zeta C_p T_t + M c_p T_x - \lambda T_{xx} = \zeta C_p (T_f - T_c)\,\phi\,(T, Y) \quad \ldots\ [1]$$

$$\zeta Y_t + M Y_x - D\zeta Y_{xx} = -\zeta\phi\,(T, Y) \quad \ldots\ [2]$$

$$\zeta_t + M_x = 0 \quad \ldots\ [3]$$

where $\phi(T, Y)$ is the chemical source function, and all the other symbols have the usual meanings. For the purposes of stability analysis, one assumes:

$$T = T_f\{\bar{\theta} + \tau(x, t)\} \quad \ldots\ [4]$$

$$Y = \overline{Y} + y(x, t) \quad \ldots\ [5]$$

$$M = \overline{M}\{1 + \mu(x, t)\} \quad \ldots\ [6]$$

$$\phi = \bar{\phi} + \bar{\phi}_\theta \tau + \bar{\phi}_Y y \quad \ldots\ [7]$$

$(^-)$ signifies that the function satisfies the steady state equations. Straightforward substitution of equations 4, 5, 6 and 7 into equations 1 and 2 keeping only linear terms in the perturbations yields:

$$\tau_t + \theta\tau_x - \theta\tau_{xx} - \psi'\tau - \phi_Y\eta = -\theta\theta_x\mu \quad \ldots\ [8]$$

$$\eta_t + \theta\eta_x - N\theta\eta_{xx} + \psi'\tau + \phi_Y\eta = -\theta Y_x\mu \quad \ldots\ [9]$$

The independent variables have been suitably non-dimensionalized:

$$\psi' = (1 - \theta_c)\{\phi_\theta - \phi/\theta\}$$

and

$$\eta = (1 - \theta_c)\, y$$

The superior bar has been omitted. One may without loss in generality set

$$Y_x = -\{1 + g(x; \nu)\}\,\theta_x \quad \ldots\ [10]$$

where $g(x; \nu) \ll 1$, and $g(x; 0) \equiv 0$. We may now add equations 8 and 9 setting $\tau + \eta = h$.

$$h_t + \theta h_x - \theta h_{xx} = \theta\{\nu\eta_{xx} + \theta_x g(x; \nu)\,\mu\} \quad \ldots\ [11]$$

Within the framework of a linear perturbation theory, the RHS of equation 11 may be neglected since both terms are of second order small. Neglecting those terms leaves an equation that is identical to the one that is obtained if the Lewis number is set identically equal to unity.

This note presents results of one phase of research carried out at the Jet Propulsion Laboratory, California Institute of Technology under Contract No. DA-04-495-Ord 18, sponsored by the Department of the Army, Ordnance Corps.

J. MENKES

Jet Propulsion Laboratory,
California Institute of Technology

(Received October 1958)

Classified Contents

Aldehyde formation during low temperature oxidation, influence of hydrocarbon structure on, 441
Alkyl silanes, spontaneous ignition of, 244
Application of well-stirred reactor theory to the prediction of combustor performance, 13

Burning times of liquid fuel drops in a convection–radiation field, 443
Butane–air and methane–air mixtures, investigations on the inflammability ranges of, ignited by electric sparks, 171
Butane-2,3- and 1,4-diol dinitrates, combustion of the, and some aldehyde–nitrogen dioxide mixtures, 157

Calculation of properties of gases at elevated temperatures, 412
Carbonaceous residues from diffusion flames, a note on polycyclic hydrocarbons in association with, 437
Coal dust clouds, variation with temperature of the explosibility characteristics of, using electric spark ignition, 35
Combustible gases, ignition of, by flames, 3
Combustion of the butane-2,3- and 1,4-diol dinitrates and some aldehyde–nitrogen dioxide mixtures, 157
Comments related to flame blow-off from rectangular burners, 107
Concentration of hydroxyl and of oxygen atoms in gases from lean hydrogen–air flames, 286
Confined jets and recirculation phenomena with cold air, 383
Cork dust, speed of flame in slowly moving clouds of, 365

Decomposition flame of liquid ozone–oxygen mixtures, 348
Detonatability envelope of gaseous fuming nitric acid–*n*-heptane–nitrogen mixtures as a function of initial pressure, 129
Diesel engines, relation between fuel injection and combustion in, 438
Drops in a convection–radiation field, burning times of liquid fuel, 443

Effect of pressure on turbulent burning velocity, 109
Experimental study of a reversed jet flameholder, 333

Flameholder, experimental study of a reversed jet, 333
Flame stability, influence of Lewis number on, 449
Flashback of laminar and turbulent burner flames at reduced pressure, 253
Formation of polycyclic hydrocarbons in diffusion flames, 267
Free radicals, some recent developments concerning, (a review), 193

Gas characteristics in the Chapman–Jouguet state, semi-empirical determination of, 226
Gaseous nitric acid–hydrocarbon flames, 181
Gases at elevated temperatures, on the calculation of the properties of, 412

Hydrazine decomposition, kinetics of, in a laminar non-isothermal flow, 149
Hydrazine flame, 137
Hydrogen–air flames, concentration of hydroxyl and of oxygen atoms in gases from lean, 286
Hydrogen–air flames held on porous burners, hydroxyl concentrations in rich, 229
Hydrogen diffusion flame as an inflammable gas detector, 446
Hydroxyl concentrations in rich hydrogen–air flames held on porous burners, 229

Ignition of combustible gases by flames, 3
Inflammable gas detector, the hydrogen diffusion flame as an, 446
Influence of hydrocarbon structure on aldehyde formation during low temperature oxidation, 441
Influence of Lewis number on flame stability, 449
Inhibition of methane–air flames by gaseous aluminium chloride, 105
Investigations on the inflammability ranges of methane–air and butane–air mixtures ignited by electric sparks, 171

Kinetics of hydrazine decomposition in a laminar non-isothermal flow, 149

Laminar flame theory, 101, 225

Measuring burning velocity, use of constant-volume bomb technique for, 273
Measuring flame and exhaust gas termperatures, note on monochromatic radiation pyrometry for, 330
Methane–air and butane–air mixtures, investigations on the inflammability ranges of, ignited by electric sparks, 171
Methane–air flames, inhibition of, by gaseous aluminium chloride, 105
Methyl nitrite decomposition flame, 55
Monochromatic radiation pyrometry for measuring flame and exhaust gas temperatures, 330

Nitric acid–*n*-heptane–nitrogen mixtures, detonatability envelope of gaseous fuming, as a function of initial pressure, 129
Nitric acid–hydrocarbon flames, gaseous, 181
Note on Spalding's centroid formula, 328

Ozone–oxygen mixtures, on the decomposition flame of liquid, 348

Polycyclic hydrocarbons, formation of, in diffusion flames, 267
Polycyclic hydrocarbons in association with the carbonaceous residues from diffusion flames, 437
Prediction of combustor performance, application of well-stirred reactor theory to, 13
Premixed spherical flames, 103
Propane, separation of products of cool flame oxidation of, 117

Recent developments and notes, 83, 208, 305, 421
Recirculation phenomena, confined jets and, with cold air, 383
Rectangular burners, comments related to flame blowoff from, 107
Relation between fuel injection and combustion in diesel engines, 438
Review of some unusual stationary flame reactions, 69

Semi-empirical determination of gas characteristics in the Chapman–Jouguet state, 226
Separation of the products of cool flame oxidation of propane, 117
Seventh International Symposium on Combustion—a brief survey, 322
Some recent developments concerning free radicals (a review), 193
Spalding's centroid formula, note on, 328
Spectroscopic studies on temperature gradients in flames, 353
Speed of flame in slowly moving clouds of cork dust, 365
Spontaneous ignition of alkyl silanes, 244
Stationary flame reactions, review of some unusual, 69

Temperature gradients in flames, spectroscopic studies on, 353
Turbulent burning velocity, effect of pressure on, 109

Use of constant-volume bomb technique for measuring burning velocity, 273

Variation with temperature of the explosibility characteristics of coal dust clouds, using electric spark ignition, 35

Author Index

ADLER, J. and SPALDING, D. B.: Laminar flame theory, 225
AGNEW, J. T.: *See* ESCHENBACH, R. C. and AGNEW, J. T.
AGOSTON, G. A., NOON, A. W. and WITHERLY, T. D.: Experimental study of a reversed jet flameholder, 333
ALLEN, D. H. and LONG, R.: A note on the influence of hydrocarbon structure on aldehyde formation during low temperature oxidation, 441
AMDUR, I. and ROSS, J.: On the calculation of properties of gases at elevated temperatures, 412
ARDEN, E. A. and POWLING, J.: The methyl nitrite decomposition flame, 55
ARTHUR, J. R., COMMINS, B. T., GILBERT, J. A. S., LINDSEY, A. J. and NAPIER, D. H.: Formation of polycyclic hydrocarbons in diffusion flames, 267
AUSTEN, A. E. W. and LYN, W. T.: The relation between fuel injection and combustion in diesel engines, 438

BADAKHSHAN, A., GARNER, F. H. and LONG, R.: A note on polycyclic hydrocarbons in association with the carbonaceous residues from diffusion flames, 437
BONNELL, A. H.: *See* HOTTEL, H. C., WILLIAMS, G. C. and BONNELL, A. H.
BURGESS, D. S.: *See* WOLFHARD, H. G. and BURGESS, D. S.
BURGOYNE, J. H.: review of *Dangerous Properties of Industrial Materials*, 435

CARPENTER, D. L. and DAVIES, D. R.: The variation with temperature of the explosibility characteristics of coal dust clouds, using electric spark ignition, 35
COMMINS, B. T.: *See* ARTHUR, J. R., COMMINS, B. T., GILBERT, J. A. S., LINDSEY, A. J. and NAPIER, D. H.
CURTET, R.: Confined jets and recirculation phenomena with cold air, 383

DALMAI, GISÈLE: Investigations on the inflammability ranges of methane–air and butane–air mixtures ignited by electric sparks, 171
DAVIES, D. R.: *See* CARPENTER, D. L. and DAVIES, D. R.

EDWARDS, P. D. and LONG, R.: The hydrogen diffusion flame as an inflammable gas detector, 446
ESCHENBACH, R. C. and AGNEW, J. T.: Use of the constant-volume bomb

technique for measuring burning velocity, 273
ESSENHIGH, R. H. and WOODHEAD, D. W.: Speed of flame in slowly moving clouds of cork dust, 365
— *See* MASDIN, E. G. and ESSENHIGH, R. H.

FERGUSON, R. E.: *See* YOKLEY, C. R. and FERGUSON, R. E.
FINE, B.: Effect of pressure on turbulent burning velocity, 109
— The flashback of laminar and turbulent burner flames at reduced pressure, 253
FRIEDMAN, R. and LEVY, J. B.: Inhibition of methane–air flames by gaseous aluminium chloride, 105
FRISTROM, R. M.: Premixed spherical flames, 103

GARNER, F. H.: *See* BADAKHSHAN, A., GARNER, F. H. and LONG, R.
GILBERT, J. A. S.: *See* ARTHUR, J. R., COMMINS, B. T., GILBERT, J. A. S., LINDSEY, A. J. and NAPIER, D. H.
GILBERT, M.: Kinetics of hydrazine decomposition in a laminar non-isothermal flow, 149
— The hydrazine flame, 137
GRIFFITHS, S. T. and WILSON, R. R.: The spontaneous ignition of alkyl silanes, 244
GROSSMAN, M.: *See* TOURIN, R. H. and GROSSMAN, M.
GRUMER, J. and HARRIS, MARGARET E.: Comments related to flame blowoff from rectangular burners, 107

HARRIS, MARGARET E.: *See* GRUMER, J. and HARRIS, MARGARET E.
HOTTEL, H. C., WILLIAMS, G. C. and BONNELL, A. H.: Application of well-stirred reactor theory to the prediction of combustor performance, 13

KASKAN, W. E.: Hydroxyl concentrations in rich hydrogen–air flames held on porous burners, 229
— The concentration of hydroxyl and of oxygen atoms in gases from lean hydrogen–air flames, 286
KIRKBY, W. A.: Recent developments and notes, 83, 208, 305, 421

LEVY, J. B.: *See* FRIEDMAN, R. and LEVY, J. B.
LINDSEY, A. J.: *See* ARTHUR, J. R., COMMINS, B. T., GILBERT, J. A. S., LINDSEY, A. J. and NAPIER, D. H.
LONG, R.: *See* ALLEN, D. H. and LONG, R.
— *See* BADAKHSHAN, A., GARNER, F. H. and LONG, R.
LONG, R.: *See* EDWARDS, P. D. and LONG, R.
LYN, W. T.: *See* AUSTEN, A. E. W. and LYN, W. T.

MACCALLUM, N. R. L.: Comments related to flame blowoff from rectangular burners, 108
MANSON, N.: Semi-empirical determination of gas characteristics in the Chapman–Jouguet state, 226
MASDIN, E. G. and ESSENHIGH, R. H.: Burning times of liquid fuel drops in a convection–radiation field, 443
MENKES, J.: A note on Spalding's centroid formula, 328
— A note on the influence of the Lewis number on flame stability, 449
MERTENS, J. and POTTER, R. L.: Gaseous nitric acid–hydrocarbon flames, 181
MINKOFF, G. J.: Seventh International Symposium on Combustion—a brief survey, 322
— Some recent developments concerning free radicals (a review), 193

NAPIER, D. H.: *See* ARTHUR, J. R., COMMINS, B. T., GILBERT, J. A. S., LINDSEY, A. J. and NAPIER, D. H.
NOON, A. W.: *See* AGOSTON, G. A., NOON, A. W. and WITHERLY, T. D.

PARKER, W. G.: A review of some unusual stationary flame reactions, 69
PERRY, M. G.: review of *Sixth Symposium (International) on Combustion*, 327
POTTER, R. L. and WAYMAN, D. H.: The detonatability envelope of gaseous fuming nitric acid–*n*-heptane–nitrogen mixtures as a function of initial pressure, 129
— *See* MERTENS, J. and POTTER, R. L.
POWLING, J. and SMITH, W. A. W.: The combustion of the butane-2,3- and 1,4-diol dinitrates and some aldehyde–nitrogen dioxide mixtures, 157
— *See* ARDEN, E. A. and POWLING, J.

ROSS, J.: *See* AMDUR, I. and ROSS, J.

SANDRI, R.: Laminar flame theory, 101
— On the decomposition flame of liquid ozone–oxygen mixtures in a tube, 348
SMITH, W. A. W.: *See* POWLING, J. and SMITH, W. A. W.
SPALDING, D. B.: Laminar flame theory, 101
— review of *Heat Exchangers*, 436
— *See* ADLER, J. and SPALDING, D. B.
TOURIN, R. H.: Spectroscopic studies on temperature gradients in flames, 353
— and GROSSMAN, M.: Note on monochromatic radiation pyrometry for measuring flame and exhaust gas temperatures, 330

WAYMAN, D. H.: *See* POTTER, R. L. and WAYMAN, D. H.
WILLIAMS, G. C.: *See* HOTTEL, H. C., WILLIAMS, G. C. and BONNELL, A. H.
WILSON, R. R.: *See* GRIFFITHS, S. T. and WILSON, R. R.
WITHERLY, T. D.: *See* AGOSTON, G. A., NOON, A. W. and WITHERLY, T.D.
WOLFHARD, H. G. and BURGESS, D. S.: The ignition of combustible gases by flames, 3
WOODHEAD, D. W.: *See* ESSENHIGH, R. H. and WOODHEAD, D. W.
YOKLEY, C. R. and FERGUSON, R. E.: Separation of the products of cool flame oxidation of propane, 117

Name Index

ADAMS, E. N. 101, 225, 226
ADAMS, G. K. 63, 68, 70, 74, 76, 81, 82, 137, 157, 170
ADLER, J. 226
AGNEW, J. T. 273
AGOSTON, G. A. 96, 333
ALBERTSON, M. L. 389, 411
ALBORN, J. 136
ALEXEJEW, D. 71, 81
ALLEN, D. H. 443
ALTMAN, D. 81, 82, 95, 147
AMDUR, I. 412, 420
ANDERSON, R. C. 71, 72, 81, 82
ARDEN, E. A. 55, 78, 82, 170
ARKLESS, F. 432
ARMSTRONG, G. T. 213
ARTHUR, J. R. 267, 272, 437, 438
ATEN, C. F. 200, 206
AUSTEN, A. E. W. 441
AVERY, W. H. 14, 33
AVETISYANTS, L. B. 84
AVRAMENKO, L. 241, 243, 297, 304

BADAKHSHAN, A. 107, 438
BAILEY, J. J. 212
BAINES, W. D. 403, 411
BAKER, M. L. 34
BALDWIN, R. R. 198, 206, 297, 304
BARBERO, L. P. 381
BARRÈRE, M. 99
BARROW, R. F. 243, 304
BARTHOLOMÉ, E. 73, 82
BASS, A. M. 243
BASU, D. 372, 382
BAXTER, W. P. 304
BEAL, A. J. 381
BENEDICT, W. S. 353, 358, 364
BENNET, W. J. 94, 97
BENSON, H. E. 212
BENSON, J. N. 203, 207
BERETS, D. J. 136, 227, 228
BERINGER, R. 196, 205
BERKOVITCH, I. 310
BERL, W. G. 14, 33
BERLAD, A. L. 262, 266
BIRD, R. B. 192, 420
BIRSE, E. A. B. 140, 148
BLACKTIN, S. C. 35, 54
BLACKWOOD, J. D. 423
BLANC, M. V. 11
BLAYDEN, H. E. 218
BLINOV, V. I. 221
BLOOM, R., Jr 85
BLUNDELL, A. 311
BOLLINGER, L. 116
BOLLINGER, L. E. 266
BONNELL, A. H. 13
BOORD, C. E. 127, 128
BOSNJAKOVIC, F. 312
BOTHA, J. P. 243
BOUDOUARD, O. 447, 449
BOWERS, V. A. 205, 207
BOWSER, M. L. 306
BOYER, M. H. 75, 82, 136, 181, 183, 185, 187, 192, 266
BOYLE, A. R. 39, 54
BREWSTER, H. M. 448, 449
BRINKLEY, RUTH F. 88
BRINKLEY, S. R., Jr 129, 136
BROIDA, H. P. 195, 197, 200, 203, 205, 206, 243
BROMLEY, L. A. 255, 266
BROTHERTON, T. D. 82
BROUGHTON, J. W. 351
BROWN, H. W. 207
BROWN, K. C. 372, 381, 382
BRUNN, L. M. 212
BRUNSVOLD, N. J. 85
BRYCE, W. A. 198, 206
BUCHANAN, R. A. 307
BULEWICZ, E. M. 243, 304
BURDEN, M. C. 82
BURGESS, D. S. 3, 197, 206
BURGESS, M. J. 447, 449
BURGESS, R. 199, 206
BURGOYNE, J. H. 82, 219, 372, 382, 429, 436, 446
BURKE, E. 82
BYINGTON, H. W. 136, 192

CALCOTE, H. F. 321
CALDER, D. S. 68
CALDWELL, F. R. 285, 317
CALLEAR, A. B. 119, 128, 199, 206
CALLOMON, J. H. 200, 206
CALVERT, J. G. 201, 206
CAMBEL, A. B. 333, 334, 347
CAMPBELL, C. E. 200, 206
CAMPBELL, D. E. 348, 352
CAMPBELL, E. S. 81, 82
CARHART, H. W. 426
CARPENTER, D. L. 35, 39, 54

CARRINGTON, T. 197, 206
CARSLAW, H. S. 347
CASSEL, H. M. 370, 371, 372, 381
CAVE-BROWNE-CAVE, T. R. 421
CHAMBERLAIN, E. A. C. 443
CHAMBERS, L. A. 423
CHARWAT, A. F. 95
CHESTERS, J. H. 431
CHOUDHURY, A. P. R. 313
CLARK, T. P. 111, 116
CLOUSTON, J. G. 205
CLOWES, F. 449
CLUSIUS, K. 200, 206
COCHRAN, E. L. 205, 207
COCKCROFT, Sir JOHN 210, 211
COHEN, E. S. 319
COHEN, L. 446
COHEN DE LARA, G. 404, 411
COLE, T. 203, 207
COLEMAN, E. H. 446, 449
COMMINS, B. T. 267, 437, 438
CONSTANT, HAYNE 305
CONWAY, J. B. 317
COOK, E. B. 116
COOK, E. G. 284, 285
COOLIDGE, A. S. 420
COOPER, J. C. 83
COOPER, R. L. 272, 437, 438
CORNER, J. 225, 226
CORRSIN, S. 389, 411
COURANT, R. 276, 285
COWARD, H. F. 91, 449
CRAIG, O. 382
CRAYA, A. 383, 397, 398, 401, 402, 404, 406, 409, 410, 411
CROSSWHITE, H. M. 231, 243
CROTTY, W. W. 243, 304
CULLEN, R. E. 113, 116
CULLIS, C. F. 252, 310, 443
CURTET, R. 383, 397, 398, 401, 402, 404, 406, 409, 410, 411
CURTISS, C. F. 192, 348, 352, 420
CVETANOVIC, R. J. 119, 128
CYBULSKI, W. B. 382
CYPHERS, J. A. 113, 116

DAI, Y. B. 389, 411
DALBY, F. W. 205, 207
DALMAI, GISÈLE 171, 180
DALY, E. F. 353, 364
DAMKÖHLER, G. 114, 116, 431
DAS GUPTA, A. K. 372, 381
DAVIES, C. N. 98
DAVIES, D. R. 35
DAVIS, R. F. 88
DAY, R. J. 83
DE GREY, A. 371, 382
DEISSLER, R. G. 148, 156
DELBEL, E. 438
DELBOURGO, R. 180
DE LORENZI, O. 382
DEMPSTER, P. B. 105, 107
DENNISTON, D. W. 431
DESTY, D. H. 122, 128, 449
DEVORE, P. 425
DEZUBAY, E. A. 14, 33
DIEDERICHSEN, J. 283, 285, 446
DIEKE, G. H. 231, 243
DI PIAZZA, J. T. 180
DITTRICH, R. T. 92
DIXON, H. B. 72, 82, 227, 228
DIXON-LEWIS, G. 430
DOAN, R. L. 428
DOLAN, J. E. 105, 107
DONNELLY, J. A. 95
DOUGLAS, A. E. 200, 206
DOUSMANIS, G. C. 206
DOWNEY, A. R. 243, 304
DOWS, D. A. 204, 205, 207
DRESSLER, K. 204, 207
DREW, C. M. 127, 128
DRUMMOND, L. J. 157, 170
DUGGER, G. L. 105, 107, 255, 266, 278, 285
DUGLEUX, P. 180
DUMORTIER, J. 318
DUNCAN, A. B. F. 304
DURIE, R. A. 79, 82
DURR, A. 220, 371, 372, 381
DWYER, R. J. 243, 304

EDSE, R. 266
EDWARDS, D. H. 215
EDWARDS, J. W. 198, 206
EDWARDS, P. D. 449
EGERTON, Sir ALFRED 34, 82, 90, 215, 421, 430
EGY, W. L. 372, 382
EKLUND, S. 210
ELLIOTT, J. F. 307
ELLIS, J. W. 364
ELTENTON, G. C. 194, 198, 205
ERHARD, K. H. L. 198, 206
ESCHENBACH, R. C. 273, 277, 285
ESSENHIGH, R. H. 86, 218, 365, 372, 382, 446
EUSTIS, R. H. 333, 347
EVANS, MARJORIE W. 347
EVERETT, A. J. 197, 205
EYE, M. 423
EYRAUD, C. 425
EYRING, H. 148

FABRI, J. 431
FAIRBAIRN, A. R. 72, 82, 195, 199, 205, 206
FEHLING, R. 208
FENIMORE, C. P. 241, 243, 297, 304
FERGUSON, R. E. 117, 199, 206
FERRIE, F. 285
FETTING, F. 313
FIELD, J. H. 212
FIELD, J. P. 347
FINE, B. 109, 116, 253, 266
FINHOLT, A. E. 252
FIOCK, E. F. 285, 317

FISHEL, J. B. 272
FOERING, L. 136
FOK, N. V. 221
FONER, S. N. 194, 198, 203, 205, 206, 207
FORST, W. 309
FÖRTHMANN, E. 389, 411
FORSTALL, W. 394, 411
FOURÉ, C. 431
FRAEIJS DE VEUBEKE, B. 99
FRAENKEL, G. K. 205
FRANKLIN, ROSALIND E. 306
FRASER, R. P. 98
FRAZEE, J. D. 81
FREAMO, M. 195, 205
FRECH, M. F. 136, 189, 192
FRÉLING, E. 180
FRENCH, F. J. 252
FRIAUF, J. B. 227, 228
FRIEBERTSHAUSER, P. E. 75, 82, 136, 181, 183, 186, 187, 192, 266
FRIEDMAN, R. 82, 107
FRIEDRICHS, K. O. 276, 285
FRISTROM, R. M. 104, 105
FROST, A. A. 148
FROST, E. E. 34, 333, 347

GALLAGHER, J. 207
GARNER, F. H. 105, 107, 438
GARSIDE, J. E. 116
GAYDON, A. G. 192, 193, 195, 197, 199, 200, 202, 205, 206, 215, 243, 303, 304, 438
GAZLEY, C. 266
GÉRARD, P. L. 218
GERSTEIN, M. 82, 247
GHORMLEY, J. 206
GHOSH, B. 372, 382
GIBSON, F. C. 83, 306
GIGUÈRE, P. A. 198, 206, 309
GILBERT, J. A. S. 267, 272, 437, 438
GILBERT, M. 81, 82, 95, 137, 147, 148, 149, 156, 330
GLASSTONE, S. 148
GLEIM, E. J. 12
GLICK, C. F. 420
GLIKSMAN, J. 423
GODSAVE, G. A. E. 446
GODWIN, E. 424
GOLDBERG, S. A. 208
GOLDSMITH, M. 446
GORDON, A. S. 95
GORDY, W. 201, 206
GORIN, E. 201, 206
GRAETZ, L. 144, 148, 156
GRAHAM, A. J. 107
GRAVES, C. C. 92
GRAY, J. A. 56, 68
GRAY, P. 55, 68, 70, 75, 78, 81, 82, 138, 147, 192
GREEN, H. L. 98
GREEN, T. E. 68
GREENE, E. F. 136, 195, 200, 205, 206, 227, 228, 308
GREENWALD, H. P. 372, 382
GREIFER, B. 83
GRIFFITHS, S. T. 244
GROBMAN, J. S. 92
GROSSE, A. V. 79, 82, 221, 317, 348, 351
GROSSMAN, M. 332
GROVER, J. H. 431
GRUMER, J. 108, 116, 128, 284, 285
GUÉNOCHE, H. 179, 180
GUEST, P. G. 43, 54
GUMZ, W. 88
GURUSWAMY, S. 372, 381

HALL, A. R. 55, 68, 69, 70, 75, 81, 82, 139, 147, 148, 170, 192, 433, 445, 446
HALPERN, C. 213
HARDCASTLE, J. W. 220
HARDING, J. T. 207
HARDY, F. R. F. 310
HARKNESS, A. L. 420
HARRIS, MARGARET E. 107, 108
HART, A. B. 70, 81
HART, R. W. 14, 33
HARTECK, P. 68
HARTMANN, I. 372, 382
HARVEY, K. B. 203, 206, 207
HARVEY, T. J. 422
HASHMAN, J. S. 198, 206
HASKINS, J. F. 272
HASLAM, R. T. 382
HATTORI, H. 372, 382
HAWTHORNE, W. R. 209
HAY, R. 308
HAYNES, W. P. 212
HEALD, M. A. 196, 205
HEATH, D. F. 200, 206
HELLER, L. W. 382
HELLWIG, K. 81
HENKEL, M. J. 136
HENRY, P. M. 363
HERON, J. 197, 205
HERZBERG, G. 195, 199, 201, 204, 205, 206, 207, 243, 355, 364
HERZFELD, C. M. 203, 206, 207
HERZFELD, K. F. 420
HIGGINS, W. F. 72, 82
HINKAMP, J. B. 209
HINSHELWOOD, C. N. 63, 68, 137, 147, 312, 315
HINZE, J. O. 389, 411
HIROSHI JINNO, 411
HIRSCHFELDER, J. O. 192, 348, 352, 420
HOBBS, J. C. 382
HOGG, A. 431
HOLDEN, C. 431
HORN, G. 411
HORNBECK, G. A. 243, 304, 332, 356, 363, 364
HORNER, E. C. A. 206
HOTTEL, H. C. 12, 13, 34, 89, 319
HOWARTH, L. 148, 156

HRYNISZAK, W. 436
HUBBARD, E. H. 83, 86
HÜBNER, J. 111, 116
HUDSON, R. L. 194, 198, 205, 206
HULSE, C. 411
HUMMEL, H. 136
HUMPHREY, N. B. 72, 82

IEVLEVA, Z. V. 316
IIDA, H. 431
INGOLD, K. U. 198, 206
ISLES, G. L. 430

JACKSON, B. 116
JACKSON, J. L. 248, 252
JAEGER, J. C. 347
JAKOB, M. 148, 156
JAMES, C. G. 243, 304
JAMES, H. J. 420
JAMES, R. S. 12
JAUMOTTE, A. 99
JEN, C. K. 196, 205, 207
JENKINS, G. I. 35, 54
JENNINGS, K. R. 203, 207
JENSEN, R. A. 389, 411
JESSUP, R. S. 214
JOHNSON, A. E. 91
JOHNSON, I. 200, 206
JOHNSON, J. E. 426
JOHNSTON, H. S. 136
JOHNSTON, W. C. 113, 116
JONES, E. 366, 382
JONES, G. W. 81, 241, 243, 297, 304, 449
JONES, L. M. 372, 382
JONES, R. A. 198, 206
JONES, W. R. D. 53
JORDAN, J. E. 420
JOST, W. 3, 12

KANE, G. P. 443
KANE, W. R. 284, 285
KANTROWITZ, A. 195, 205
KAPP, N. M. 266
KARLOVITZ, B. 431
KASKAN, W. E. 229, 243, 286, 304
KASSEL, L. S. 145, 147
KAUFMAN, F. 304
KAVANAGH, G. M. 71, 81
KEBELY, V. 116
KENNEDY, R. E. 81
KHUDYAKOV, G. N. 221
KIESS, N. H. 200, 206
KINNEY, C. R. 438
KIRKBY, W. A. 93, 223, 321, 332, 434
KIRKWOOD, J. G. 129, 136
KIRSCHENBAUM, A. D. 79, 82, 221
KISLIG, F. 371, 372, 382
KISTIAKOWSKY, G. B. 135, 136, 190, 192, 203, 207, 215, 227, 228, 304
KITAGAWA, T. 82
KLÄUKENS, H. 111, 116
KLEIN, E. 313
KLEIN, R. 68, 202, 206
KLING, R. 312
KNEWSTUBB, P. F. 211
KONDRATIEV, V. 243
KORNFELD, G. 71, 81
KOSTKOWSKI, H. J. 197, 206, 243
KREEVOY, M. M. 420
KREISINGER, H. 382
KRIEBEL, A. R. 347
KUETHE, A. M. 316
KUHN, L. P. 165, 170
KYDD, P. H. 304
KYRYAKOS, G. 128

LAFFITTE, P. 180
LAIDLER, K. H. 207
LAIDLER, K. J. 148
LANE, W. R. 98
LEACH, H. A. 147
LE CHATELIER, N. 447, 449
LECK, J. H. 98
LEE, J. C. 70, 81, 138, 147
LE FEVRE, E. J. 419, 420
LEROY, D. J. 119, 128
LEVY, A. 429
LEVY, J. B. 68, 107
LEWIS, B. 3, 12, 180, 191, 192, 227, 228, 230, 243, 266, 285, 288, 304, 317, 347, 348, 351, 421
LEWIS, G. N. 195, 205
LINDEMANN, O. 137
LINDSEY, A. J. 267, 272, 437, 438
LINNETT, J. W. 73, 82, 203, 207, 317
LIPKIN, D. 195, 205
LIVINGSTON, R. 196, 197, 205, 206
LLEWELLYN, F. J. 39, 54
LONG, R. 107, 438, 443, 449
LONG, V. D. 219, 372, 381, 382
LONGFIELD, J. E. 68
LONGWELL, J. P. 15, 34, 313, 333, 347
LONIE, G. 308
LORELL, J. 105
LORENTSO, R. 241, 243, 297, 304
LOSSING, F. P. 194, 205
LUCQUIN, M. 425
LYN, W. T. 441

MACCALLUM, N. R. L. 107, 108
MCCARTY, M. 206, 207
MCCORMICK, C. G. 201, 206
MCCOUBREY, J. C. 170
MCDONALD, G. E. 82, 247
MCGRORY, F. 423
MCKINNEY, H. 136
MCLENNAN, J. C. 202, 206
MCNESBY, J. R. 127, 128
MADER, P. P. 423
MADOR, I. L. 201, 206
MANSON, N. 228, 285
MANTON, J. 113, 116, 266, 284, 285
MARBLE, F. E. 155, 347

MARKSTEIN, G. H. 180, 320
MARSKELL, W. G. 87
MARTIN, D. G. 216
MARTIN, W. T. 333, 347
MARUSCHAK, P. 136
MARVIN, C. F. 285, 317
MASANAGA KUNUGI, 411
MASCOLO, R. W. 116
MASDIN, E. G. 446
MASON, C. M. 83, 306
MASON, E. A. 420
MASON, T. N. 382
MASON, W. 372, 382
MATHESON, M. S. 196, 205
MEARS, T. W. 214
MEISSNER, H. P. 100
MELVILLE, H. W. 140, 148
MENAPACE, H. 128
MENKES, H. R. 316
MENKES, J. 330, 449, 450
MERTENS, J. 181
MESSERLY, G. H. 136
MESTRE, A. 313
MEUNIER, J. 224
MILLÁN, G. 95, 146, 147
MILLER, E. 82, 192
MILLIGAN, D. E. 203, 207
MILLIKEN, B. B. 113, 116, 266, 284, 285
MINKOFF, G. J. 193, 195, 197, 198, 199, 205, 206, 207, 322
MITCHELL, J. W. 68
MONKHOUSE, A. C. 92
MOORE, G. E. 243, 304
MOORE, N. P. W. 202, 206, 216
MORGAN, G. H. 284, 285
MOTT, B. W. 210
MRAZ, C. L. 333, 347
MUKAI, M. 272
MULLEN, J. D. 311
MULLINS, B. P. 244, 252
MUNDAY, S. D. C. 99
MURPHREE, E. V. 428
MURRAY, R. C. 69, 81, 139, 148
MYERS, J. W. 208

NALBANDJAN, A. B. 221
NAPIER, D. H. 267, 272, 437, 438
NEEDHAM, D. P. 68, 77, 82, 170, 190, 192, 309
NEUBERGER, D. 304
NEWBY, M. P. 405, 408, 409, 410, 411
NEWTON, Miss J. 68
NICHOLSON, H. M. 347
NINOMIYA, M. 304
NOON, A. W. 96, 333, 347
NOREEN, A. E. 333, 347
NORMAN, I. 195, 205
NORRISH, R. G. W. 90, 195, 196, 198, 205, 206, 304

O'DONOVAN, K. H. 317
OLDENBERG, O. 243, 304
OLSEN, L. O. 332, 356, 364

OOTUKA, H. 82
ORLICK, C. A. 78, 82
ORNING, A. A. 382
OSTERLÉ, J. F. 394, 411
OURA, H. 304

PAHNKE, A. J. 85
PARKER, W. G. 63, 68, 69, 73, 74, 82, 136, 192
PATTERSON, W. L., Jr 308
PAULING, L. 355, 364
PEARLMAN, H. 420
PEARSON, R. G. 148
PEARSON, S. W. 431
PEASE, R. N. 216
PEIRCE, T. J. 86, 87
PELLAM, J. R. 202, 206, 207
PENNER, S. S. 95, 147, 197, 206, 225, 226, 334, 347, 348, 352
PERRIN, F. 210
PERRY, J. H. 108, 449
PERRY, M. G. 218, 327, 382
PERRY, R. W. 195, 205
PETERSON, C. 262, 266
PEYRON, M. 203, 206
PHILLIPS, V. D. 82
PIGFORD, R. L. 347
PIMENTEL, G. C. 205, 207
PIPENBERG, K. J. 85
PLYLER, E. K. 332, 358, 364
POLYAKOV, M. V. 425
PONCELET, J. 216
PORTER, G. 72, 82, 195, 196, 205, 207, 271, 272, 304, 308
POTTER, A. E., Jr 262, 266
POTTER, R. L. 129, 136, 181, 191, 192
POWLING, J. 55, 68, 77, 78, 82, 105, 157, 170, 190, 192, 215, 309
PRATT, M. W. T. 55, 78, 82, 192
PRESCOTT, R. 347
PRETTRE, M. 425
PRIEDE, T. 427
PROUT, W. E. 71, 81

RALLIS, C. J. 317
RAMSAY, D. A. 195, 200, 204, 205, 206, 207
RAMSPERGER, H. C. 145, 148
RANQUE, G. J. 215
RASBASH, D. J. 445, 446
REDWOOD, B. 449
REED, R. I. 202, 206
REICHARDT, H. 389, 411
REITER, S. H. 116
RESNICK, H. 71, 81
RIBAS-MARQUÈS, I. 370, 382
RIBAUD, G. M. 89
RICE, F. O. 62, 68, 195, 204, 205, 207
RICE, G. S. 372, 382
RICE, J. L. 14, 33
RICE, O. K. 145, 148
RICE, W. E. 420
RICHARDSON, J. F. 99

RICHARDSON, J. M. 129, 136
RIEKE, F. F. 243, 304
RIVIÈRE, M. 409, 411
ROBB, J. C. 199, 206
ROBERTSON, A. J. B. 198, 206
ROBERTSON, W. W. 72, 82
ROBINSON, G. W. 197, 204, 206, 207
ROBINSON, H. 35, 54
RODEBUSH, W. H. 304
RODOWSKAS, E. L. 62, 68
ROEDER, C. H. 285, 317
ROGOWSKI, Z. E. 445, 446
ROSE, H. E. 427
ROSEN, P. 14, 33, 420
ROSIN, P. 208
ROSS, J. 412, 420
ROSSER, W. A., Jr 107
ROUSE, H. 389, 411
ROY, N. K. 372, 382
ROZLOVSKII, A. I. 64, 68, 74, 82
RUBIN, F. L. 266
RUDINGER, G. 320
RUDRAKANCHANA, S. 82
RUEGG, F. W. 213
RUHERWEIN, R. 197, 205
RUMMEL, K. 271, 272
RUSSELL, R. P. 382

SAAD, M. A. 217
SALEH, M. A. 310
SANDERS, T. M. 206
SANDRI, R. 101, 348, 351
SANZ, S. 146, 147
SATTERFIELD, C. N. 12, 71, 81
SAUNDERS, O. A. 34, 315
SAX, N. I. 435
SCHAAF, V. P. 78, 82, 309
SCHAFFER, A. 333, 347
SCHALLA, R. L. 82, 247, 250, 252
SCHATZ, P. N. 420
SCHAWLOW, A. L. 206
SCHAY, G. 82
SCHEER, M. D. 68
SCHELKIN, K. I. 305
SCHERBER, F. I. 204, 207
SCHIFF, H. I. 197, 205
SCHMIDT, H. 89, 332
SCHNEIDER, G. 423
SCHOEN, L. J. 68, 201, 202, 206
SCHOLL, J. R. 136, 192
SCHULTZ, H. 107, 108
SCHWARTZ, R. N. 420
SCOTT, F. H. 306
SCOTT, R. P. W. 446, 449
SCRIVENER, J. 68, 76, 82
SCURLOCK, A. C. 431
SEAGER, J. 381
SECCO, E. A. 198, 206
SELLE, H. 68
SEMENOV, N. N. 221, 312
SETZER, H. J. 82, 192
SHAW, G. T. 61, 68
SHAW, S. K. 382
SHERMAN, R. A. 89, 330, 332
SHERWOOD, T. K. 347
SHOOSMITH, J. 201, 206
SHORE, L. 116, 266
SHORIN, S. N. 84
SHRUM, I. 202, 206
SIESTRUNCK, R. 431
SIDDALL, R. G. 431
SILVERMAN, S. 332, 353, 364
SIMMONS, R. F. 80, 82, 107, 198, 206
SIMPSON, C. J. S. M. 73, 82
SIMPSON, H. C. 446
SINGER, J. M. 113, 116, 284, 285
SKIRROW, G. 79, 82, 311
SLAWSKY, Z. I. 420
SLOOTMAKERS, P. J. 216
SMALL, N. J. H. 442, 443
SMALLER, B. 196, 205
SMITH, M. L. 382
SMITH, P. B. 92
SMITH, R. W., Jr 208
SMITH, S. R. 95
SMITH, W. A. W. 68, 78, 82, 157, 170
SOMERS, L. M. 180
SPALDING, D. B. 14, 34, 90, 101, 146, 148, 225, 226, 243, 320, 328, 329, 430, 436, 446
SPAULDING, W. P. 136
SPEALMAN, M. L. 304
SPIERS, H. M. 382
SPOKES, G. N. 215
SPOLAN, I. 81
SQUIRE, H. B. 388, 390, 411
STARK, G. W. V. 445, 446
STEACIE, E. W. R. 61, 68, 193, 201, 205, 206
STEHLING, F. C. 81
STEINBERGER, R. 78, 82, 309
STIMSON, H. F. 332
STINSON, E. W. 382
STOCKS, G. W. 70, 81, 137, 147
STRASSER, A. 12, 68
STRENG, A. G. 82, 348, 351
STRICKLAND-CONSTABLE, R. F. 98, 100
STRONG, J. 353, 364
STYLE, D. W. G. 56, 68, 206
SUGDEN, T. M. 211, 243, 304
SUMMER, D. 206
SUMMERFIELD, M. 116
SUMMERS, C. R. 306
SUNAVALA, P. 411
SURUGUE, I. 313
SUTHERLAND, G. B. B. M. 353, 364
SZWARC, M. 140, 144, 148, 156

TAFFANEL, J. 220, 371, 372, 381
TAILBY, S. R. 310
TANDLER, W. S. 332
TANFORD, C. 63, 68, 216
TANNENBAUM, S. 252
TAO, YU-SHENG 136
TAYLOR, D. C. 147

TAYLOR, E. H. 196, 205
TAYLOR, G. I. 276, 285
TAYLOR, J. 308
TAYLOR, J. A. 63, 68
TAYLOR, J. H. 353, 364
TAYLOR, R. L. 308
TEBBENS, B. D. 272
TEMPLE, R. G. 442, 443
TERRES, E. 429
TESNER, P. A. 316
THEILE, H. 76, 82
THOMAS, C. A. 107
THOMAS, J. F. 272
THOMPSON, R. J. 136
THORP, C. E. 352
THORP, N. 438
THRING, M. W. 86, 87, 89, 90, 219, 220, 405, 408, 409, 410, 411, 431, 446
THRUSH, B. A. 195, 196, 203, 205, 207
THURLOW, G. G. 313
TICKNER, A. W. 194, 205
TIDESWELL, F. V. 376, 382
TOONE, B. 432
TOPONAK, T. 191
TORREY, J. D. 272
TOURIN, R. H. 332, 353, 364
TOWNEND, D. T. A. 434, 443
TOWNES, G. H. 198, 206
TOWNSEND, A. A. 411
TRINKS, W. 382
TROUNCE, P. C. 422
TROUNCER, J. O. 388, 390, 411
TSIEN, H. S. 431
TURNER, D. W. 310

UBBELOHDE, A. R. 252, 442, 443
UBEROI, M. S. 316
UNDERWOOD, G. 219

VANDENKERCKHOVE, J. 99
VAN DER HEGGE ZIJNEN, B. G. 389, 411
VAN DOLAH, R. W. 88
VAN TIGGELEN, A. 216
VEGARD, L. 202, 206
VEH, P. O. 271, 272
VERON, M. 318
VICKERS, J. M. F. 215
VIOLETT, T. D. 82
VOLLHARDT, F. 208
VOLPI, G. G. 190, 192, 304
VON ELBE, G. 3, 12, 180, 228, 230, 243, 266, 285, 288, 304, 317, 347, 348, 351
VON KÁRMÁN, T. 95, 143, 147, 148, 225, 226, 348, 352, 421
VON ROSENBERG, H. 116
VON SMOLUCHOWSKI 98

WAGSTAFF, J. B. 307
WALKER, P. L., Jr 83
WALSH, A. D. 198, 201, 206, 442, 443
WALTERS, W. D. 68
WARREN, D. R. 198, 206
WARREN, J. A. 209
WATERS, S. 449
WATT, J. D. 306
WAYMAN, D. H. 129, 136, 191, 192
WEBER, H. C. 100
WEDGWOOD, P. 437, 438
WEEKS, D. J. 315
WEIL, C. W. 116
WEINBERG, F. J. 82, 214, 429
WEINSTEIN, A. A. 394, 411
WEISS, M. A. 15, 34, 333, 347
WELLS, F. E. 431
WESTBROOK, E. A. 81
WHARTON, W. W. 82
WHEELER, R. V. 382, 447, 449
WHITE, A. G. 366, 382
WHITE, J. R. 136
WHITTLE, E. 195, 205, 207
WHITTLE, Sir FRANK 210
WIEZEVICH, P. G. 244, 246, 252
WILDE, D. G. 381
WILDE, K. A. 225, 226
WILHELM, R. H. 313
WILKE, C. R. 255, 266
WILLE, R. 312
WILLIAMS, D. 116
WILLIAMS, F. 334, 347
WILLIAMS, F. W. 95
WILLIAMS, G. C. 12, 13, 34
WILLIAMS, G. T. 215
WILLIAMS, H. L. 372, 382
WILLIAMS, K. G. 426
WILSON, E. B. 355, 364
WILSON, M. J. G. 224
WILSON, R. R. 244
WINKLER, C. A. 198, 206
WINWARD, A. 272
WISDOM, J. C. 421
WISE, H. 105, 107, 136, 189, 192
WITHERLY, T. D. 96, 333
WOHL, K. 114, 116, 243, 253, 262, 266
WOLFHARD, H. G. 3, 12, 55, 63, 68, 70, 72, 74, 75, 76, 79, 80, 81, 82, 105, 107, 136, 170, 181, 190, 192, 197, 200, 206, 243, 254, 266, 283, 285
WOOD, B. 105
WOOD, W. W. 129, 136
WOODHEAD, D. W. 365, 372, 381, 382
WRIGHT, C. C. 83
WRIGHT, F. H. 96, 155, 330

YASAITIS, E. L. 196, 205
YOKLEY, C. R. 117
YOST, D. M. 207
YU-SHENG TAO 136

ZEELENBERG, A. P. 90
ZELDES, H. 196, 205, 206
ZUKOSKI, E. E. 94, 155, 347